SYNTHESIS, CHARACTERIZATION AND EVALUATION OF POLY(ACRYLIC ACID)-*GRAFT*-POLY(ETHYLENE GLYCOL)'S AS BOUNDARY LUBRICANTS FOR TREATMENT OF OSTEOARTHRITIS

A Dissertation

Presented to the Faculty of the Graduate School

of Cornell University

in Partial Fulfillment of the Requirements for the Degree of

Doctor of Philosophy

By

Ming-Chee Tan

May 2015

THE SYNTHESIS, CHARACTERIZATION AND IN VIVO EVALUATION OF POLY(ACRYLIC ACID)-*GRAFT*- POLY(ETHYLENE GLYCOL)'S AS BOUNDARY LUBRICANTS FOR THE TREATMENT OF OSTEOARTHRITIS

Ming-Chee Tan, Ph.D.

Cornell University, 2015

Osteoarthritis (OA) is a debilitating disease affecting the joints such as hips, knees, and shoulders. It involves degradation of the cartilage tissue and is generally irreversible given the limited self-repair mechanisms of cartilage. To aid in preservation of cartilage, the body produces lubricin – a natural boundary lubricant that binds the surface of cartilage and protects it against wear. In rat models of OA, supplementation of lubricin has been shown to prevent OA disease progression. In OA joints, production of lubricin is impaired and the mass production of lubricin has proven difficult and infeasbile. However, biomimicry can allow us to design, via synthetic routes, molecules that can have the same functionality of lubricin in the joints. Following the hypothesis that lubricin's boundary lubricating properties are tied to its structure, it is possible to apply biomimetic design criteria to create synthetic lubricin-like molecules.

In this work, a combinatorial library of polymer brushes composed of poly(acrylic acid) (pAA) and poly(ethylene glycol) (PEG) are synthesized to mimic the structure and function of lubricin and to screen for how several parameters influence function. The parameters involve different molecular weights of pAA and PEG as well as grafting ratios (PEG:AA). The pAA was synthesized via RAFT polymerization and PEG was conjugated via condensation chemistry at the given grafting ratios. The resulting 27 polymers are called poly(acrylic acid)-*graft*-poly(ethylene glycol) (pAA-*g*-PEG). The stability of these polymers

was tested to determine ideal storage conditions and potential degradation products in what is called a forced degradation study. Here the polymers are subjected to accelerated oxidative and hydrolytic (acidic and basic) conditions. The results demonstrate resistance to hydrolysis but prone to oxidation especially of the PEG component.

To characterize the pAA-*g*-PEG's, a novel method involving Fourier transform infrared spectroscopy (FTIR) and either single value decomposition (SVD) or partial least squares (PLS) modeling was employed. The hypothesis is that the FTIR spectra of pAA-*g*-PEG is a composition of pure pAA and PEG spectra. A series of known mass mixtures of pAA and PEG were spun coated on CaF_2 slides and their spectra captured. They were then decomposed in Matlab either through SVD or PLS and compared to their known pAA mass fractions in a calibration graph. Decomposed pAA-*g*-PEG spectra were then be compared to this graph to determine pAA mass fraction and percent conjugation of PEG side chains. However, the results demonstrated effectiveness only for lower grafting ratios (0.5 and 0.25) but were ineffective for the highest grafting ratio of 2.

Finally, the evaluation of pAA-*g*-PEG's as boundary lubricants were done in vitro on bovine cartilage explants and in vivo on rat models of OA. In both in vitro and in vivo studies, pAA(60)-2-PEG(2) (60,000 g/mol pAA; grafting ratio 2; 2,000 g/mol PEG), demonstrated the greatest reduction in coefficient of friction compared to negative controls. In vitro binding time constant (~20 minutes) was much less than synovial clearance time (~5 hours). In vivo studies also showed through histological analysis chondroprotection of cartilage in OA rats compared to controls, meaning it protected against OA disease progression.

BIOGRAPHICAL SKETCH

Ming-Chee Tan was born March 20th, 1987 in New York City, NY, USA. He received a Bachelor of Science in Mechanical Engineering from SUNY Binghamton University, Binghamton, NY and graduated summa cum laude. Did materials research as an undergraduate with Professor Cho. Is awardee of the Giant Nevus Morgan Fellowship 2010-2012 and a co-winner of the Advanced Materials Enabled Innovation business competition in 2013. He has started his PhD studies in the department of Biomedical Engineering at Cornell University under the auspices of Dr. David Putnam.

ACKNOWLEDGEMENTS

To my father and mother, Check Lee Tan and Lan Hua Sun, for whom I owe my life. To Dr. Putnam for offering me this wonderful research opportunity with all its surprises, difficulties and moments of joy. His expansive knowledge has taught me much over the years about research, clinical translation of medicine and business. My thanks my committee member Dr. Bonassar and his student Kirk Samaroo, who as my collaborators brought this project forward. Dr. Christober Ober, for his time and advice. I would also like to thank all of my collaborators on this project: Dr. Petersen, Dr. Gourdon, Dr. Andresen-Eguiluz, and Aliyah Barrett. Special thanks to Dr. Minglin Ma for attending my defense on such short notice.

My gratitude to the Morgan family for providing a generous fellowship as well as NYSTAR and NIH for their funding. CCMR and the NBTC for the instrumentation and advice I have gotten over the years. I am especially grateful to all the members of the Putnam Lab for the all the laughs and fun times we have had over the years. I am very blessed to have been part of such a team.

To my Father and Mother,

Check Lee Tan and Lan Hua Sun

TABLE OF CONTENTS

LIST OF FIGURES

LIST OF TABLES

CHAPTER 1

INTRODUCTION

1.1 Osteoarthritis

Osteoarthritis (OA) is a leading cause of disability in adults caused through chronic and acute damage to the tissues surrounding joints such as knees, hips and ankles[1]. In general, due to the constant wear and limited self-repair mechanisms of joint tissues, they are particularly susceptible to chronic degradation over a patient's lifetime. OA is assessed according to severity of the condition, ranging from mild, moderate and severe; and given its chronic nature most cases of osteoarthritis will continue to increase in severity over a patient's lifetime. According to the Center for Disease Control (CDC) in the US, there were 27 million adults with OA in 2003[2] and by 2030 there may be as many as 67 million people with some form of arthritis[3]. One in two people may by the age of 85 and two in three people who are obese will develop knee OA[4], making knee OA the most prevalent form of OA. People active in sporting activities are particularly susceptible to joints injuries such as a torn ACL. Children under 18 years of age who have endured joint injuries may be 10 times more likely to develop OA[5]. In 2005, the annual health care burden of OA exceeded $185 billion[6] and the costs are expected to rise due to the aging baby-boomer generation and increasing obesity rates in the US. As of right now, it is a widespread disease where medical science as yet to develop a viable treatment to cure or at least inhibit the disease progression.

1.2 Current treatment options for osteoarthritis

There are many treatment options for OA, depending on the severity and condition of the patient. Treatment options are differentiated into surgical and non-surgical, the latter of

which is most preferred except in severe circumstances when surgery is required. Current non-surgical treatments for osteoarthritis include lifestyle management such as exercise and medication for symptom relief[7]; of the latter the most common drugs are non-steroidal anti-inflammatories[8] and intra-articular corticosteroid injections[9,10] both of which do not inhibit disease progression. In fact, the latter treatment may lead to further cartilage damage due to the patient inability to feel the pain – usually an important indicator of damage[10]. Another non-surgical therapy is the oral supplementation of chondroitin sulfate and glucosamine, both of which are components of a healthy cartilage and are hypothesized to help maintain joint integrity. However, clinical studies on the supplements have cast doubt onto their efficacy to inhibit OA disease progression[11,12]. On the extreme end, a longer term for treating with osteoarthritic knees is total joint replacement[7] but is usually only considered when other medical treatments fail. Another approach to the treatment of OA, and the topic of this thesis, is to administer lubricants into the joint to help protect the cartilage against repeated wear and friction, and to relieve pain and slow disease progession. This idea has in the past been extensively studied with regards to two naturally occurring biolubricants found in the human body which are hyaluronic acid (HA) and lubricin. Both HA and lubricin are found naturally in the synovial fluid of human joints, such as the knees, and both contribute to the lubricity of the joints. However, the mechanism through they lubricate are significantly different from each other, that is they each have their own unique way to decrease friction between two surfaces.

1.3 Joint lubrication

There are two extremes of lubrication regimes known as hydrodynamic and boundary[13]. In hydrodynamic mode lubrication there is a thick liquid film separating the two contact surfaces where viscosity of the film plays a significant role; boundary mode lubrication meanwhile has almost no fluid between the contact surfaces and surface roughness plays a larger role. A Stribeck curve based on the Hersey number readily demonstrates an example of this (**Fig 1.1**). The Hersey number allows quantification of lubrication conditions, and when combined tribological analyses, it can differentiate the various regimes of lubrication based on coefficient of friction. The Hersey number is given in the equation below.

$$H = \frac{Velocity * Viscosity}{Pressure * Roughness} \quad (1)$$

Another way to create Stribeck curves is to use the Sommerfeld number instead of the Hersey number. The Sommerfeld number is a more modern form of the Hersey number also applicable in understanding tribology[14]. An advantage in applying the Sommerfeld number in analyzing tissue lubrication modes is that corresponds well to porous materials[15] and softer, elastic materials[16,17]. In general the Sommerfeld number involves the contact width of the contacting surfaces while Hersey factors in the surface roughness, important for the consideration of pressurized film layers[17]. Cartilage is a natural tissue that is both porous and elastic, corresponding to soft matter, and these materials tend not to enter pure hydrodynamic mode as readily. In human joints, all such modes of lubrication are encountered but boundary mode not only experiences the highest coefficient of friction but is possibly the most common

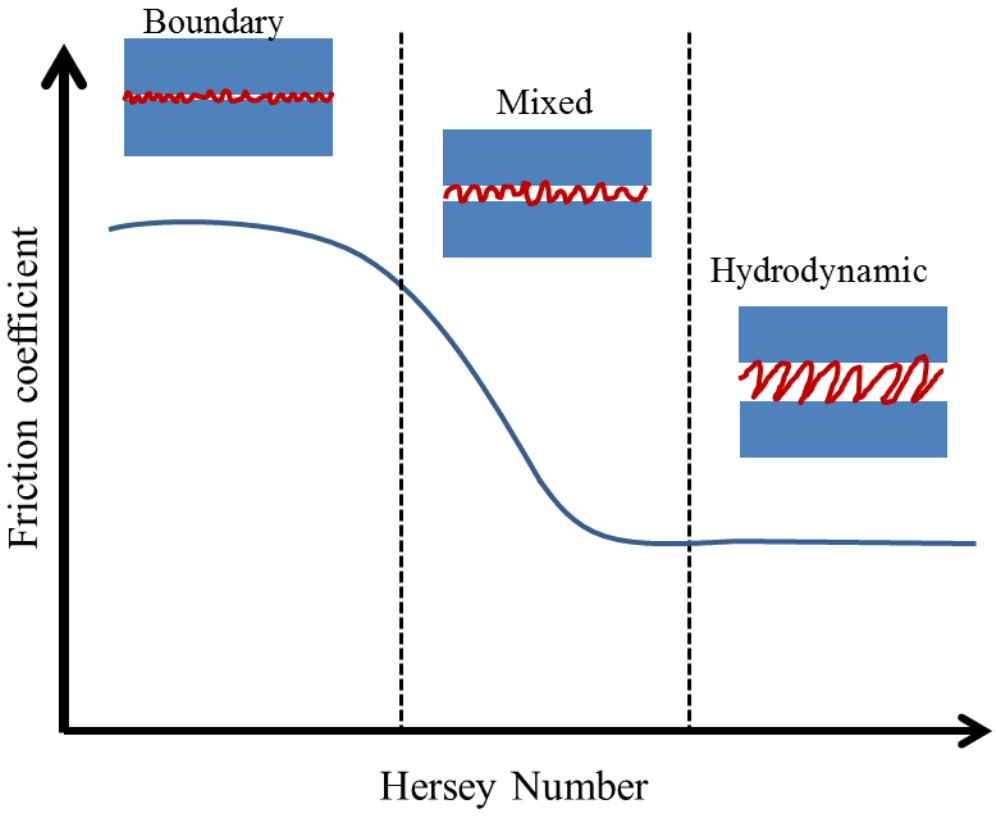

Figure 1.1 An example of a Stribeck curve with friction plotted against Hersey number. The red line separating the surfaces represent a fluid film. Modes of lubrication correspond to fluid film thickness separating the two surfaces. Boundary mode has minimal fluid film presence, hydrodynamic mode has maximal, while mixed is an intermediate between the two.

due to the slower movements people normally engage in such as walking and standing compared to running activities like sprinting or jogging.

1.4 Hyaluronic Acid and Lubricin

HA is a naturally occurring glycosasminoglycan found within the synovial fluid of the joints and lubricates by increasing the viscosity of the synovial fluid; this reduces friction in the mixed and hydrodynamic mode of lubrication on articular cartilage[18]. Therapeutically, HA is injected intra-articularly to treat OA[19]. Some clinical studies of HA have shown little long term efficacy in inhibiting OA disease progression when injected by itself[20–24], while other studies claim to demonstrate efficacy[25]. A recent study demonstrated efficacy in a rat model of OA by modifying the tissue to retain HA on the cartilage surface[26], thus altering the surface properties and perhaps driving it towards boundary mode lubrication. However, by itself HA is not an effective boundary lubricant and its effectiveness as a stand-alone treatment for OA is controversial, with some possible benefits to relieve pain[25,27] but with inconsistent benefit on OA disease progression[28].

Lubricin, a high molecular weight glycoprotein (**Fig 2**), is also a biolubricant found within the synovial fluid that binds to the articular cartilage surfaces and reduces friction in the boundary mode[29–32]. In rat models of OA, intra-articular supplementation of native lubricin was shown to inhibit disease progression[33,34]; LUB:1 a truncated recombinant form of lubricin also exhibited similar effects in rat OA models[35,36]. Lubricin's effectiveness in inhibiting OA disease progression may be due to reducing friction in the boundary mode instead of hydrodynamically. Boundary mode is where the highest frictional forces are experienced and has thinnest fluid film separating the contact surfaces; this may be why HA

supplementation is ineffective on its own in inhibiting OA disease progression. In fact, it is suggested both HA and lubricin supplementation is needed to properly lubricate weight-bearing joints such as the knee in inhibiting the disease progression[37]. However, to date, the large-scale recombinant manufacture of both lubricin and LUB:1 remains challenging owing to multiple amino acid repeats in the protein core, as well as the high degree of glycosylation[38,39] making it impractical to advance to clinical studies. To this end, more studies must be conducted on lubricin to understand its function and ways to develop lubricin-like molecules that can provide similar lubricating abilities to lubricin. Lubricin's lubricating ability appears to rely on its unique brush-like structure, involving a peptide backbone and oligosaccharide side chains that contributes the most to its high molecular weight. In the presence of water, the hydrophilic oligosaccharides swell and cause the molecule to form an extended structure that when bounded to a surface, may provide boundary lubrication.In this way lubricin can be compared to brush polymers in structure and function[40,41]. Since lubricin resembles a brush structure (**Fig 1.2**), synthetic polymer brushes can easily be generated and analyzed to elucidate their general properties that, in turn, can lead to the creation of bioinspired lubricating materials. This can provide greater insight into how lubricin functions as a lubricant based on its unique structure.

1.5 Lubricin and polymer brushes

There is a plethora of work in the scientific literature concerning polymer brushes for the purposes of lubrication some inspired by lubricin. These studies not only create lead to synthetic lubricants but because of the modifiability of polymer brushes, an insight in lubrication mechanism can be elucidated. Spencer et al. has done much work synthesizing a

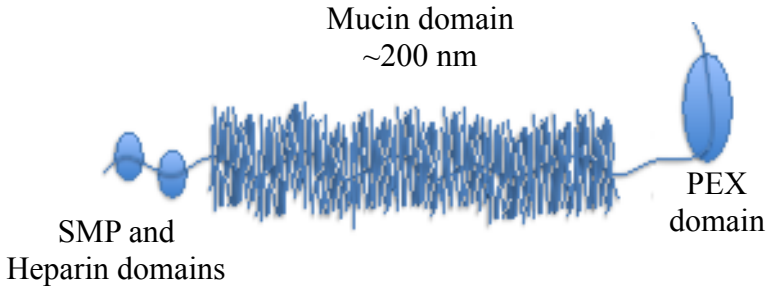

Figure 1.2: Schematic of a lubricin molecule. The mucin domain is the largest part composed of dense oligosaccharide chains resembling a "brush" like structure, ~200 nm in length40. The end termini are composed of somatomedin (SMP), heparin and homeopexin (PEX), which are important for lubricin interactions with other molecules and cartilage tissue respectively.

series of lubricin inspired polymer brush analogues. They have synthesized polymer brushes with poly(L-lysine) backbones grafted with either poly(ethylene glycol)[42–45] or dextran[46,47]. Poly(L-lysine)-*graft*-poly(ethylene glycol) (PLL-*g*-PEG) consists of a polycationic lysine backbone with neutral PEG side chains absorbable onto negatively charged substrates via the positively charged backbone. They demonstrated adsorption onto oxide surfaces and profoundly reduced boundary friction in aqueous solutions[42,48]. The polymer would absorb flatly onto the substrate while the PEG chains would solvate and extend outwards. The coefficient of friction was reduced by half compared to aqueous control in their studies. Further they demonstrated that by increasing the molecular weight of the PEG side chains, they were able to further decrease the coefficient of friction. The Spencer group also worked with dextran grafted onto PLL instead of PEG as the side chains. Dextran is a type of hydrophilic polysaccharide of varying molecular weights; polysaccharides in general are carbohydrates found on a variety of biomolecules including proteoglycan such as lubricin and is vital to lubrication[49]. They found that poly(L-lysine)-*graft*-dextran (PLL-*g*-dex) was able to lower friction on oxide surfaces but generally was not more effective than PLL-*g*-PEG. In their work they concluded that friction was most effectively reduced when their backbone was well anchored to their substrates and when PEG side chains were well solvated[45].

Claesson et al. has designed polymers similar to Spencer et al. of methacryloxyethyl trimethylammonium chloride (METAC) and PEG-methylether methacrylate (PEO_{45}MEMA) as a random copolymer called PEO_{45}MEMA:METAC-X, with X corresponding to the mole % of charged METAC segments in the backbone[50,51]. One major difference between Claesson's and Spencer's work is the positioning of the adsorbed polymers on the substrate – PLL-*g*-PEG lubricates best when it lays flat on the substrate but PEO_{45}MEMA:METAC-X actually

functions better when partially adhered via its backbone than when completely adsorbed flat via its backbone[50,52], this latter is more in line with the how lubricin functions on cartilage surfaces[40].

Israelachvili et al. has recently developed another polymer brush inspired by the structure of lubricin following an ABA block copolymer structure where the A groups is composed of quaternized 2-(dimethylaminoethyl) methacrylate (qDMAEMA) and the core or B is a statistical copolymer of methyl methacrylate (MMA) and MMA conjugated with poly(2-methacryloyloxyethyl phosphorylcholine) (PMPC)[53]. Abbreviated PMPC ABA, this polymer was bound to mica substrates via the qDMAEMA end groups, while the core brush structure would hydrate and expand in aqueous solvents. This is in contrast to Spencer et al or Claesson's work where the polymer brushes either laid flat (complete backbone interaction) or experienced partial adherence (partial backbone interaction). Iasraelachvili et al's reasoning was that lubricin and typical polymer brush lubricants form linear polymer loops (attached from one end) that are inefficient when considering bridging effects between surfaces and poor frictional dynamics under high shearing speeds. In fact, Israelachvili was able to demonstrate excellent lubricating properties under a range of normal forces (0-12 mN) and sliding speeds (0.001-100 μm/s) equaling to less than half of lubricin in PBS on mica.

In conclusion, there are many polymer brushes inspired by the lubrication properties of lubricin and synthesized for that specific application. What has been ascertained from these studies is that the effective lubrication of polymer brushes relies heavily on 1) effective adherence onto substrate surfaces, 2) the length and density of the side chains under "good" solvent conditions and 3) the conformation of the conformation of polymer brushes bound to surfaces.

1.6 Characteristics of polymer brushes for lubrication

The unique properties of polymer brushes stem from having long side chains closely packed together in a small area. The many researched applications of polymer brushes are beyond the scope of this chapter and the focus will be on topics germane to this thesis. Polymer brushes have been extensively researched for their potential as surface coatings for the purposes of anti-adhesion[54–57], anti-microbial[55,58–61] and even as lubricating layers[62–64]. Often polymer brush coatings function for several of these purposes at once, such as anti-adhesive and anti-microbial. Examples of these include poly(2-hydroxyethyl methacrylate) grafted with chitosan[54], peptide modified pluronic[55] and PEG based brushes[56]. Anti-adhesive properties of polymer brushes, particular of those composed of PEG, are often studied as surface coatings. The reasons are these characteristics not well-known but are speculated to be due to the formation of a steric barrier or increased osmotic pressure as a result of polymer brush hydration[65]. In fact, this may be related to why polymer brushes can also function as excellent boundary lubricants. If the polymer brushes have interchain repulsion and strong interactions with a good solvent, then they will naturally swell and form a cushioning layer that may repel proximal contacting surfaces. In general, the packing density of the side chain and their interactions with their environment provide brush polymers with very interesting properties at the molecular level. In a given volume the polymer brushes can occupy much more space than a linear polymer, which could form a pressurized, steric barrier depending on its environmental interactions.

1.7 Synthesis of polymer brushes

Polymer brushes have been synthesized to produce a range of structures including varying backbone lengths, side chain functionalities and even grafting densities. The general methods of producing polymer brushes can be grouped into *grafting through*, *grafting onto*, and *grafting from* (**Fig 1.3**). Each of these synthetic techniques has its own peculiar strengths and weaknesses for generating polymer brushes. Grafting through involves polymerization of macromonomers that themselves are oligomers or polymers such as the polymerization of poly(ethylene glycol) methyl ether acrylate (PEGMA) by ATRP[66] or the copolymerization of methylacrylic acid (MAA) and PEGMA[67]. Grafting through can create well defined polymer brushes with densely packed side chain groups but is limited by monomer selection. Utilizing large macromonomers has the weakness of limited the percent conversion as steric hindrance and increasing of viscosity can prematurely terminate the reaction leading to limited repeat units of polymer brush[68]. Grafting onto, involves a linear polymer with functional groups such as carboxylic acids conjugated with telechelic polymers. These telechelic polymers become side chains on linear polymer, examples of this includes PLL-*g*-PEG[42] and PLL-*g*-dex[46] by Spencer et al. The polymer brush backbone and side chain to be prepared independently provided that their respective functionalities allow conjugation to take place, as a result large polymers and a diversity of side chains can be employed to create a large and varied polymer brush. However, due to steric hindrance the packing density of the side chains may be very limited, and the polymer and side chain molecules require complementary functional groups that allow them to be linked through methods such as nucleophilic substation[69–71] or click chemistry[72–74]. Grafting from, relies on utilizing a polymer backbone whose functional groups can function as initiation sites for monomers allowing the growth of side chains directly from

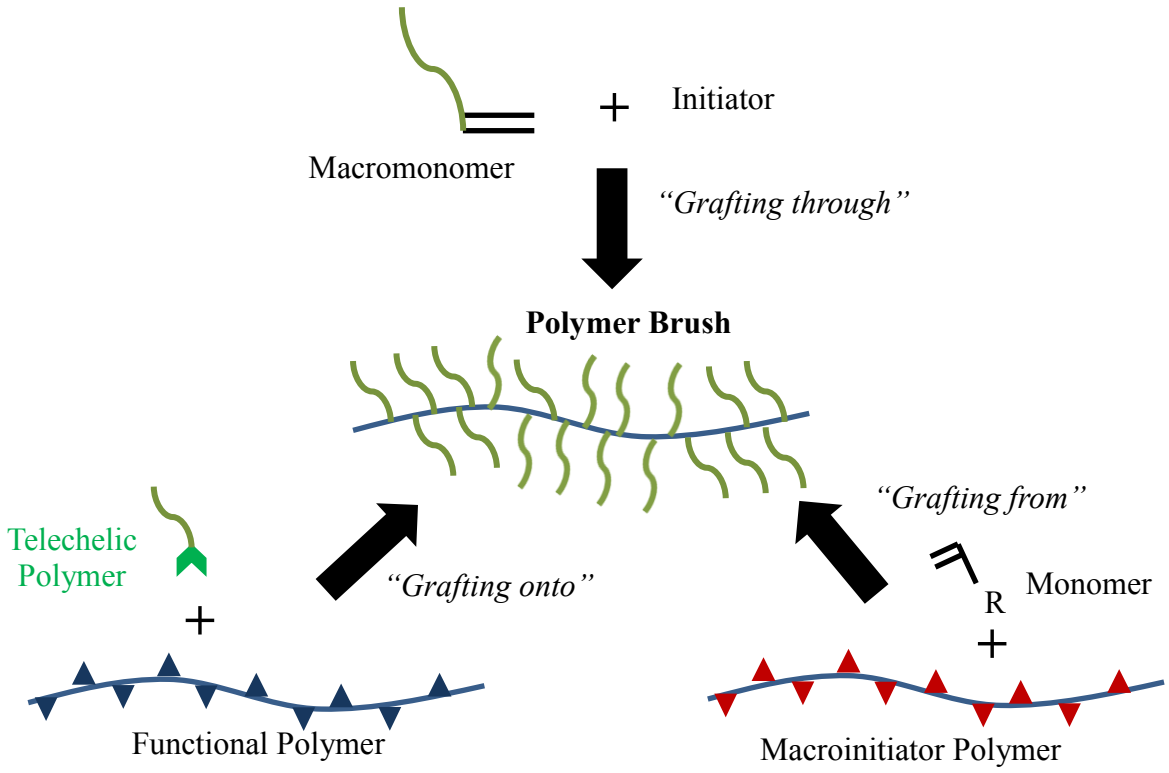

Figure 1.3: Three general synthetic schemes to produce polymer brushes.

the backbone; polymerization methods include anionic[75] and atom transfer radical polymerization (ATRP)[53,76]. This allows the generation of a polymer brush with narrow molecular weight distributions and long backbones. However, the reaction is limited by the initiation efficiency of the polymer backbone as well as steric hindrance of the side chain monomers leading to limited packing density and side chain lengths. A more thorough description of polymer brush synthesis techniques can be found in a review article by Sheiko et al.[77]

1.8 Synthesis of lubricin-like polymer brushes

Synthesis of polymer brushes have well-defined routes but their ability to fully replicate the density and length of lubricin has not yet been fully accomplished. Lubricin's persistence length is approximately ~200 nm[40] and has such a densely packed core of oligosaccharides that it forms a very stiff rod-like formation. Of the polymers investigated so far, to the knowledge of this author, none have been able to fully reproduce this through a synthetic polymer route or thoroughly investigated it as a lubricin replacement for arthritic conditions. The difficulties include the ability to produce a very long backbone combined with hydrophilic side chains – grafting through can produce a dense stiff polymer brush but is limited by the length of the backbone, grafting from can utilize a large backbone but may not produce dense or long side chain, while grafting onto may use large backbone and side chains but may not readily produce lead to densely packed side chains.

To this end, we aim to design and synthesize a series of synthetic polymer brushes to mimic the structure of lubricin and determine if the synthetic lubricin analogs can, in fact, lubricate in the boundary mode and what structural parameters of the brush architecture influences lubrication, following the hypothesis that lubricin's lubricating ability is due solely to its structure.

The synthetic lubricin anaolog consists of a polymer backbone of poly(acrylic acid) (pAA) grafted with poly(ethylene glycol) (PEG) as the side chains. The structural parameters to be investigated include the size of the polymer backbone (60, 105, 145 kDa), the size of the PEG's (2, 5, 10 kDa) as well as the grafting ratio of PEG to acrylic acid monomers (PEG/AA = 0.5, 1, 2). A combinatorial library of polymers was synthesized according to these parameters before lubrication testing, to eliminate the time consuming method of iterative polymer synthesis, and to try to improve lubrication in boundary mode. Through a combinatorial approach a wide range of polymer architectures was synthesized and then tested to identify promising architectures; this allows for efficiency when the desired parameters are unknown.

1.9 References

1. Guccione, A. The effects of specific medical conditions on the functional limitations of elders in the Framingham Study. *Am. J. Public Health* **84,** 351–358 (1994).

2. Lawrence, R. C. *et al.* Estimates of the prevalence of arthritis and other rheumatic conditions in the United States. Part II. *Arthritis Rheum.* **58,** 26–35 (2008).

3. Hootman, J. M. & Helmick, C. G. Projections of US prevalence of arthritis and associated activity limitations. *Arthritis Rheum.* **54,** 226–9 (2006).

4. Murphy, L. *et al.* Lifetime risk of symptomatic knee osteoarthritis. *Arthritis Rheum.* **59,** 1207–13 (2008).

5. LaBella, C. R., Hennrikus, W. & Hewett, T. E. Anterior cruciate ligament injuries: diagnosis, treatment, and prevention. *Pediatrics* **133,** e1437–50 (2014).

6. Kotlarz, H., Gunnarsson, C. L., Fang, H. & Rizzo, J. a. Insurer and out-of-pocket costs of osteoarthritis in the US: evidence from national survey data. *Arthritis Rheum.* **60,** 3546–53 (2009).

7. Sinusas, K. Osteoarthritis: diagnosis and treatment. *Am. Fam. Physician* **85,** 49–56 (2012).

8. Scott, D. L. *et al.* The long-term effects of non-steroidal anti-inflammatory drugs in osteoarthritis of the knee: a randomized placebo-controlled trial. *Rheumatology (Oxford).* **39,** 1095–101 (2000).

9. Arroll, B. & Goodyear-Smith, F. Corticosteroid injections for osteoarthritis of the knee: meta-analysis. *BMJ* **328,** 869 (2004).

10. Hauser, R. The deterioration of articular cartilage in osteoarthritis by corticosteroid injections. *J. Prolotherapy* 107–123 (2009). at <http://www.journalofprolotherapy.com/pdfs/issue_02/issue_02_10_deterioration_cartilage.pdf>

11. Sherman, A. L., Ojeda-Correal, G. & Mena, J. Use of glucosamine and chondroitin in persons with osteoarthritis. *PM R* **4,** S110–6 (2012).

12. Vangsness, C. T., Spiker, W. & Erickson, J. A review of evidence-based medicine for glucosamine and chondroitin sulfate use in knee osteoarthritis. *Arthroscopy* **25,** 86–94 (2009).

13. Bhushan, B. *Introduction to tribology*. (John Wiley & Sons, 2002).

14. Philipossian, A. & Olsen, S. Fundamental Tribological and Removal Rate Studies of Inter-Layer Dielectric Chemical Mechanical Planarization. *Jpn. J. Appl. Phys.* **42,** 6371–6379 (2003).

15. Murti, P. R. K. Hydrodynamic lubrication of long porous bearings. *Wear* **18,** 449–460 (1971).

16. Bongaerts, J. H. H., Fourtouni, K. & Stokes, J. R. Soft-tribology: Lubrication in a compliant PDMS–PDMS contact. *Tribol. Int.* **40,** 1531–1542 (2007).

17. Pitenis, A. A. *et al.* Polymer Fluctuation Lubrication in Hydrogel Gemini Interfaces. *Soft Matter* **10,** 8955–8962 (2014).

18. Tadmor, R., Chen, N. & Israelachvili, J. N. Thin film rheology and lubricity of hyaluronic acid solutions at a normal physiological concentration. *J. Biomed. Mater. Res.* **61,** 514–23 (2002).

19. Mabuchi, K., Tsukamoto, Y., Obara, T. & Yamaguchi, T. The effect of additive hyaluronic acid on animal joints with experimentally reduced lubricating ability. *J. Biomed. Mater. Res.* **28,** 865–70 (1994).

20. Lo, G., LaValley, M., McAlindon, T. & Felson, D. Intra-articular hyaluronic acid in treatment of knee osteoarthritis: a meta-analysis. *Jama* **290,** 3115–3121 (2003).

21. Rutjes, A. W. S. *et al.* Viscosupplementation for Osteoarthritis of the KneeA Systematic Review and Meta-analysis. *Ann. Intern. Med.* **157,** 180–191 (2012).

22. Felson, D. Osteoarthritis of the knee. *N. Engl. J. Med.* **354,** 841–848 (2006).

23. Curran, M. P. Hyaluronic acid (Supartz®): a review of its use in osteoarthritis of the knee. *Drugs Aging* **27,** 925–41 (2010).

24. Colen, S. & Bekerom, M. van den. Hyaluronic Acid in the Treatment of Knee Osteoarthritis. *BioDrugs* **26,** 257–268 (2012).

25. Chang, K.-V., Hsiao, M.-Y., Chen, W.-S., Wang, T.-G. & Chien, K.-L. Effectiveness of intra-articular hyaluronic acid for ankle osteoarthritis treatment: a systematic review and meta-analysis. *Arch. Phys. Med. Rehabil.* **94,** 951–60 (2013).

26. Singh, A. *et al.* Enhanced lubrication on tissue and biomaterial surfaces through peptide-mediated binding of hyaluronic acid. *Nat. Mater.* (2014). doi:10.1038/nmat4048

27. Bannuru, R. R., Natov, N. S., Dasi, U. R., Schmid, C. H. & McAlindon, T. E. Therapeutic trajectory following intra-articular hyaluronic acid injection in knee osteoarthritis--meta-analysis. *Osteoarthritis Cartilage* **19,** 611–9 (2011).

28. Jubb, R., Piva, S., Beinat, L., Dacre, J. & Gishen, P. A one-year, randomised, placebo (saline) controlled clinical trial of 500-730 kDa sodium hyaluronate (Hyalgan) on the radiological change in osteoarthritis of the knee. *Int. J. Clin. Pract.* **57,** 467–474 (2003).

29. Gleghorn, J. P. & Bonassar, L. J. Lubrication mode analysis of articular cartilage using Stribeck surfaces. *J. Biomech.* **41,** 1910–8 (2008).

30. Gleghorn, J. P., Jones, A. R. C., Flannery, C. R. & Bonassar, L. J. Boundary mode lubrication of articular cartilage by recombinant human lubricin. *J. Orthop. Res.* **27,** 771–7 (2009).

31. Swann, D. & Radin, E. The molecular basis of articular lubrication I. Purification and properties of a lubricating fraction from bovine synovial fluid. *J. Biol. Chem.* **247,** 8069–8073 (1972).

32. Jay, G. D., Haberstroh, K. & Cha, C. J. Comparison of the boundary-lubricating ability of bovine synovial fluid, lubricin, and Healon. *J. Biomed. Mater. Res.* **40,** 414–8 (1998).

33. Elsaid, K. a *et al.* The impact of forced joint exercise on lubricin biosynthesis from articular cartilage following ACL transection and intra-articular lubricin's effect in exercised joints following ACL transection. *Osteoarthritis Cartilage* **20,** 940–8 (2012).

34. Jay, G. D. *et al.* Prevention of cartilage degeneration and gait asymmetry by lubricin tribosupplementation in the rat following anterior cruciate ligament transection. *Arthritis Rheum.* **64,** 1162–71 (2012).

35. Flannery, C. R. *et al.* Prevention of cartilage degeneration in a rat model of osteoarthritis by intraarticular treatment with recombinant lubricin. *Arthritis Rheum.* **60,** 840–7 (2009).

36. Jay, G. D. *et al.* Prevention of cartilage degeneration and restoration of chondroprotection by lubricin tribosupplementation in the rat following anterior cruciate ligament transection. *Arthritis Rheum.* **62,** 2382–91 (2010).

37. Das, S. *et al.* Synergistic interactions between grafted hyaluronic acid and lubricin provide enhanced wear protection and lubrication. *Biomacromolecules* **14,** 1669–77 (2013).

38. Jay, G. D. Lubricin and surfacing of articular joints. *Curr. Opin. Orthop.* **15,** 355–359 (2004).

39. Jones, A. & Gleghorn, J. Binding and localization of recombinant lubricin to articular cartilage surfaces. *J. Orthop. Res.* **12,** 10–12 (2007).

40. Zappone, B., Ruths, M., Greene, G. W., Jay, G. D. & Israelachvili, J. N. Adsorption, lubrication, and wear of lubricin on model surfaces: polymer brush-like behavior of a glycoprotein. *Biophys. J.* **92,** 1693–708 (2007).

41. Coles, J. M., Chang, D. P. & Zauscher, S. Molecular mechanisms of aqueous boundary lubrication by mucinous glycoproteins. *Curr. Opin. Colloid Interface Sci.* **15,** 406–416 (2010).

42. Müller, M., Lee, S., Spikes, H. & Spencer, N. The influence of molecular architecture on the macroscopic lubrication properties of the brush-like co-polyelectrolyte poly (L-lysine)-g-poly (ethylene glycol)(PLL-g-PEG) adsorbed on oxide surfaces. *Tribol. Lett.* **15,** 395–405 (2003).

43. Ramakrishna, S. N., Espinosa-Marzal, R. M., Naik, V. V, Nalam, P. C. & Spencer, N. D. Adhesion and friction properties of polymer brushes on rough surfaces: a gradient approach. *Langmuir* **29,** 15251–9 (2013).

44. Lee, S. & Spencer, N. D. Aqueous lubrication of polymers: Influence of surface modification. *Tribol. Int.* **38,** 922–930 (2005).

45. Perry, S. S. *et al.* Tribological properties of poly(L-lysine)-graft-poly(ethylene glycol) films: influence of polymer architecture and adsorbed conformation. *ACS Appl. Mater. Interfaces* **1,** 1224–30 (2009).

46. Perrino, C., Lee, S., Choi, S. W., Maruyama, A. & Spencer, N. D. A Biomimetic Alternative to Poly (ethylene glycol) as an Antifouling Coating: Resistance to Nonspecific Protein Adsorption of Poly (L -lysine)-graft-dextran. *Langmuir* **24,** 8850–8856 (2008).

47. Perrino, C., Lee, S. & Spencer, N. D. End-grafted Sugar Chains as Aqueous Lubricant Additives: Synthesis and Macrotribological Tests of Poly(l-lysine)-graft-Dextran (PLL-g-dex) Copolymers. *Tribol. Lett.* **33,** 83–96 (2008).

48. Huang, N. *et al.* Poly (L-lysine)-g-poly(ethylene glycol) Layers on Metal Oxide Surfaces: Surface-Analytical Characterization and Resistance to Serum and Fibrinogen Adsorption. *Langmuir* **17,** 489–498 (2001).

49. Jay, G. D., Harris, D. A. & Cha, C. Boundary lubrication by lubricin is mediated by O-linked β (1-3) Gal-GalNAc oligosaccharides. *Glycoconj. J.* **18,** 807–815 (2001).

50. Pettersson, T., Naderi, A., Makuška, R. & Claesson, P. Lubrication properties of bottle-brush polyelectrolytes: An AFM study on the effect of side chain and charge density. *Langmuir* **24,** 3336–3347 (2008).

51. Krivorotova, T., Makuska, R., Naderi, a., Claesson, P. M. & Dedinaite, a. Synthesis and interfacial properties of novel cationic polyelectrolytes with brush-on-brush structure of poly(ethylene oxide) side chains. *Eur. Polym. J.* **46,** 171–180 (2010).

52. Iruthayaraj, J., Olanya, G. & Claesson, P. M. Viscoelastic Properties of adsorbed bottle-brush polymer layers studied by quartz crystal microbalance - Dissipation measurements. *J. Phys. Chem. C* **112,** 15028–15036 (2008).

53. Behavior, A. *et al.* Bioinspired Bottle-Brush Polymer Exhibits Low Friction and Amontons-like Behavior. *J. Am. Chem. Soc.* **136,** 6199–6202 (2014).

54. Yang, W. J. *et al.* Biomimetic anchors for antifouling and antibacterial polymer brushes on stainless steel. *Langmuir* **27,** 7065–76 (2011).

55. Muszanska, A. K. *et al.* Antiadhesive polymer brush coating functionalized with antimicrobial and RGD peptides to reduce biofilm formation and enhance tissue integration. *Biomacromolecules* **15,** 2019–26 (2014).

56. Fan, X., Lin, L. & Messersmith, P. B. Cell fouling resistance of polymer brushes grafted from ti substrates by surface-initiated polymerization: effect of ethylene glycol side chain length. *Biomacromolecules* **7,** 2443–8 (2006).

57. Hwangbo, K.-H., Kim, Y.-J. & Cho, K. Y. Fabrication of protein-resistant blend based on PVDF-HFP and amphiphilic brush copolymer made from PMMA and PEGMA. *Appl. Surf. Sci.* **263,** 291–296 (2012).

58. Gao, G. *et al.* Antibacterial surfaces based on polymer brushes: investigation on the influence of brush properties on antimicrobial peptide immobilization and antimicrobial activity. *Biomacromolecules* **12,** 3715–27 (2011).

59. Roosjen, A., Mei, H. C. Van Der, Busscher, H. J. & Norde, W. Microbial Adhesion to Poly (ethylene oxide) Brushes : Influence of Polymer Chain Length and Temperature. 10949–10955 (2004).

60. Nejadnik, M. R. *et al.* Bacterial colonization of polymer brush-coated and pristine silicone rubber implanted in infected pockets in mice. *J. Antimicrob. Chemother.* **62,** 1323–5 (2008).

61. Nejadnik, M. R., van der Mei, H. C., Norde, W. & Busscher, H. J. Bacterial adhesion and growth on a polymer brush-coating. *Biomaterials* **29,** 4117–21 (2008).

62. Raviv, U. *et al.* Lubrication by charged polymers. *Nature* **425,** 163–5 (2003).

63. Nomura, A., Okayasu, K., Ohno, K., Fukuda, T. & Tsujii, Y. Lubrication Mechanism of Concentrated Polymer Brushes in Solvents: Effect of Solvent Quality and Thereby Swelling State. *Macromolecules* **44,** 5013–5019 (2011).

64. Bielecki, R. M., Crobu, M. & Spencer, N. D. Polymer-Brush Lubrication in Oil: Sliding Beyond the Stribeck Curve. *Tribol. Lett.* **49,** 263–272 (2012).

65. Gennes, P. de. Conformations of polymers attached to an interface. *Macromolecules* **1075,** 1069–1075 (1980).

66. Neugebauer, D., Zhang, Y. & Pakula, T. Densely-grafted and double-grafted PEO brushes via ATRP. A route to soft elastomers. *Macromolecules* **36,** 6746–6755 (2003).

67. Rinaldi, D. & Hamaide, T. copolymerization of methacrylic acid and poly (ethylene glycol) methyl ether methacrylate in the presence of a hydrophobic chain transfer agent in organic solution. *J. Polym. Sci. Part A Polym. Chem.* **47,** 3045–3055 (2009).

68. Yamada, K., Miyazaki, M., Ohno, K., Fukuda, T. & Minoda, M. Atom Transfer Radical Polymerization of Poly(vinyl ether) Macromonomers. *Macromolecules* **32,** 290–293 (1999).

69. Schmolke, H., Hartwig, S. & Klages, C.-P. Poly(acrylic acid)-graft-poly(ethylene glycol) preparation and adsorption on polyelectrolyte multilayers (PEMs) for custom-made antiadhesive surfaces. *Phys. Status Solidi* **208,** 1290–1300 (2011).

70. Pelet, J. M. & Putnam, D. An in-depth analysis of polymer-analogous conjugation using DMTMM. *Bioconjug. Chem.* **22,** 329–37 (2011).

71. Thompson, K. & Michielsen, S. Novel synthesis of N-substituted polyacrylamides: Derivatization of poly(acrylic acid) with amines using a triazine-based condensing reagent. *J. Polym. Sci. Part A Polym. Chem.* **44,** 126–136 (2006).

72. Ranjan, R. & Brittain, W. J. Synthesis of High Density Polymer Brushes on Nanoparticles by Combined RAFT Polymerization and Click Chemistry. *Macromol. Rapid Commun.* **29,** 1104–1110 (2008).

73. Rahane, S. B., Hensarling, R. M., Sparks, B. J., Stafford, C. M. & Patton, D. L. Synthesis of multifunctional polymer brush surfaces via sequential and orthogonal thiol-click reactions. *J. Mater. Chem.* **22,** 932 (2012).

74. Ranjan, R. & Brittain, W. J. Tandem RAFT Polymerization and Click Chemistry: An Efficient Approach to Surface Modification. *Macromol. Rapid Commun.* **28,** 2084–2089 (2007).

75. Ederle, Y., Isel, F., Grutke, S. & Lutz, P. J. Anionic polymerization and copolymerization of macromonomers: kinetics, structure control. *Macromol. Symp.* **132,** 197–206 (1998).

76. Tsarevsky, N. V & Matyjaszewski, K. "Green" atom transfer radical polymerization: from process design to preparation of well-defined environmentally friendly polymeric materials. *Chem. Rev.* **107,** 2270–99 (2007).

77. Sheiko, S. S., Sumerlin, B. S. & Matyjaszewski, K. Cylindrical molecular brushes: Synthesis, characterization, and properties. *Prog. Polym. Sci.* **33,** 759–785 (2008).

CHAPTER 2

SYNTHESIS AND STABILITY OF pAA-*g*-PEG'S

Following the hypothesis that the lubrication ability of lubricin is tied to its structure, a library of polymers was synthesized to replicate lubricin's brush-like structure. In particular, the long protein backbone, hydrophilic oligosaccharide side chains and C-terminus binding site were mimicked through synthetic polymer chemistry. Poly(acrylic acid) (pAA) was chosen to form the backbone of the polymer, the side chains would were be composed of hydrophilic PEG side chains and the C-terminus binding site was a thiol group exposed on one end of the polymer backbone. The main parameters to be investigated were the length of the backbone, length of the PEG side chains, and the density of the PEG side chains. The specific molecular parameters are given in **Table 2.1**. The polymers are synthesized in a two-step process: a) RAFT polymerization of acrylic acid to produce poly(acrylic acid) and b) conjugation of PEG onto pAA using conjugation chemistry to produce poly(acrylic acid)-*graft*-PEG (pAA-*g*-PEG).

In addition, the chemical stability of the polymers was investigated via forced degradation study to better understand what environmental factors pose the greatest hindrance to long-term storage. This stability analysis provides insight to how the polymer might change over time in a formulation and probes its potential shelf-life if it were it to become a medical device.

Table 2.1. Structural molecular parameters for the library of pAA-*g*-PEG

Parameter	**Poly(acrylic acid) $\bar{M}_n$ (g/mol)**	**PEG $\bar{M}_n$ (g/mol)**	**Grafting feed Ratios (PEG/AA)**
Range	60,000 105,000 145,000	2,000 5,000 10,000	2 1 0.5

2.1 Synthesis of the pAA-*g*-PEG library

2.1.1 Introduction

RAFT Polymerization of Acrylic Acid

Poly(acrylic acid) is a very common polyelectrolyte polymer investigated for many purposes either alone or as a formulation component including drug delivery[1–4], dispersants[5,6], and super-absorbent material[7]. This polymer contains carboxylic acids as its functional group which allows for easy post-polymerization modifications and is very useful as a pH responsive material. It's pH responsiveness has been studied for LCST systems[8] and as a hydrogel component[9]. Most importantly its long history of use in biological systems, low toxicity and low immunogenicity makes it a suitable biomaterial for a variety of biomedical uses. Of interest is its hydrophilicty and super-absorbency that makes it's an interesting material to incorporate into a biolubricant; the characteristic of many boundary mode lubricants is the ability to retain water to create a lubricating layer on a surface[10].

Poly(acrylic acid) (pAA) was synthesized via Reversible Addition-Fragmentation Chain Transfer (RAFT) polymerization; an unique free radical polymerization technique developed in 1998 by Rizaardo et al.[11]. This technique requires a RAFT chain transfer agent (CTA) and a free radical initiator to polymerize a given monomer. The RAFT agent provides control and protection for a propagating chain to prevent early termination and rapid monomer conversion (**Fig 2.1**). The important outcome of this method includes more a controlled polymerization and narrower molecular weight distributions compared to conventional free radical polymerization, and it is applicable to a wide range of monomers (especially acid monomers), solvent conditions (includes water) and complex architectures[12]. The RAFT agent can also be chosen to functionalize the end of the polymers, such as utilizing

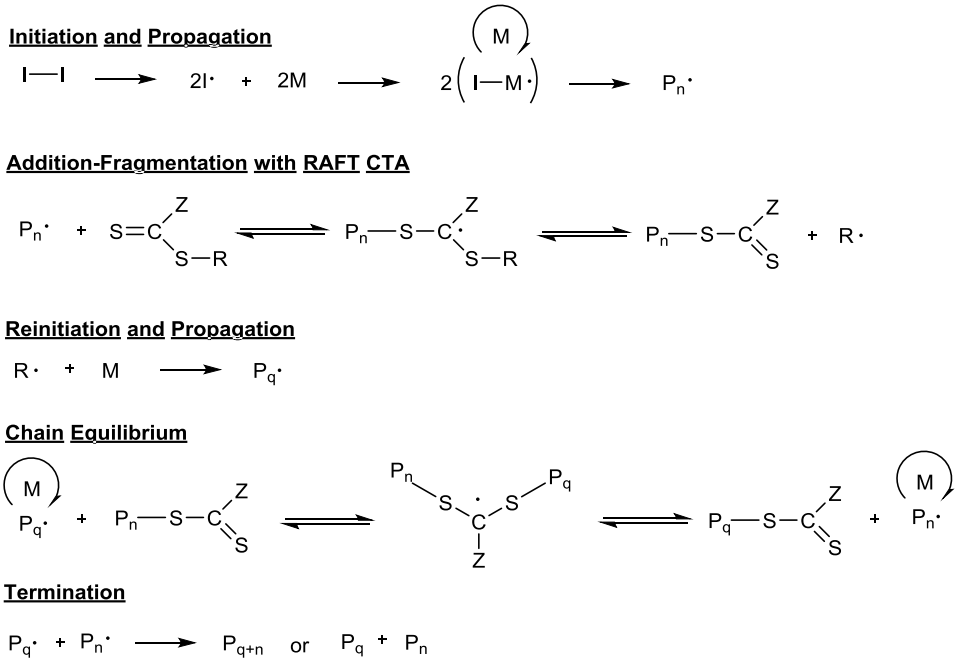

Figure 2.1: RAFT polymerization mechanism. P_n and P_q are polymers; P_n• and P_q• propagating radicals; I is initiator; M is monomer; R and Z are constituent groups dependent on the specific RAFT CTA.

thiocarbonylthio as the RAFT CTA, which can be cleaved to expose a thiol end group allowing for further chemical functionalization.

PEG conjugation via DMTMM activation

PEG has a long history in the biomedical field for its superior biological properties and interactions within the human body[13]. Its unique properties include solubility in water, biocompatibility, lack of immunogenicity and ease of production. It is known that within the human body PEG elicits no adverse immunogenic responses such as macrophage recruitment or inflammatory response. It can increase the circulatory time of nanoscale materials when conjugated to their surface and is good at masking the immunogenic and antigenic effects of peptides, termed in the literature as a "stealth" effect[14]. PEG has also been known to easily clear from the body through renal excretion and does not readily undergo enzymatic degradation. Of particular interest is the high hydrophilicity of PEG, which has been studied extensively for usage as a film component for its lubricating[15,16] and anti-fouling[17,18] properties. PEG with one end or both ends functionalized allows it to be easily conjugated onto substrates to impose biological inertness.

Condensation chemistry is a method of attaching molecules onto a variety of different substrates through activated functional groups such as activated esters from carboxylic acid, making them very reactive to amines or hydroxyls to form an amide or ester bond respectively[19,20]. Many condensing agents have been developed over the years but carbodiimides such as dicyclohexylcarbodiimide (DCC) and N-(3-dimethylaminopropyl)-N'-ethylcarbodiimide (EDC) are some of the most common condensing agents. However, some difficulties in their usage include requiring organic solvents and anhydrous conditions, as well

as complicated purification steps to remove side products. 4-(4,6-Dimethoxy-1,3,5-triazine-2-yl)-4-methylmorpholinium chloride (DMTMM) is a more recently developed condensing agent more recently developed and can perform one-step conjugation of both small and large molecules (**Fig 2.2**). It can be utilized in solvents such as water, alcohols and tetrahydrofuran and so does not require a tightly controlled environment. It has been used successfully in reactions between nucleophilic molecules and polymers[21–23], and successfully with acrylate polymers[24]. DMTMM is useful due to its effectiveness in aqueous and ambient conditions. This is in contrast to the use of carbodiimides such as (DCC) and (EDC) which are more commonly used but may require organic solvents, inert conditions and difficult purification steps[19,25], and hence are not as cost-effective.

2.1.2 Method and Materials

2.1.2.1 Materials

Acrylic acid (AA, 99.5%) stabilized with 200 ppm 4-methoxyphenol, methanol (99.8%) and sodium borate buffer were obtained from VWR (Radnor, PA, USA). 4,4' azobis (4-cyanopentanoic acid) (A-CPA) and 4-cyano-4-(phenylcarbonothioylthio)pentanoic acid (CPA-DB) (>97% HPLC) was obtained from Sigma-Aldrich (St. Louis, MO, USA). Methoxy-poly(ethylene glycol)-amine powder (PEG-NH_2) was obtained from Jenkem Technologies (Beijing, PRC) and 4-(4,6-dimethoxy-1,3,5-triazin-2-yl)-4-methylmorpholinium chloride (DMTMM) was from TCI America (Portland, OR, USA). All chemicals were used as received unless otherwise specified.

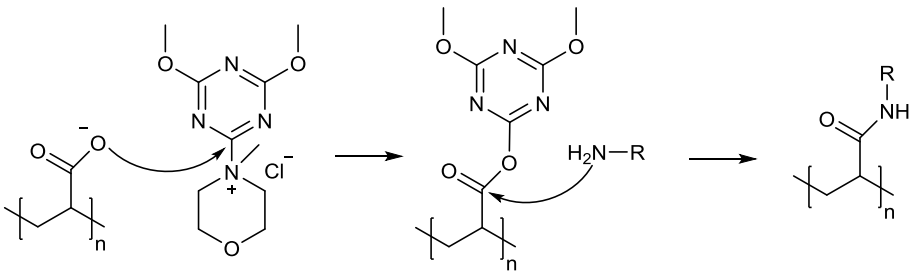

Figure 2.2: DMTMM conjugation mechanism. DMTMM activates carboxylate ion, which is then attacked by primary amine (nucleophile) to form amide bond. R refers to any molecule.

2.1.2.2 Equipment

M_n and polydispersity indices (PDI) for pAA were obtained using a Waters gel permeation chromatography (GPC) system equipped with two Ultrahydrogel™ columns (Waters) in series (500 Å and 250 Å), 1515 isocratic HPLC pump and 2414 refractive index detector with the temperature controlled at 30°C. The mobile phase employed was phosphate buffer saline (pH 7.4) at a rate of 0.8 ml min^{-1} calibrated with poly(methacrylic acid), sodium salt standards. ^{1}H NMR of pAA was performed using an Inova 400 MHz or Inova 600 spectrometer with deuterium oxide (D_2O) as the solvent. Resonances were referenced to HOD at 4.79 ppm.

2.1.2.3 Synthesis and characterization of poly(acrylic acid) backbone (pAA).

Polyacrylic acid was synthesized by RAFT polymerization, as previously reported by our group[26], using acrylic acid (AA), A-CPA as initiator (I) and CPA-DB as chain transfer agent (CTA) under anhydrous, airtight and dark conditions (**Fig 1**). For this study, a scaled up version of the previously reported reaction was developed[26]. The general reaction scheme is as follows: AA (0.95 ml, 13.8mmol) was added to a flame dried 5 ml brown ampule with one flea magnet, to which CPA-DB (5.3 mg, 19 x 10^{-3} mmol) dissolved in 2.9 ml of nitrogen-purged methanol was added, followed by A-CPA (1.3 mg, 4.63 x 10^{-3} mmol) dissolved in 0.7 ml of nitrogen-purged methanol. Nitrogen gas was bubbled through the reaction mixture after addition of each reagent for several minutes to prevent oxygen gas influx. After the last nitrogen purge the reaction ampule was flamed sealed, placed in a 60 ^oC oil bath to initiate polymerization and allowed to stir for 48 hours. Upon reaction completion the ampule neck was broken to expose the reactants to air and the solution cooled in ice to stop the

polymerization. The solution was diluted with 0.01 M NaOH, dialyzed against deionized water for 3 days, with water changes twice daily, and then lyophilized to obtain a white, waxy powder. Characterization: ^{1}H NMR (INOVA 400 MHz, D_2O, ppm): δ1.5-2.0 (pAA-CH_2-), δ 2.25-2.75 (pAA-CH-).

2.1.2.4 Synthesis of pAA-*g*-PEG polymer brushes.

The pAA-*graft*-PEG (pAA-*g*-PEG) copolymer was synthesized by polymer analogous conjugation of monoamine-functionalized PEG to the pAA backbone using DMTMM as the condensing agent based on a procedure reported by our lab[27]. The general reaction is as follows: pAA (107,600 g/mol M_n, 10mg, 139 mmol of AA) and PEG-amine (2000 g/mol M_n, 610 mg, 305 mmol of PEG) were dissolved by stirring in ~0.1 M borate buffer (3 ml, pH 8.5) in a 10 ml flask with magnetic stir bar. DMTMM (79 mg, 285 mmol) dissolved in 0.1 M borate buffer (0.6 ml) was added drop-wise to the solution and the pH adjusted to 6-7 using 1 N HCl. The concentration of pAA was maintained at ~3.3 g/L, assuming corresponding molar ratios of PEG would dissolve at the corresponding volumes, otherwise reaction solutions were maintained at PEG concentrations of 185 g/L. This is due to difficulties of dissolving a high mass of large M_n PEG at certain molar ratios relative to AA monomers while maintaining buffer solution volume relative to pAA concentrations at 3 g/L, this results in trying to dissolve a large mass of PEG in insufficient buffer. As a result instead of maintaining buffer solution volumes relative to pAA at ~3 g/L; it was adjusted in some scenarios to 185 g/L relative to PEG mass. Each conjugation reaction was conducted for 24 hours at room temperature, dialyzed against deionized water for 3 days and lyophilized to obtain a white powder. The assigned nomenclature for the polymer brushes are given as pAA(*a*)-*g*-PEG(*b*),

where *a* and *b* are molecular weights of pAA and PEG respectively, and *g* is the grafting ratio defined by the moles of PEG grafted to the pAA backbone divided by the moles of AA monomers in the pAA backbone.

2.1.3 Results and Discussion

2.1.3.1 RAFT polymerization of AA

pAA was synthesized using 4,4' azobis (cyanopentanoic acid) (A-CPA) and 4-cyanopentanoic acid dithiobenzoate (CPA-DB) as initiator (I) and CTA respectively. The kinetics of this combination of initiator and CTA on acid acrylate polymerization has been well characterized previously by Pelet[26,28] formerly of the Putnam Lab. The reaction scheme is given in. **Fig 2.3.**

Employing the kinetic results from Pelet's previous work, we scaled-up the reaction volume by ~1.6 times while maintaining all other reaction conditions the same. This was done to produce a larger quantity of pAA from each to eliminate experimental error; as well as to help determine potential challenges with future industrial scale-ups of pAA synthesis. Initiator:CTA ratios were maintained at 0.25 in all reactions, while the AA concentrations were varied relative to CTA. The results are given in **Table 2**, we chose the molecular weights of 60, 105 and 145 kDa specifically because their contour lengths are approximiately 0.6, 1, and 1.5 times respectively the hydrodynamic size of lubricin[29]. This allowed a range of polymer backbone lengths to be explored in this study.

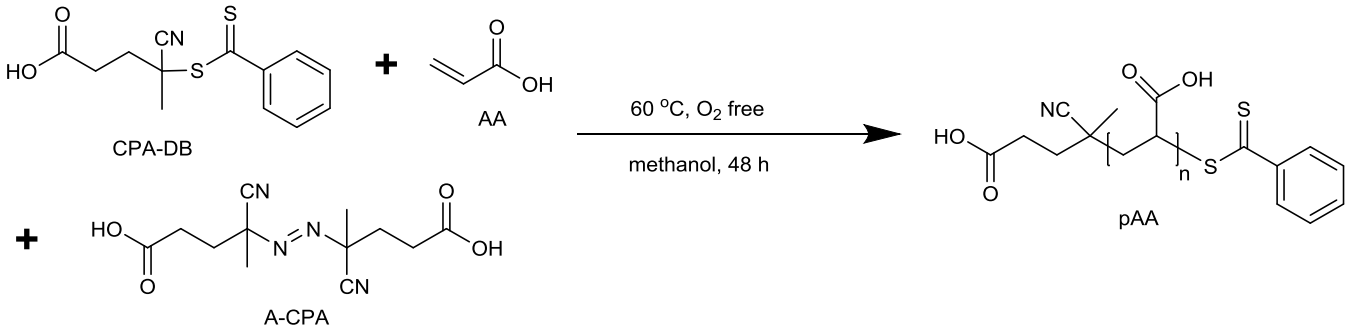

Figure 2.3: Synthesis schematic of poly(acrylic acid) (pAA) by RAFT polymerization

Table 2.2. Molecular weights of synthesized pAA[a]. Includes theoretical and sample experimental values

Concentration of AA (M)	**[AA]:[CTA]**	**Theoretical M_n (g/mol)**	**Experimental M_n[b,c] (g/mol) (GPC)**	**Polydispersity (PDI)[b]**
3	762	60,000	61,700	1.34
5	1259	105,000	104,200	1.31
8	2509	145,000	145,600	1.28

[a] RAFT polymerization of AA were conducted in methanol @ 60^{o}C, while maintaining [I]:[CTA]=0.25 under airtight, oxygen-free conditions and varying [AA] and [AA]:[CTA].

[b] Determined by gel permeation chromatography (GPC)

[c] Author determined it acceptable if within 5% of theoretical molecular weight.

To achieve molecular weights greater than M_n 100,000 with acceptable PDIs (i.e., ≤1.35), AA concentrations greater than 3 M were required to avoid deviations from the theoretical M_n (**Table 2.2**). This is likely from the high concentration of AA required to reach higher molecular weights combined with the low [CTA]. This combination of reaction scale-up with the synthesis of high M_n pAA may also explain the higher PDI (>1.3) relative to our previously reported work. It is likely that to achieve even higher molecular weights (M_n 200,000 or greater) with narrow PDI's, even higher monomer concentrations along with modified reaction conditions will be necessary.

2.1.3.2 PEG conjugation

PEG was grafted onto pAA via condensation chemistry. Condensation chemistry involves the reaction of the carboxylate groups such as the carboxylic acids of pAA with a condensing agent forming activated esters. This activated ester is very reactive to nucleophiles; readily forming stable ester or amide bonds. 4-(4,6-Dimethoxy-1,3,5-triazine-2-yl)-4-methylmorpholinium chloride (DMTMM) is one such condensing agent that allows one-step condensation reactions between nucleophilic molecules and polymers[21–23], and successfully with acrylate polymers[24]. DMTMM is useful due to its effectiveness in aqueous and ambient conditions. This is in contrast to the use of carbodiimides such as dicyclohexyl carbodiimide (DCC) and N-(3-dimethylaminopropyl)-N'-ethylcarbodiimide (EDC) which are more commonly used but may require organic solvents, inert conditions and difficult purification steps[19,25], hence ar not as cost-effective.

The reagents used in this condensation reaction were methoxy-PEG-amine, pAA and DMTMM in an aqueous borate buffer. The reaction scheme is given in **Fig. 2.4**. The reaction

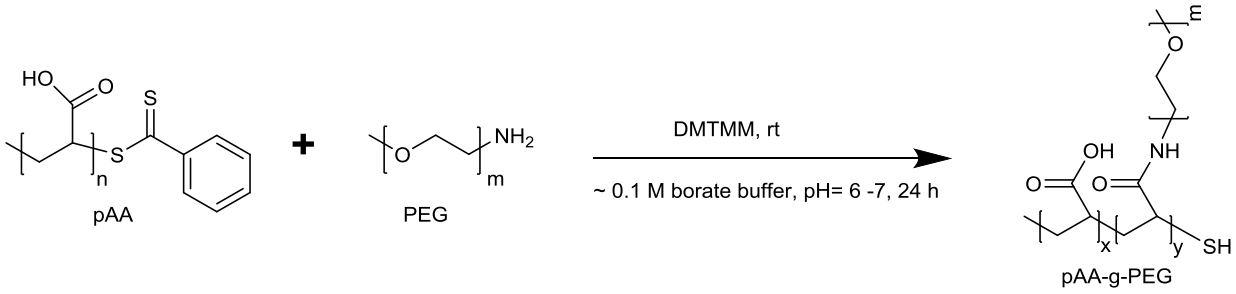

Figure 2.4: Grafting of PEG onto pAA using DMTMM condensing agent

conditions for efficient conjugation of primary amines onto acrylate polymers using DMTMM was characterized previously in our lab by Pelet[27]. The reaction was performed in ~0.1M borate buffer with pH adjusted to 6-7. The grafting ratios was defined as the moles of PEG to moles of AA monomer in pAA (PEG:AA). PEG:AA was varied in each reaction while maintaining DMTMM:PEG ratios at 1:1 under ambient conditions. During the reaction the thiocarbonylthio end groups of the pAA would be cleaved to expose a free thiol, a common occurrence in the presence of nucleophiles, such as primary amines[30]. Unreacted reagents and the DMTMM byproduct N-methylmorpholine (NMM)[23] were removed by water dialysis and product was then lyophilized. The resulting poly(acrylic acid)-*graft*-PEG (pAA-*g*-PEG) consisted of a hydrocarbon backbone with varying ratios of PEG to carboxylic acid side chains and a thiol terminus. **Table 2.3** lists the entire combinatorial library of pAA-*g*-PEG that was synthesized. The assigned nomenclature for the polymer brushes are given as pAA(*a*)-*g*-PEG(*b*), where *a* and *b* are molecular weights of pAA and PEG respectively, and *g* is the grafting ratio defined by the moles of PEG grafted to the pAA backbone divided by the moles of AA monomers in the pAA backbone. **Fig 2.5**, shows ^{1}H NMR spectra of pAA and pAA(60)-0.5-PEG(2) as examples.

2.1.4 Conclusions

A library of polymer brushes pAA-*g*-PEG was successfully synthesized to mimic the structure of lubricin and help to determine lubrication as a function of structure. The polymerization of pAA using RAFT agents allowed well-controlled production of high molecular weight pAA with low PDI's; and the DMTMM conjugation of PEG to pAA was a simple, inexpensive reaction under ambient, aqueous conditions. This two-step synthetic

scheme was designed to allow for inexpensive production of large quantities of the hydrophilic polymer brush, pAA-*g*-PEG, for potential use as a biolubricant. Conjugation of the higher PEG molecular weights (5,000/10,000 g/mol) was more difficult due to requiring a larger mass of PEG at the same grafting ratios (1:1, 1:2) than the smaller PEG (2,000 g/mol). In addition, the solubility of the resulting polymers were not identical (See **Appendix**) especially the pAA-*g*-PEG's utilizing pAA with molecular weight 105,000 g/mol or greater and PEG 5,000 g/mol or greater, many of these were insoluble in aqueous solvents after lyophilization possibly due to unintentionally physical cross-linking due to their sizes.

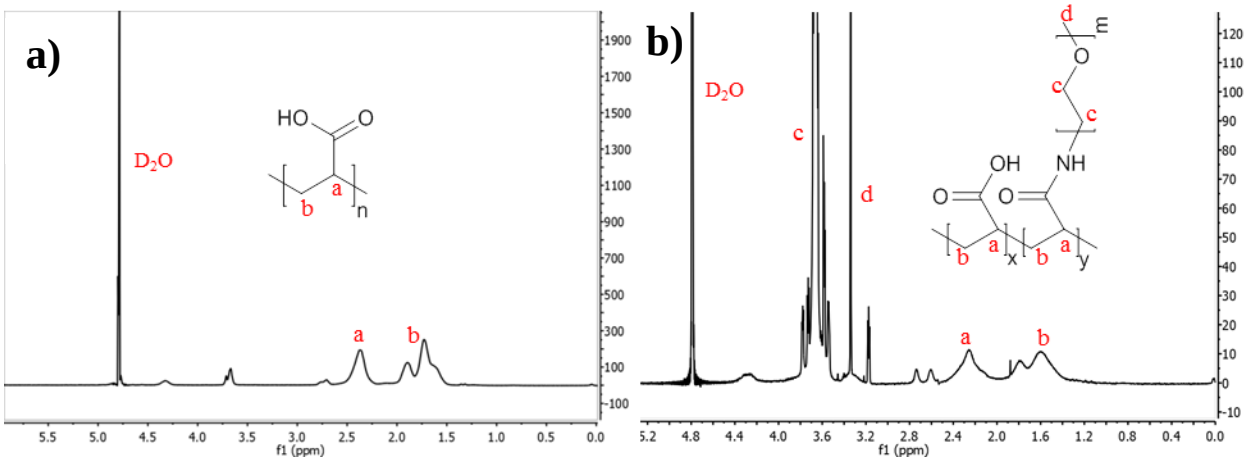

Figure 2.5: ^{1}H NMR of **a)** 60 kDa pAA in D_2O, a and b corresponds to the pAA backbone carbons at ~1.6 and ~2.3 ppm respectively. A double peak at 3.5-3.6 ppm corresponds to methylation of carboxyl group from methanol solvent (~<15%). A peak at 2.8 ppm and 4.2 ppm may be related to dimerization of acrylic acid before polymerization(<7%), which retains carboxylic acid functionality albeit with slight extension from backbone. **B)** pAA(60)-0.5-PEG(2) in D_2O. c corresponds to the PEG hydrogens at ~3.5 ppm and d corresponds to PEG methoxy protons while the pAA backbone hydrogens are also present.

Table 2.3. Table of pAA-*g*-PEG polymer brushes[a]

Nomenclature[b]	pAA backbone (g/mol)[c]	MW of PEG side chains (g/mol)	PEG:AA grafting ratio[d]
pAA(145)-2-PEG(10)	145000	10000	2
pAA(145)-1-PEG(10)	145000	10000	1
pAA(145)-0.5-PEG(10)	145000	10000	0.5
pAA(145)-2-PEG(5)	145000	5000	2
pAA(145)-1-PEG(5)	145000	5000	1
pAA(145)-0.5-PEG(5)	145000	5000	0.5
pAA(145)-2-PEG(2)	145000	2000	2
pAA(145)-1-PEG(2)	145000	2000	1
pAA(145)-0.5-PEG(2)	145000	2000	0.5
pAA(105)-2-PEG(10)	105000	10000	2
pAA(105)-1-PEG(10)	105000	10000	1
pAA(105)-0.5-PEG(10)	105000	10000	0.5
pAA(105)-2-PEG(5)	105000	5000	2
pAA(105)-1-PEG(5)	105000	5000	1
pAA(105)-0.5-PEG(5)	105000	5000	0.5
pAA(105)-2-PEG(2)	105000	2000	2
pAA(105)-1-PEG(2)	105000	2000	1
pAA(105)-0.5-PEG(2)	105000	2000	0.5
pAA(60)-2-PEG(10)	60000	10000	2
pAA(60)-1-PEG(10)	60000	10000	1
pAA(60)-0.5-PEG(10)	60000	10000	0.5
pAA(60)-2-PEG(5)	60000	5000	2
pAA(60)-1-PEG(5)	60000	5000	1
pAA(60)-0.5-PEG(5)	60000	5000	0.5
pAA(60)-2-PEG(2)	60000	2000	2
pAA(60)-1-PEG(2)	60000	2000	1
pAA(60)-0.5-PEG(2)	60000	2000	0.5

[a] Reactions were conducted at room temperature in ~0.1 M borate buffer for 24 hours; pH adjusted to between 6-7.

2.2 Forced degradation

2.2.1 Introduction

Many pharmaceuticals are typically stored for prolonged periods of time prior to use and can be subjected to a variety of environmental stressors that may adversely affect their safety and efficacy. In particular, the FDA requires stability testing on pharmaceuticals before they can be approved for clinical use. This process can help determine the proper formulation to maximize shelf life. Typically, mandatory long-term stability studies following ICH guidelines would take at least 12 months while accelerated stability studies would be 6 months[31]. The stability tests would help determine what degradation products would form as a result of the formulation and environment stressors. Forced degradation studies on the other hand can allow the development of degradation products in a matter of weeks to allow their rapid identification[32]. Forced degradation of drug or drug products utilizes conditions that are even more severe than accelerated stability tests, such as highly acidic conditions or elevated temperatures, in an effort to decompose the drug or drug substance. The data developed from forced degradation studies can be utilized to develop and analyze much longer stability tests. In essence, forced degradation provides an initial insight into the drug or drug product stability via its degradation products.

Herein, we report the forced degradation of pAA-*g*-PEG and its pure polymer components to determine their initial degradation products. In this particular case, pAA-*g*-PEG would be used as a biolubricant dissolved in an aqueous solution and ideally stored in the same way. Forced degradation studies are performed based prototype formulations of the drug or drug substance in either the solid or liquid state[32,33]. The prototype formulation of pAA-*g*-PEG would in solution, therefore the main stressors to be investigated are oxidative

and hydrolytic in nature[33], and would focus on what products would form as a result of forced oxidation or forced hydrolysis. This information can be useful, to refine the formulation depending on what environmental stressors may degrade the material.

From among the polymer library, pAA(60)-2-PEG(2) and its independent polymer components were chosen for this forced degradation study. Since the chemical composition was the same throughout the library with the only variance being the size of the polymer components, pAA(60)-2-PEG(2) can be assumed to be a representative material. Two polymers tested in addition to pAA(60)-2-PEG(2) are pAA ($\bar{M}_n$ 60,000 g/mol) and methoxy-PEG-amine (PEG) ($\bar{M}_n$ 2,000 g/mol).

2.2.2 Materials and Methods

2.2.2.1 Materials

pAA(60)-2-PEG(2), 60000 g/mol ($\bar{M}_n$) pAA were synthesized as described in section 2.1. Methoxy-poly(ethylene glycol)-amine powder (PEG-NH_2) was obtained from JenKem Technologies (Beijing, PRC). Hydrogen peroxide (30%), HCl (10 N) and NaOH (10 N) was purchased from the Cornell University Chemical stockroom (Ithaca, NY, USA) and each diluted with deionized (DI) water to form 3% hydrogen peroxide, 0.1 N HCl and 0.1 N NaOH. 1X and 10X phosphate buffered saline solution (PBS) was purchased from VWR ((Radnor, PA, USA). PD10 columns were purchased from GE Healthcare Life Sciences (Pittsburge, PA, USA).

2.2.2.2 Equipment

M_n and polydispersity indices (PDI) for pAA were obtained using a Waters gel permeation chromatography (GPC) system equipped with two Ultrahydrogel™ columns, 1515 isocratic HPLC pump and 2414 refractive index detector with the temperature controlled at 30°C. The mobile phase employed was phosphate buffered saline (pH 7.4) at a rate of 0.8 ml min^{-1} calibrated with poly(methacrylic acid), sodium salt standards. ^{1}H NMR was performed using an Inova 600 MHz spectrometer with deuterium oxide (D_2O) as the solvent.

2.2.2.3 Forced Oxidation

Either pAA, PEG or pAA(60)-2-PEG(2) were dissolved in 1X PBS with 3% hydrogen peroxide at 3 mg/ml at room temperature to induce oxidation. Samples were drawn at 6 hours, 3 days, and 7 days and then lyophilized. Degradation was quantitatively analyzed using ^{1}H NMR of the unaltered time point samples in D_2O at 10 mg/ml. For GPC analysis, the time samples were desalted through a PD10 column to remove PBS salts, lyophilized, and then dissolved in GPS PBS mobile phase before injection.

2.2.2.4 Forced Hydrolysis

Either pAA, PEG or pAA(60)-2-PEG(2) were dissolved in 0.1 N HCl or 0.1 N NaOH at 3 mg/ml and reacted at 40^{o}C under reflux with cold water. Samples were drawn at 6 hours, 3 days, and 7 days, neutralized and then lyophilized. Degradation was quantitatively analyzed using ^{1}H NMR in D_2O at 10 mg/ml. For GPC analysis, the time point samples were dissolved in GPC PBS mobile phase before injection.

2.2.3 Results and discussion

2.2.3.1 Forced Oxidation

The forced oxidation experiments took place in PBS with 3% hydrogen peroxide to control for pH (7.4). Unfortunately, the residual PBS salts made analysis more problematic as they would create negative GPC baseline peaks and had to be removed before running the samples. To accomplish the salt removel, the samples in PBS had to be run through a PD10 desalting column to remove only the PBS salts. For ^{1}H NMR analysis no desalting took place as it could have potentially removed degradation products of interest.

Utilizing ^{1}H NMR, both PEG and pAA(60)-2-PEG(2) demonstrated chemical changes and degradation products under oxidative conditions up to 7 days. They evolved the same peaks near the same range of chemical shifts since PEG is the only component appearing to oxidize. For brevity only the pAA(60)-2-PEG(2) ^{1}H NMR's are shown in **Fig 2.6**, here the samples begin to evolve new peaks around 4.2-4.5 ppm beginning on the third day of oxidation and become more pronounced by the seventh day. These peaks are relatively broad and can range in number from 1-3 separate peaks in the same vicinity. Pure pAA(60)-2-PEG(2) and PEG have similar spectra due to the preponderance of PEG in the polymer brush and both evolve similar degradation peaks in their spectra. No changes to pAA were observed through ^{1}H NMR (data not shown), suggesting that the PEG component of pAA(60)-2-PEG(2) is the only component susceptible to degradation.

Several potential degradation products of PEG are shown in **Fig 2.7.** These are based on an oxidation study done on much smaller PEG's (400 g/mol)[34] containing hydroxyl end groups; known reactions that occur on tetrahydrofuran (THF), an alkane with an ether

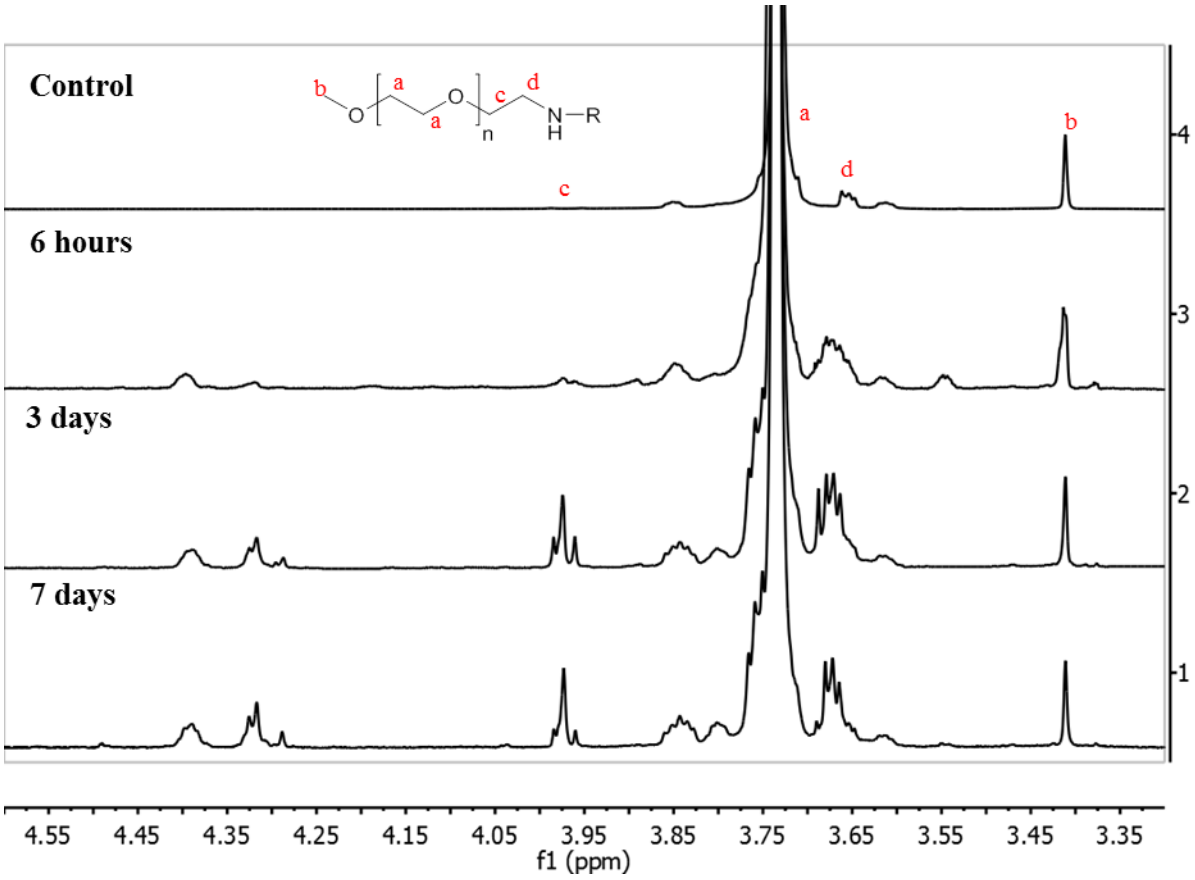

Figure 2.6: ^{1}H NMR of the oxidation of pAA(60)-2-PEG(2) in 3% hydrogen peroxide PBS over 7 days. PEG peaks are at 3.4 ppm (-OC**H**$_3$), 3.68 (-O-CH$_2$-C**H**$_2$-NH-), 3.72-3.9 ppm (-O-C**H**$_2$-C**H**$_2$-O-), 3.98 (O-C**H**$_2$-CH$_2$-NH-), **R** corresponds to pAA backbone. Peaks corresponding to oxidation are around 4.2-.4.4 ppm and steadily increase over 7 days. Oxidation of PEG ($\bar{M}_n$ 2000 g/mol) evolve peaks at the same chemical shifts. Peaks scaled for viewing of oxidation peaks hence c is not clear in control pAA(60)-2-PEG(2).

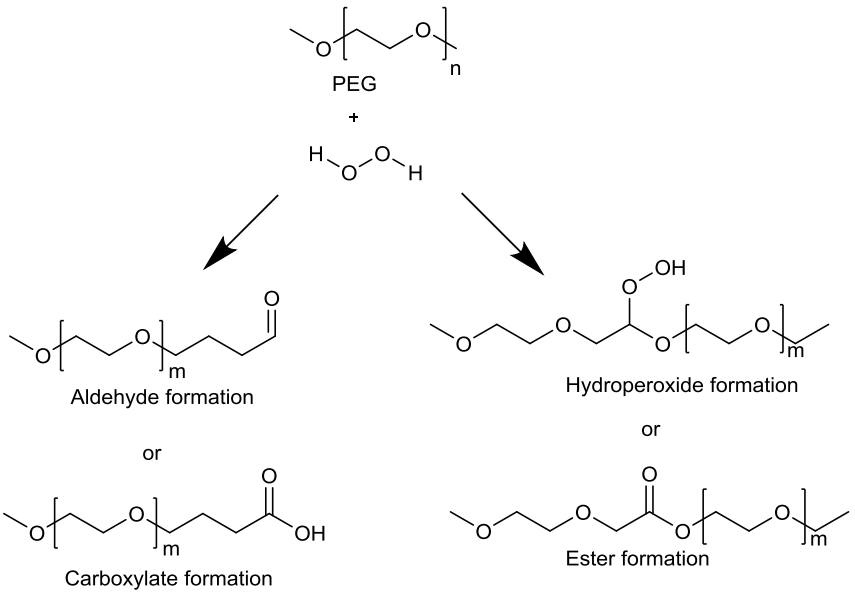

Figure 2.7: Potential oxidation products of PEG in 3% hydrogen peroxide over time as determined by prediction ^{1}H NMR.

group[35]; and predictive NMR. Specifically, the peroxide can create a carboxylate or aldehyde on the PEG chains. The peroxides can also attach to a carbon adjacent to oxygen on PEG and form a hydroperoxide or ester, both of which deshield the nearby protons and increase their chemical shifts.

While the % degradation cannot be confirmed without determining the exact degradation structure(s), the peak ratios can nonetheless be analyzed to confirm degradation changes over time. To do this, the degradation peaks existing around 4.2-4.5 ppm where integrated and divided by the methyl singlet peak near 3.4 ppm; this methyl peak corresponds to the end group of PEG and is relatively stable. The graphs of peak ratios versus time of both PEG and pAA(60)-2-PEG(2) are given in **Fig. 2.8**. Both demonstrated a reaction that occurs linearly over the time period investigated. This implies a continuous rate of oxdiation and that no observed plateau, indicating incomplete oxidation of the materials.

The GPC traces (**Fig. 2.9**) also demonstrate a slight broadening over time and a small shift to the right in the chromograph, suggesting either cleavage of PEG chains, cross-linking or some other alteration to their excluded volumes caused by oxidation. GPC traces for pAA(60)-2-PEG(2) could not be properly obtained due to the large size of the polymer and difficulties filtering it. The pAA traces showed maintained their general shape and show no noticeable broadening or narrowing; further confirming that pAA did not oxidize in this study.

2.2.3.2 Forced Hydrolysis

The forced hydrolysis of pAA, PEG and pAA(60)-2-PEG(2) yield no noticeable changes over the seven days of the experiments. Neither 0.1 N HCl or 0.1 N NaOH caused any identifiable

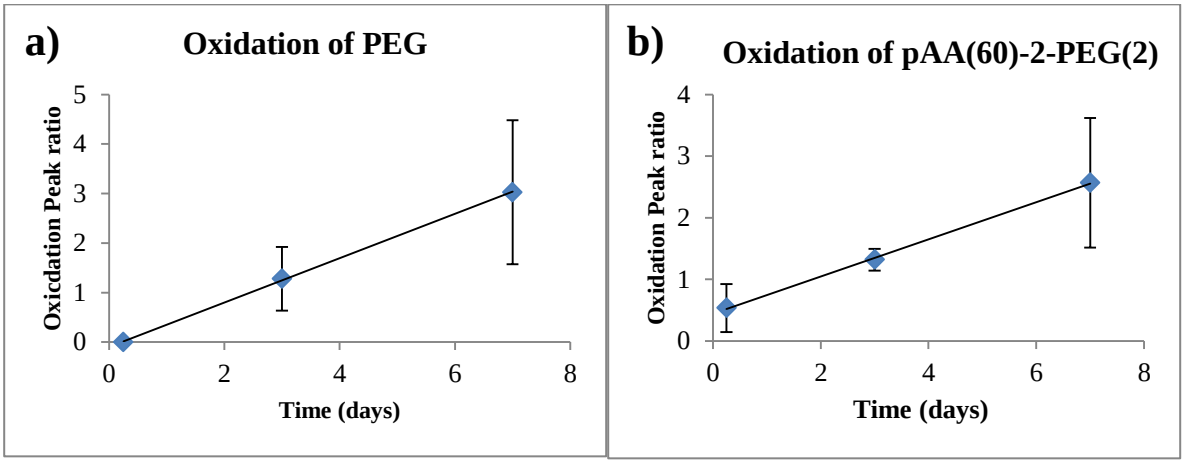

Figure 2.8: Ratio of ^{1}H NMR oxidation peaks to PEG methyl peak versus time for **a)** PEG (n=3) and **b)** pAA(60)-2-PEG(2) (n=3). The oxidation peaks (4.2-4.5 ppm) were integrated and divided by the integration of the PEG methyl peak (3.3-3.45 ppm). The methyl end group of the PEG is a very stable, and produces a strong singlet in NMR making it an ideal reference peak. The graphs suggest a continuous rate of oxidation.

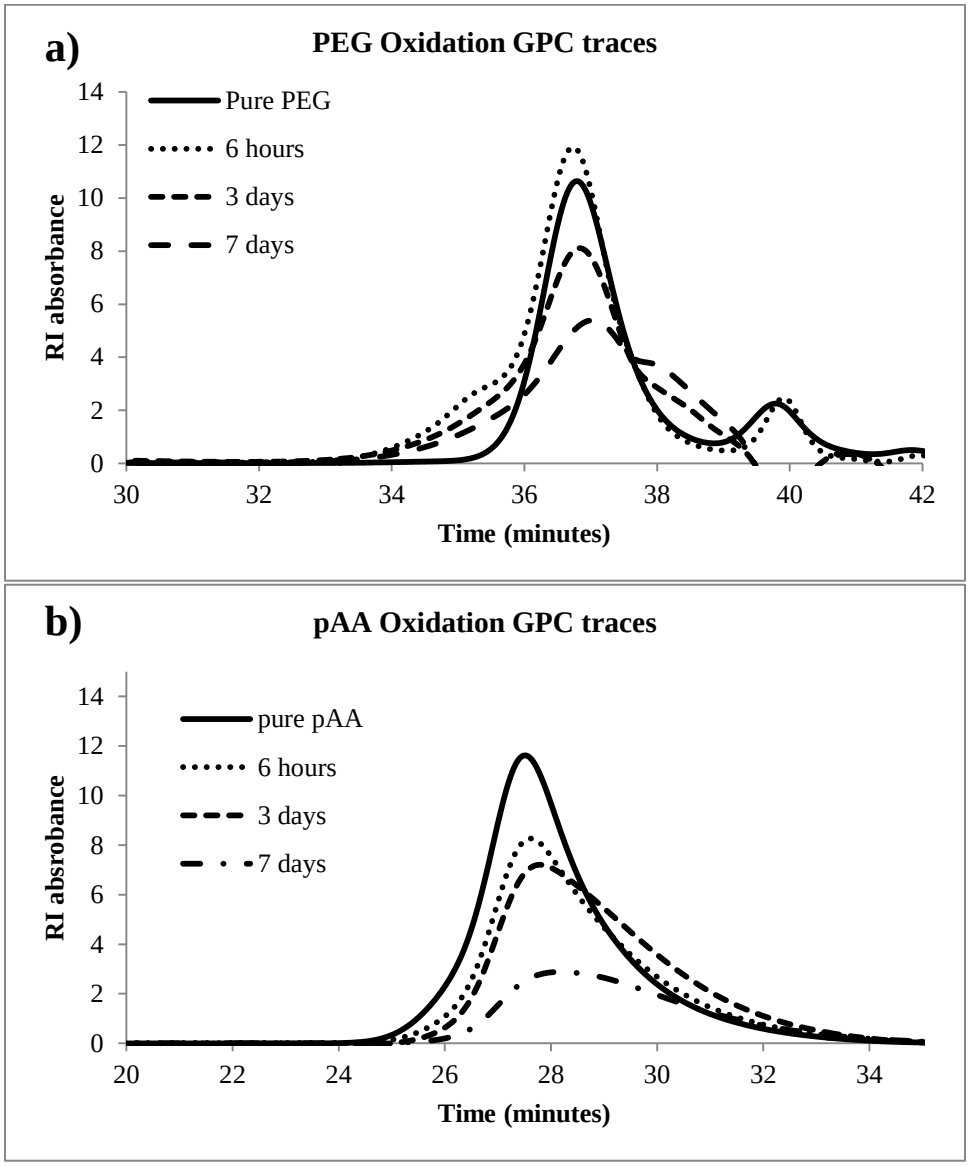

Figure 2.9: GPC traces of **a)** PEG and **b)** pAA oxidation time samples. A slight broadening of the traces occurs over time for PEG but pAA appears to maintain the general shape and location of the traces.

changes in the ^{1}H NMR spectra of the polymer involved (data not shown). In addition the GPC traces of the pAA or PEG samples were identical to their negative controls.

2.2.4 Conclusions

The forced degradation experiment of pAA(60)-2-PEG(2) demonstrated that oxidation is the main route of degradation in these studies. The PEG chains are the main reactants to hydrogen peroxide and the rate of oxidation follows a linear relationship or first-order trend. Hydrolysis by either 0.1 N HCl or 0.1 N NaOH did not occur on any of the polymers investigated and demonstrated no changes. GPC was utilized in this study to analyze the samples but is limited by solvent selection – a better approach may be to apply high pressure liquid chromatography (HPLC) to better separate out the constituents without the need for desalting columns.

2.3 References

1. Yuk, S., Cho, S. & Lee, H. pH-sensitive drug delivery system using OW emulsion. *J. Control. release* **37,** 69–74 (1995).

2. Lele, B. S. & Hoffman, a S. Mucoadhesive drug carriers based on complexes of poly(acrylic acid) and PEGylated drugs having hydrolysable PEG-anhydride-drug linkages. *J. Control. Release* **69,** 237–48 (2000).

3. Topuzogullari, M. *et al.* Conjugation, characterization and toxicity of lipophosphoglycan-polyacrylic acid conjugate for vaccination against leishmaniasis. *J. Biomed. Sci.* **20,** 35 (2013).

4. Vernon, B., Kim, S. W. & Bae, Y. H. Insulin release from islets of Langerhans entrapped in a poly(N-isopropylacrylamide-co-acrylic acid) polymer gel. *J. Biomater. Sci. Polym. Ed.* **10,** 183–198 (1999).

5. Loiseau, J. *et al.* Synthesis and characterization of poly (acrylic acid) produced by RAFT polymerization. Application as a very efficient dispersant of CaCO3, kaolin, and TiO2. *Macromolecules* **36,** 3066–3077 (2003).

6. Whitby, C. P. *et al.* PAA/PEO comb polymer effects on rheological properties and inter-particle forces in aqueous silica suspensions. *J. Colloid Interface Sci.* **262,** 274–81 (2003).

7. Zohuriaan-mehr, M. J. & Kabiri, K. Superabsorbent Polymer Materials: A Review. *Iran. Polym. J.* **17,** 451–477 (2008).

8. Lu, X., Hu, Z. & Schwartz, J. Phase Transition Behavior of Hydroxypropylcellulose under Interpolymer Complexation with Poly(acrylic acid). *Macromolecules* **35,** 9164–9168 (2002).

9. Philippova, O., Hourdet, D., Audebert, R. & Khokhlov, A. R. pH-responsive gels of hydrophobically modified poly (acrylic acid). *Macromolecules* **30,** 8278–8285 (1997).

10. Lee, S. & Spencer, N. D. Materials science. Sweet, hairy, soft, and slippery. *Science* **319,** 575–6 (2008).

11. Chiefari, J. *et al.* Living Free-Radical Polymerization by Reversible Addition - Fragmentation Chain Transfer : The RAFT Process We wish to report a new living free-radical polymer- ization of exceptional effectiveness and versatility . 1 The living character is conferred by . **9297,** 5559–5562 (1998).

12. Chong, Y., Le, T. & Moad, G. A more versatile route to block copolymers and other polymers of complex architecture by living radical polymerization: the RAFT process. *Macromolecules* 2071–2074 (1999). at <http://pubs.acs.org/doi/pdf/10.1021/ma981472p>

13. Veronese, F. M. & Mero, A. The Impact of PEGylation on Biological Therapies. *BioDrugs* **22,** 315–329 (2008).

14. Knop, K., Hoogenboom, R., Fischer, D. & Schubert, U. S. Poly(ethylene glycol) in drug delivery: pros and cons as well as potential alternatives. *Angew. Chem. Int. Ed. Engl.* **49,** 6288–308 (2010).

15. Perry, S. S. *et al.* Tribological properties of poly(L-lysine)-graft-poly(ethylene glycol) films: influence of polymer architecture and adsorbed conformation. *ACS Appl. Mater. Interfaces* **1,** 1224–30 (2009).

16. Lee, S. & Spencer, N. D. Aqueous lubrication of polymers: Influence of surface modification. *Tribol. Int.* **38,** 922–930 (2005).

17. Xu, F. J. *et al.* Spatially well-defined binary brushes of poly(ethylene glycol)s for micropatterning of active proteins on anti-fouling surfaces. *Biosens. Bioelectron.* **24,** 779–86 (2008).

18. Bergstrand, A., Rahmani-Monfared, G., Ostlund, A., Nydén, M. & Holmberg, K. Comparison of PEI-PEG and PLL-PEG copolymer coatings on the prevention of protein fouling. *J. Biomed. Mater. Res. A* **88,** 608–15 (2009).

19. Montalbetti, C. a. G. N. & Falque, V. Amide bond formation and peptide coupling. *Tetrahedron* **61,** 10827–10852 (2005).

20. Hermanson, G. T. *Bioconjugate Techniques*. 219–223 (Academic Press, 2008).

21. Kunishima, M., Kawachi, C., Hioki, K., Terao, K. & Tani, S. Formation of carboxamides by direct condensation of carboxylic acids and amines in alcohols using a new alcohol- and water-soluble condensing agent: DMT-MM. *Tetrahedron* **57,** 1551–1558 (2001).

22. Kunishima, M., Kawachi, C., Iwasaki, F., Terao, K. & Tani, S. Synthesis and characterization of 4-(4, 6-dimethoxy-1, 3, 5-triazin-2-yl)-4-methylmorpholinium chloride. *Tetrahedron Lett.* **40,** 5327–5330 (1999).

23. Kunishima, M., Kawachi, C., Monta, J. & Terao, K. 4-(4, 6-dimethoxy-1, 3, 5-triazin-2-yl)-4-methyl-morpholinium chloride: an efficient condensing agent leading to the formation of amides and esters. *Tetrahedron* **55,** 13159–13170 (1999).

24. Thompson, K. & Michielsen, S. Novel synthesis of N-substituted polyacrylamides: Derivatization of poly(acrylic acid) with amines using a triazine-based condensing reagent. *J. Polym. Sci. Part A Polym. Chem.* **44,** 126–136 (2006).

25. Hermanson, G. T. *Bioconjugate Techniques*. (Elsevier, 2008).

26. Pelet, J. M. & Putnam, D. Poly(acrylic acid) Undergoes Partial Esterification During RAFT Synthesis in Methanol and Interchain Disulfide Bridging Upon NaOH Treatment. *Macromol. Chem. Phys.* **213,** 2536–2540 (2012).

27. Pelet, J. M. & Putnam, D. An in-depth analysis of polymer-analogous conjugation using DMTMM. *Bioconjug. Chem.* **22,** 329–37 (2011).

28. Pelet, J. M. & Putnam, D. High Molecular Weight Poly(methacrylic acid) with Narrow Polydispersity by RAFT Polymerization. *Macromolecules* **42,** 1494–1499 (2009).

29. Swann, D., Silver, F., Slayter, H., Stafford, W. & Shore, E. The molecular structure and lubricating activity of lubricin isolated from bovine and human synovial fluids. *Biochem. J* **225,** 195–201 (1985).

30. Chong, Y., Moad, G., Rizzardo, E. & Thang, S. Thiocarbonylthio end group removal from RAFT-synthesized polymers by radical-induced reduction. *Macromolecules* 4446–4455 (2007). at <http://pubs.acs.org/doi/abs/10.1021/ma062919u>

31. Services, H. Guidance for Industry of New Drug Substances and Products Guidance for Industry Q1A (R2) Stability Testing of New Drug Substances and Products. Available from <http://www.fda.gov/downloads/drugs/guidancecomplianceregulatoryinformation/guidances/ucm073369. (2003).

32. Blessy, M., Patel, R. D., Prajapati, P. N. & Agrawal, Y. K. Development of forced degradation and stability indicating studies of drugs—A review. *J. Pharm. Anal.* 1–7 (2013). doi:10.1016/j.jpha.2013.09.003

33. Hotha, K. K., Reddy, S. P. K., Raju, V. K. & Ravindranath, L. K. Forced Degradation Studies: Practical Approach - Overview of Regulatory Guidance and Literature for the Drug Products and Drug Substances. *Int. Res. J. Pharm.* **4,** 78–85 (2013).

34. Hemenway, J. N. *et al.* Formation of Reactive Impurities in Aqueous and Neat Polyethylene Glycol 400 and Effects of Antioxidants and Oxidation Inducers. *J. Pharm. Sci.* **101,** 17–20 (2012).

35. Robertson, A. Tetrahydrofuran Hydroperoxide. *Nature* **162,** 153–153 (1948).

CHAPTER 3

NOVEL CHARACTERIZATION METHOD FOR pAA-*g*-PEG's

3.1 Introduction

Polymer brushes are an ever expanding field of study with studies potential applications including surface coatings for their anti-adhesive[1–4], anti-microbial[2,5–8], lubricanting[9–11] and solution dispersing[12] properties. However, a major hurdle in understanding polymer brushes involves the proper and detailed characterization of their structure. A polymer brush is composed of a relatively long polymer backbone with polymer side chains creating a "hairy" brush-like structure. The structure may be composed of varying molecular weights of backbone and side chains, different side chain densities and different side chain polymers. The result may be a structure of indeterminate parameters depending on the method of synthesis.

In general, polymer brushes may be prepared via "grafting through", "grafting onto" and "grafting from" (**Fig 3.1**). A more thorough description of polymer brush synthesis techniques can be found in a review article by Sheiko et al.[13] "Grafting through" involves polymerization of macromonomers that themselves are oligomers or polymers such as the polymerization of poly(ethylene glycol) methyl ether acrylate (PEGMA) by ATRP[14] or the copolymerization of methylacrylic acid (MAA) and PEGMA[15]. "Grafting onto", involves a linear polymer with functional groups such as carboxylic acids conjugated with telechelic polymers. The polymers can be prepared independently. These telechelic polymers become side chains on the linear polymer, examples includes PLL-*g*-PEG[16] and PLL-*g*-dex[17] by Spencer et al. "Grafting from", relies on utilizing a polymer backbone whose functional groups can serve as initiation sites for monomers allowing the growth of side chains directly

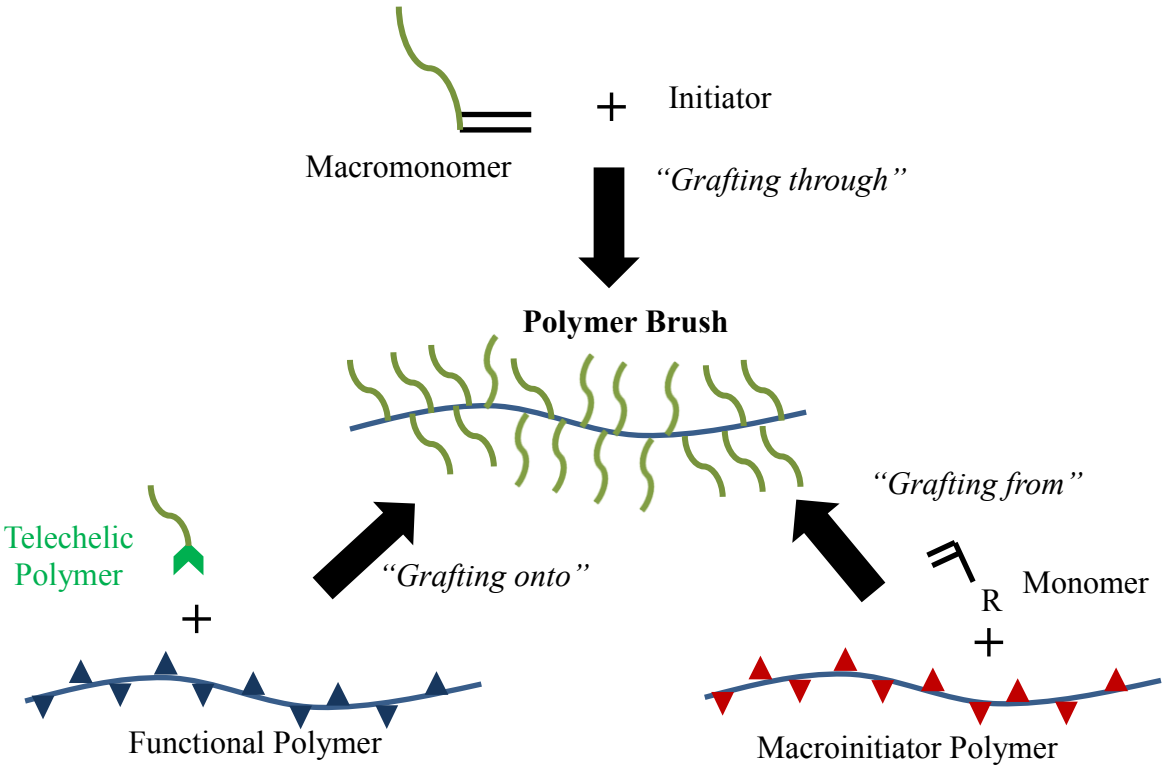

Figure 3.1: Three general synthetic schemes to produce polymer brushes.

from the backbone; polymerization methods include anionic[18] and atom transfer radical polymerization (ATRP)[19,20].

The synthesis techniques may determine the ease through which the polymer may be characterized. In "grafting through", the monomer/side chain molecular weights are well defined but high degree of polymerization may be difficult to achieve. The structure may be characterized simply by determining % conversion of monomers. If more than one monomer, the reactivity's may affect the degree of polymerization and enhance the difficulty of characterization. "Grafting from" utilizes the polymer backbone as initiation sites for polymerization of monomers to create side chains, this leads to well defined molecular weights for the backbone and side chains, but is limited by effectiveness of side chain initiation. Hence the side chain density may be difficult to quantify. "Grafting onto", involves both premade polymer backbones and side chains with corresponding reactive moieties allowing them to conjugate together. This method allows predetermined polymer molecular weights but is limited by the conjugation efficiency of the side chains onto the backbone.

Polymers brushes, especially made using "grafting from" and "grafting onto" techniques, may have varying side chain densities compared to grafting through which tend to have 100% side chain densities for homopolymers. This density variation leads to difficulties in determining both molecular weight and packing densities of the polymer brushes. In fact, the inability to characterize the molecular weights of polymer brushes is common and many investigators simply report the reactant concentrations of the polymer brush components[16,21]. This may be due to the difficulties of applying standard methodologies such as nuclear magnetic resonance (NMR) and gel permeation chromatography (GPC), which all work best

with smaller polymers that can return distinct and accurate measurements – a problem with some polymer brushes given their size and polydispersity.

Fourier transform infrared spectroscopy (FTIR) is a potential novel method for characterizing polymer brushes, in particular the density of side chains. FTIR is a common material characterization technique and is widely used across the physical, chemical and biological disciplines. In general, FTIR measures the infrared absorbance of materials across various frequencies and then converts the raw signal into interpretable spectra via Fourier transform. The frequencies at which infrared light is absorbed depend heavily on the character of molecular bonds. For example, C=O aldehyde bond stretching absorbs around 1750 cm^{-1}, while alkyl C-H stretching absorbs around 2900 cm^{-1}. The chemical structure can then be identified by the shapes, intensities and frequencies of the absorbances. An analysis of a series of spectra composed of chemical mixtures may be done by mathematical methods such as singular value decomposition (SVD) or partial least squares (PLS) modeling. SVD is a widely used method to analyze groups of data and determine their relationships with each other[22–25], while PLS is used for prediction modeling of data sets[26,27]. A chemical mixture can be analyzed alongside their pure components to create a series of standard spectra to help determine the composition of a material. Theoretically, a brush copolymer spectrum may be assumed to be composed of the pure polymer components' spectra, thus the spectra of a copolymer may be likened to a mixture of the components. And it is to the knowledge of this author such a technique has not, as of yet, been reported in the literature.

Herein, we report the evaluation of a novel methodology to apply FTIR and SVD or PLS to analyze the brush copolymers: poly(acrylic acid)-*graft*-poly(ethylene glycol) (pAA-*g*-

PEG). There the pAA-*g*-PEG spectra are compared against a calibration curve composed of pure pAA and PEG, and their mixtures in varying ratios.

3.2 Materials and Methods

3.2.1 Materials

Acrylic acid (AA, 99.5%) stabilized with 200 ppm 4-methoxyphenol, methanol (99.8%) and sodium borate buffer were obtained from VWR (Radnor, PA, USA). 4,4' azobis (4-cyanopentanoic acid) (A-CPA), 4-cyano-4-(phenylcarbonothioylthio)pentanoic acid (CPA-DB) (>97% HPLC) and hydrogen chloride–methanol solution (~1.25 M) were obtained from Sigma-Aldrich (St. Louis, MO, USA). Methoxy-poly(ethylene glycol)-amine (PEG-NH_2) was obtained from Jenkem Technologies (Beijing, PRC) and 4-(4,6-dimethoxy-1,3,5-triazin-2-yl)-4-methylmorpholinium chloride (DMTMM) was from TCI America (Portland, OR, USA). IR polish calcium fluoride (CaF_2) optical window crystals (10.0mmx1.0mm) were purchased from Crystan (Poole, Dorset, UK). Several PEG calibration standards from Polymer Standards Service (Amherst, MA, USA) were acquired courtesy of the Cornell Center for Materials Research (CCMR); their $\bar{M}_n$ and PDI are 6170, 1.06; 22100, 1.17; and 31700, 1.3 respectively. All chemicals were used as received unless otherwise specified.

3.2.2 Synthesis of pAA(60)-*g*-PEG(2)

Poly(acrylic acid) (pAA, $\bar{M}_n$60,000 g/mol) was synthesized via RAFT polymerization utilizing a [AA]:[CPA-DB]:[A-CPA] ratio of 762:0.25:1 at [AA] of 3.0 mM in methanol. It was reacted for 48 hours @ 60^{o}C under airtight, 0_2 free, and dark conditions. The polymerization was terminated by plunging the flask into an ice bath and exposing it to air.

The product was dialyzed for 3 days in deionized (DI) water and lyophilized. Molecular weight was determined by gel permeation chromatography (GPC). Poly(arylic acid)-*graft*-poly(ethylene glycol) (pAA-*g*-PEG) was synthesized via condensation chemistry facilitated with DMTMM. pAA ($\bar{M}_n$ 60,000 g/mol), methoxy-PEG-amine ($\bar{M}_n$ 2,000 g/mol), and DMTMM were dissolved in ~ 0.1 M borate buffer at [AA]:[DMTMM]:[PEG] ratios of 1:2:2, 1:0.5:0.5, and 1:0.25:0.25 with pAA dissolved at 3.3 mg/ml. The pH was adjusted to between 6 and 7 using 1 N HCl, and the reaction was left to run for 24 hours at room temperature, then dialyzed against DI water for 3 days and lyophilized. The final products are pAA(60)-2-PEG(2), pAA(60)-0.5-PEG(2) and pAA(60)-0.25-PEG(2).

3.2.3 Spin coating on Calcium Fluoride

Samples were prepared for fourier transform infrared spectroscopy (FTIR) by spin coating polymer solutions onto CaF_2 crystals. A stock of 0.1M HCl-methanol was prepared from a ~1.25 M HCl-Methanol solution. Polymer samples of either of a mixture of pAA/PEG or pAA(60)-2-PEG(2) were dissolved in 0.1 M HCl-methanol at 10 mg/ml. The polymer solution was then spin coated on the CaF_2 crystals using a Laurell WS-400A-6NPP-LITE spin coater at 750 rpm for 1 minute under N_2 gas. The samples' spectra were then generated on a Nicolet 8700 using DTEC splitting and OMNIC software. Each sample had 64 scans at resolution 2. The results were analyzed using either single value decomposition (SVD) or partial least squares modeling (PLS) of the spectra in MATLAB. The PLS algorithm library was from Dr. Liang of the Central South University, Changsha, China under the GNU general public license.

3.2.4 MALLS/SEC of pAA(60)-2-PEG(2)

pAA(60)-2-PEG(2) and PEG calibrations standards were sent to the Biophysics Resource of Keck Laboratory at the Yale School of Medicine to be analyzed by their DAWN Helios multil-angle laser light scattering size exclusion chromatraphy system (MALLS/SEC). A Superpose 6 column was used to fractionate the samples at ambient temperatures. pAA(60)-2-PEG(2) was dissolved at 3mg/ml in PBS and sonicated for 15 minutes before injection into the SEC using a dn/dc value of 0.135 ml/g.

3.2.5 ^{1}H NMR of pAA(60)-0.25-PEG(2) and pAA(60)-0.5-PEG(2)

Percent conjugation of PEG onto pAA for pAA(60)-0.25-PEG(2) and pAA(60)-0.5-PEG(2) was determined by ^{1}H NMR using an INOVA 600 MHz instrument. The samples were dissolved in deuterium oxide (D_2O) at 10 mg/ml and scanned under quantitative settings. The results were analyzed through MNova – pAA peaks at ~1.7 and ~2.4 ppm were integrated and compared to PEG methyl peak at ~3.4 ppm to determine percent conjugation.

3.3 Results and Discussion

A series of pAA-*g*-PEG brush copolymers with differing grafting densities was synthesized via the "grafting onto" schema as described in Chapter 2 of this thesis. These polymer brushes consists of well-defined polymer backbone and side chain molecular weights; however the side chain density or % conjugation of PEG is not easily determined. This characterization problem may be due to the high molecular weights of pAA (60, 105, 145 kg/mol) and PEG (2, 5, 10 kg/mol) utilized (synthesis in chapter 2 of this thesis) and the desired high degree of side chain density. The problem of characterization of side chain

density becomes evident particularly when attempting to analyze pAA-*g*-PEG through quantitative ^{1}H NMR (**Fig. 3.2**). Due to the high PEG content of the final polymer brush the H^{1} NMR spectra consists primarily of a dominating peak at ~3.5 ppm corresponding to PEG methylene groups. Thus characterization by NMR proves difficult in this situation. When attempting to utilize gel permeation chromatography (GPC) an issue arises where the pAA-*g*-PEG in solution is too large to be filtered (0.2 μm) and may potentially clog the system. Measurement of relative molecular weight by GPC employing linear polymer standards would not work well for polymer brushes, which are non-linear in dimension. As a result, conventional GPC does not give accurate molecular weights. The exception to this rule would be the use of a multi-angle laser light scattering (MALLS) GPC, which does not rely on standards but directly computes molecular weights through light scattering of the solutions. In fact, the pAA(60)-2-PEG(2)'s molecular weight was determined through MALLS GPC. However, use of this equipment is costly and not feasible for analyzing an entire brush copolymer library.

In this study, FTIR was used as an alternative approach to determine the % conjugation of the pAA-*g*-PEG's specifically composed of 60,000 g/mol pAA and 2,000 g/mol PEG. To accomplish this, the spectra of pAA and PEG was first analyzed to determine their differences and to determine the spectral regions of interest where the composition content could be measured. In **Fig. 3.3**, the spectra of pAA and PEG are shown in the frequency range of 1000-2000 cm^{-1}. This is the region where the most differences between the two polymers are observed. Specifically, the carbonyl stretching peak between 1600-1800 cm^{-1} corresponding to carboxylic acid exist in pAA but not PEG, and the distinct sharp peaks between 1000-1500 cm^{-1} corresponding to alkyl and ether stretches are very prominent in

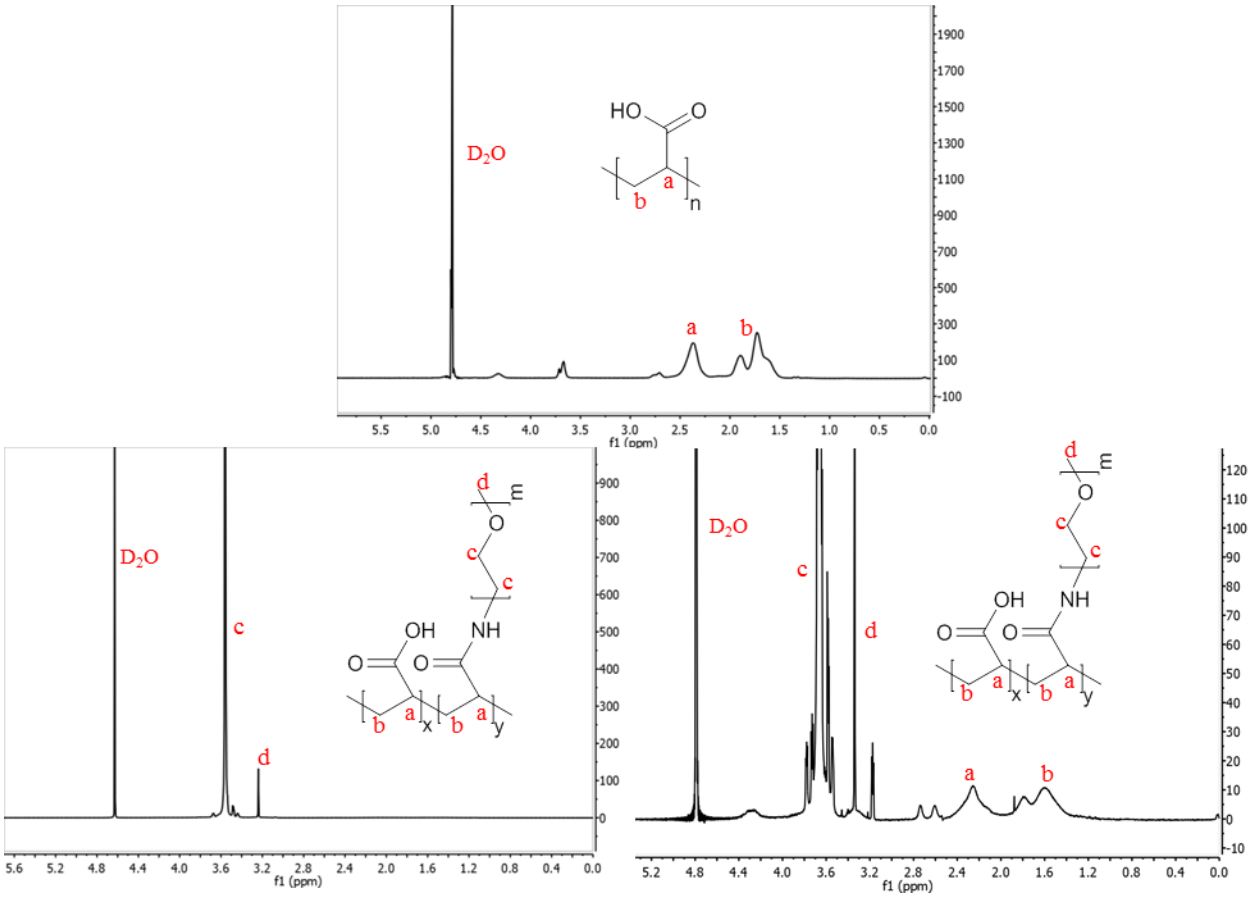

Figure 3.2: ^{1}H NMR of **a)** 60 kDa pAA in D_2O, a and b corresponds to the pAA backbone carbons at ~1.6 and ~2.3 ppm respectively. A double peak at 3.5-3.6 ppm corresponds to methylation of carboxyl group from methanol solvent (~<15%). A peak at 2.8 ppm and 4.2 ppm may be related to dimerization of acrylic acid before polymerization (<7%)[28], which retains carboxylic acid functionality albeit with slight extension from the backbone. **b)** pAA(60)-2-PEG(2) in D_2O. c corresponds to the PEG hydrogens at ~3.5 ppm and d corresponds to PEG methoxy protons while the pAA backbone hydrogens are not seen in the NMR. This is due to the overwhelming presence of the 2 kDa PEG side chains preventing visualization of the backbone hydrogens. **c)** pAA(60)-0.5-PEG(2) to demonstrate lower conjugation of PEG with pAA peaks visible. Here the pAA peaks are still visible.

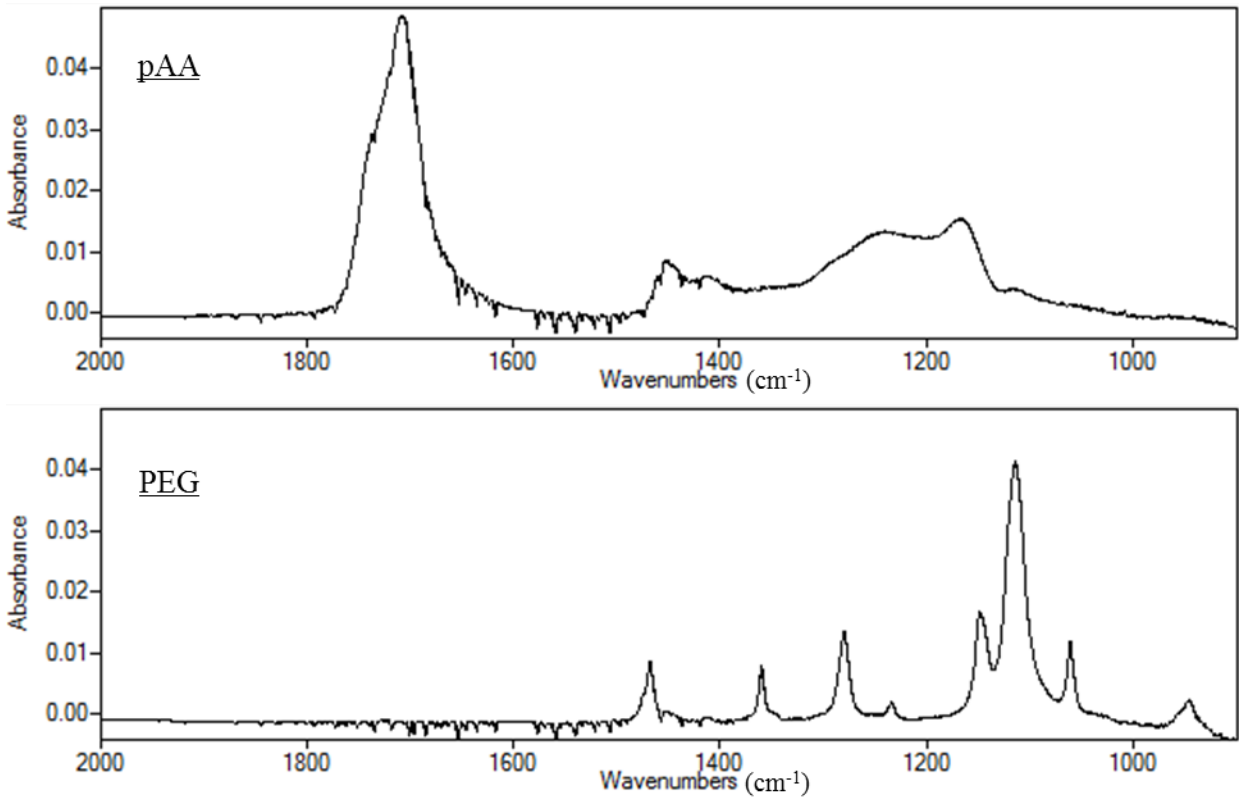

Figure 3.3: FTIR spectra of pure pAA and PEG respectively. Samples were dissolved in 0.01 M HCl-Methanol at 3mg/ml and spin coated onto CaF_2 slides. pAA has a large carbonyl peak from 1600-1800 cm^{-1}, while PEG has sharp, distinct peaks from 1000-1500 cm^{-1}.

PEG. In addition, this frequency region is very useful for quantitative analysis due to their distinct peaks, in contrast tofrequencies greater than 2000 cm^{-1} where the spectral peaks may be quite broad and have overlapping peaks with residual water.

For this study, it is hypothesized that pAA-*g*-PEGs' FTIR spectra is simply a composition of pure pAA and PEG spectra in varying ratios. Thus it would be possible to compare the FTIR spectra of pAA-*g*-PEG to the spectra of known pAA:PEG physical mixtures. But to measure a range of pAA-*g*-PEG's with different % conjugations, a calibration curve of pAA and PEG mixtures is needed. Here four different mass fractions of pAA (0.1, 0.25, 0.5, 0.75) were measured in addition to pure pAA and PEG (mass fractions of 1 and 0 respectively), creating a total of six calibration mass fractions. Nine FTIR spectra were captured for each of these fractions. The compendium of the spectra after taking the first derivative is shown in **Fig. 3.4**. The first derivative is to account for baseline differences of the spectrum. The color graph differentiates the ratios of pAA:PEG in the spectra, with 0 indicating no pAA (pure PEG) and 1 being pure pAA. As seen in the figure, the absorbance values gradually change with increasing pAA fraction.

3.3.1 Mathematical Modeling Methods

To analyze the FTIR spectral data, the various spectra were mathematically decomposed into useful components that would allow comparisons to be easily quantifiable. Two methods explored for this purpose were SVD and PLS. The general methodologies for creating the calibration or prediction curves are given in the following sections.

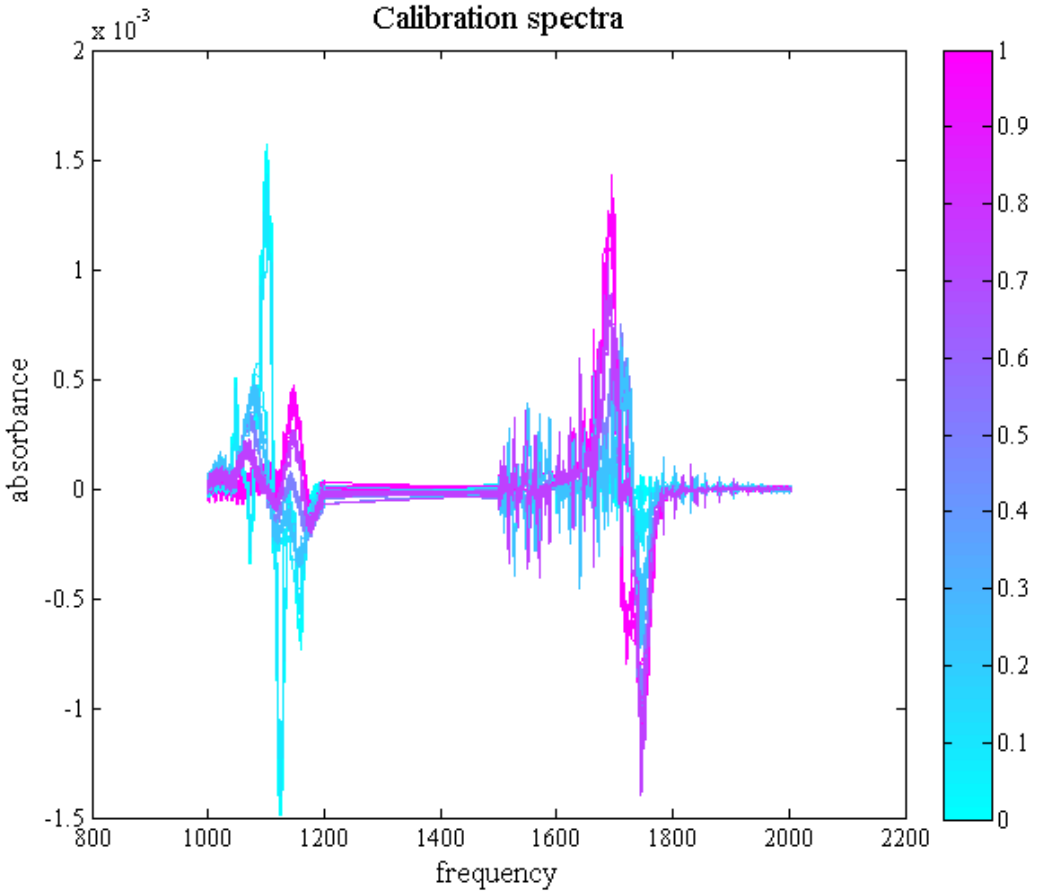

Figure 3.4: Compendium of all calibration FTIR spectra after taking first derivative used in this study. The color graph corresponds to the pAA mass fraction of the individual spectra. Here the first derivative is used to overcome differences in baselines across the samples, simplifying analysis.

3.3.2 Single Value Decomposition (SVD)

SVD can take a series of data in a matrix and break it down into its component matrices, similar to eigendecomposition, but without the limitation of square matrices. This method allows the data to be analyzed via its basis vectors and its corresponding coefficients. The component matrices can then be used to determine the principal components i.e. factors that contribute the most to the variance in the data set, which can then allow correlation of the data set.

Briefly, to create the calibration curve using SVD, a matrix '*Y*' is created composed of the absorbance values taken from the FTIR of the calibration samples and decomposed into matrices of the form:

$$Y = USV^T \qquad \text{eq (1)}$$

where *U* is the first basis vector set, *S* is the scalar matrix, and V^T is the coefficient matrix. For the Matlab code a π matrix is selected such that $X_g = U\pi$; this transforms *U* into a new basic vector X_g such that the first and second columns of $X_g$correspond to the spectral basis vectors of pure pAA and PEG respectively. Here the assumption is that the first two columns of *U* contribute the most to the differences between the pAA and PEG spectra. The coefficient matrix *Vg* is created such that $V_g = V\pi$; where the first and second column of *Vg* correspond to pAA and PEG coefficients. The pAA:PEG spectral coefficient fraction is then calculated from the first two columns in V_g (corresponding to pAA and PEG respectively) and plotted against the pAA:PEG mass fractions in Matlab (see **Appendix 3.6.2** for code).

The calibration curve created by SVD is shown in **Fig. 3.5**. The y-axis corresponds to pAA spectral coefficients fraction and follows a quadratic relationship against the pAA mass fractions. The trend suggests that the SVD code was able to link the pAA mass fractions with

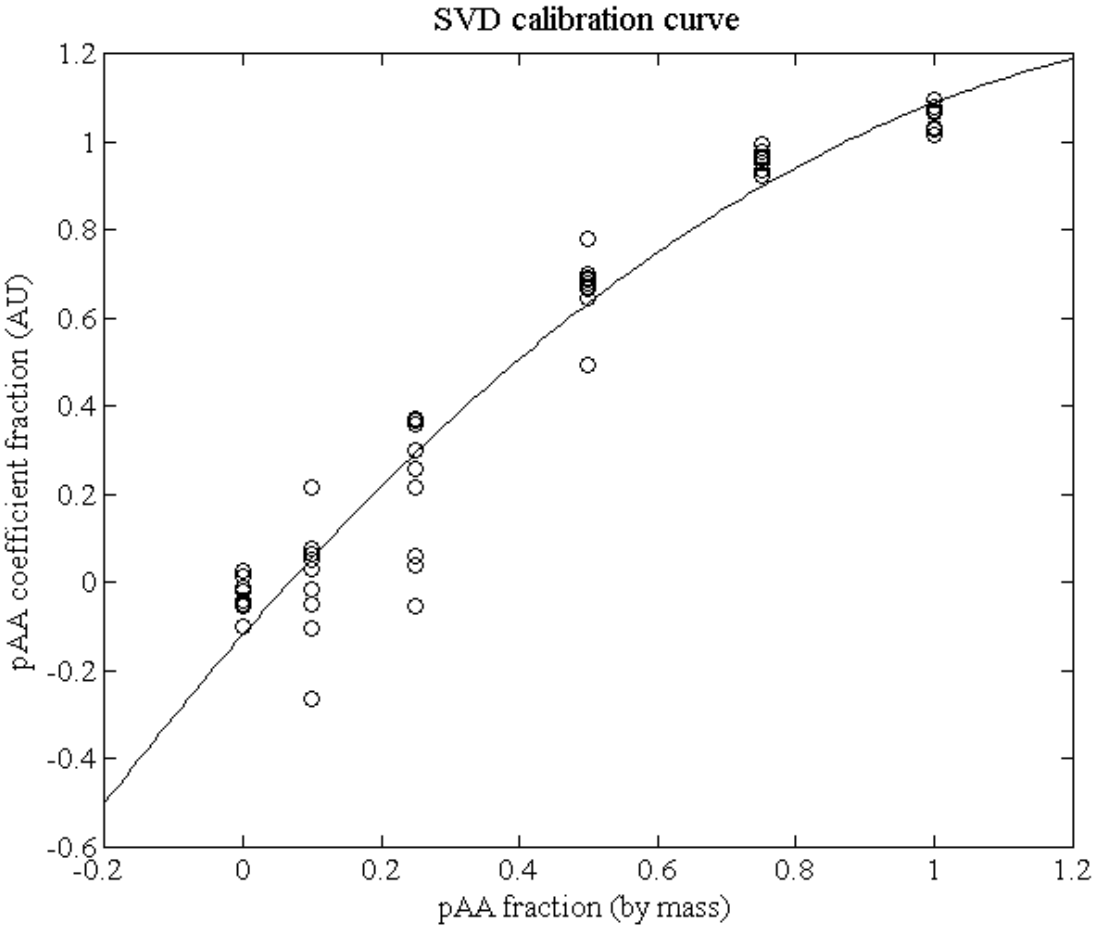

Figure 3.5: SVD calibration curve generated from the FTIR spectra of pAA and PEG. Graph correlates the spectral pAA coefficient fraction calculated using SVD with the known pAA mass fractions. Quadratic equation ($y=-0.58x^2+1.79x-0.12$) fitted to data with $r^2=0.93$.

the corresponding spectra. However, the error bars on some of the points are fairly large especially at the pAA mass fractions of 0.1 and 0.25 causing the pAA coefficient fractions to have negative values.

3.3.3 Partial Least Squares (PLS) Modeling

PLS modeling works similarly to SVD, in that it decomposes a matrix of data to determine the variance of the matrix factors, but requires not only the input data but the response data as well. In general, SVD only utilizes the input (i.e. spectral data) for the mathematical decomposition and the resulting values have to be manually compared to the response (pAA mass fraction) to create a calibration curve. PLS on the other hand utilizes both the input (spectral data) and response (pAA mass fractions) in its equations, to create a standard. This is because PLS is specifically designed to create a prediction model between two datasets by maximizing their variance and projecting it into a new space, creating a linear prediction model between input and response. The general PLS equations are given below:

$$Y = TP^T + E \qquad \text{Eq (2)}$$

$$Z = UQ^T + F \qquad \text{Eq (3)}$$

Where Y is the input matrix, Z is the response matrix, T, P, U and Q are loading matrices while E and F are the error terms. By maximizing the covariance between T and U, a linear prediction model can be created between Y and Z. A key step to this involves determining the ideal number of latent variables or loading matrix factors to minimize the error of the prediction model. In general, the more latent variables used the better the model; however, for a given dataset there exists an optimal number of latent variables such that increasing the number of latent variables makes little difference. The Matlab code derived

from Dr. Liang's code can automatically determine the optimal number of latent variables for a given data set (see **Appendix 3.6.3).** An important consideration is that increasing the number of latent variables for PLS is not the same as overfitting a curve. In PLS the increase in latent variables works to improve the predictive power of the model and does not count as observable variables, but as hidden variables instead i.e. which factors in the loading matrices provide the greatest covariance.

The prediction curve generated from PLS is given in the **Fig. 3.6**, it was generated using 11 and 27 latent variables – the optimal numbers determined by the program. The major difference between the results is of the error deviation of the data points when PLS switches from 11 latent variables to 27 latent variables, which decreases the error deviations. The RMSECV vs latent variables is shown in **Fig 3.7** demonstrating little change in cross-validation error beyond 27 latent variables. The y-axis here is the PLS input fit designed to produce a linear relationship with the known pAA mass fractions. When compared to the SVD calibration curve, PLS has much smaller error bars and has minimal negative y-values.

3.3.4 Evaluation of SVD and PLS for pAA-*g*-PEG

pAA(60)-2-PEG(2), pAA(60)-1-PEG(2), pAA(60)-0.5-PEG(2) and pAA(60)-0.25-PEG(2) were analyzed using the curves generated by both SVD and PLS. The resulting percent conjugation of PEG onto the pAA backbone was then calculated and compared to the % conjugation determined either through MALLS/SEC or ^{1}H NMR (**Table 1**). For the PLS the % conjugation was analyzed using either 11 latent variables or 27 latent variables. While **Fig 3.7** shows that beyond 27 latent variables there is no noticeable changes in error, the plot of PLS predicted pAA mass fractions pAA-*g*-PEG's versus latent variables (**Fig 3.8**) shows

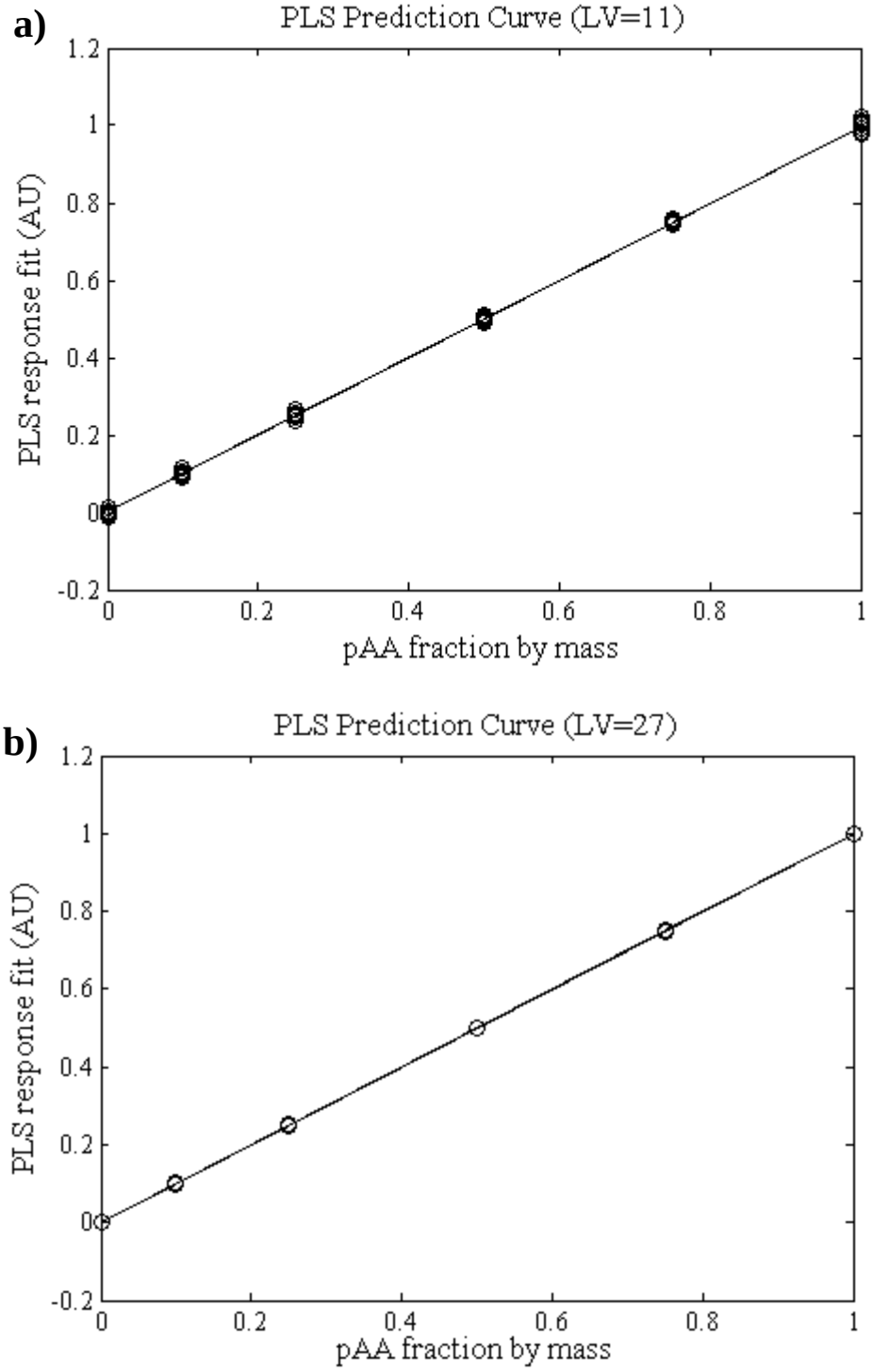

Figure 3.6: PLS prediction curve between known pAA mass fractions (x-axis) and the PLS generated input fit (y-axis) using **a)** 11 or **b)** 27 latent variables from the FTIR spectra of pAA and PEG. The fit equation is y=x, r^2~1.

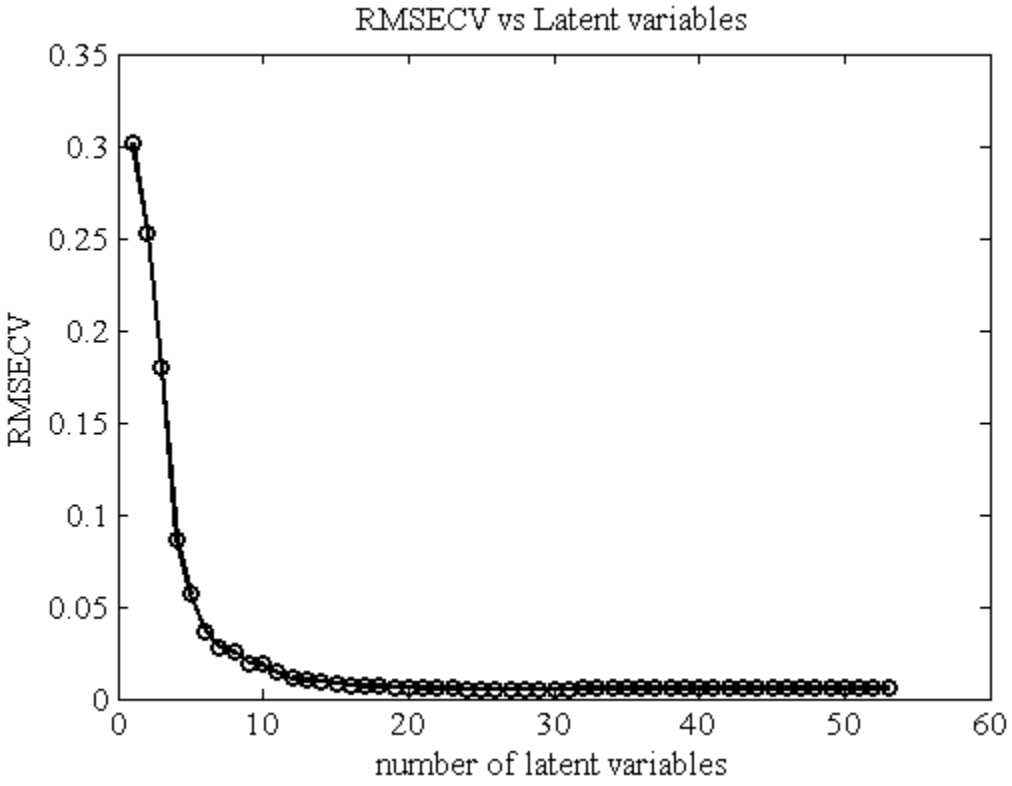

Figure 3.7: Root mean square error of cross-validation (RMSECV) of the calibration data set vs latent variables used in the PLS.

Table 3.1 Percent conjugation of PEG in pAA-*g*-PEG

Polymer	**Actual % conjugation**	**% conjugation by SVD**	**% conjugation by PLS (LV[f]=11)**	**% conjugation by PLS (LV[f]=27)**
pAA(60)-2-PEG(2)	81.2[a]	16.4 ± 4.2[c]	>100[c]	>100[c]
pAA(60)-1-PEG(2)	~100[b,e]	21.6±7.6	97.8±8.4[c]	>100[c]
pAA(60)-0.5-PEG(2)	23.1[b]	7.4 ± 2.8[d]	20 ± 0.2[d]	11.8 ± 0.3[d]
pAA(60)-0.25-PEG(2)	23.7[b]	6.9 ± 2.2[c]	19.1 ± 0.5[c]	12.3 ± 0.6[c]

[a] As determined by MALLS/GPC

[b] As determined by quantitative ^{1}H NMR

[c] Averaged from 3 samples

[d] Averaged from 4 samples taken across multiple days

[e] ^{1}H NMR pAA peaks may be too close to baseline to provide accurate results

[f] LV= latent variables

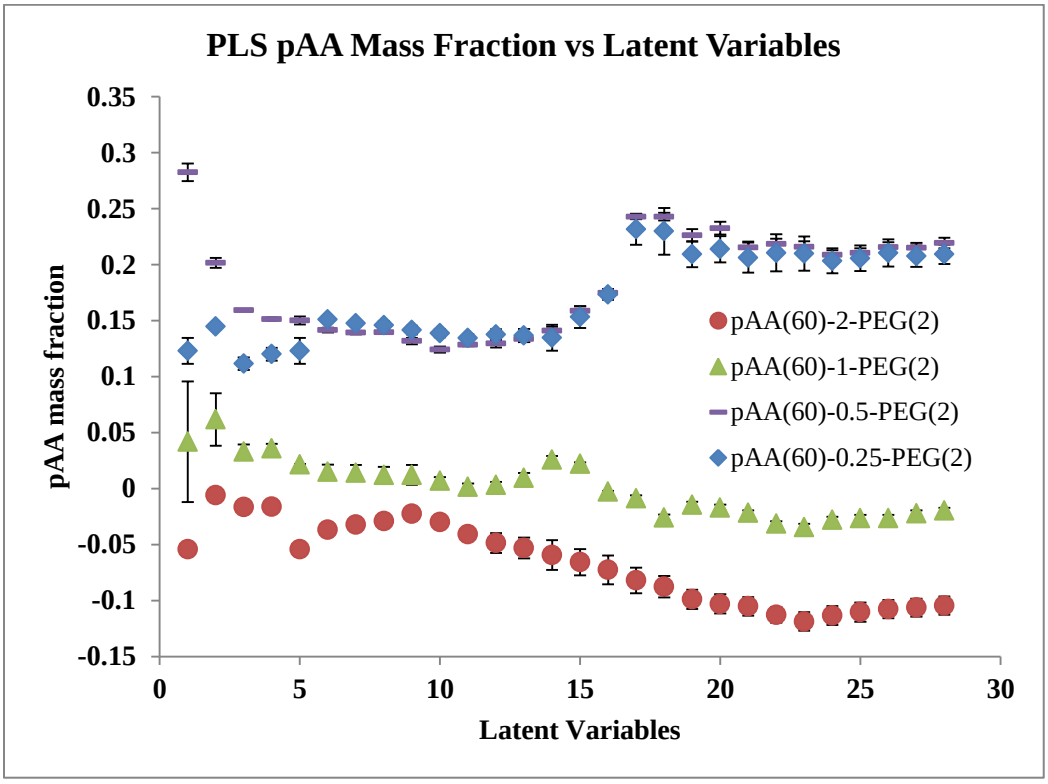

Figure 3.8: The predicted pAA mass fraction of various pAA-*g*-PEG's in PLS versus the number of latent variables used.

some differences in calculated values. There appears to be two plateaus in the graph between 5-14 latent variables and from 17-28 latent variables particularly for pAA(60)-0.5-PEG(2) and pAA(60)-0.25-PEG(2). Hence, the polymers were analyzed using both 11 and 27 variables to ascertain differences.

Table 1 shows the predicted % conjugation of PEG of the pAA-*g*-PEG's by both SVD and PLS (LV=11 and 27). The values determined by SVD when compared to the actual % conjugation numbers are significantly lower, this may be due to the significant error bars of the calibration curve (**Fig 3.5**) combined with lack of control of latent variables in the algorithm. The predicted results from PLS fall closer to the actual % conjugation values than SVD. pAA(60)-2-PEG(2) showed nearly greater than 100% suggesting that the model does not predict highly grafted % conjugation. The PLS results for pAA(60)-1-PEG(2) demonstrated a similar issue but was difficult to compare due to inaccuracies of measuring actual % conjugation using ^{1}H NMR, the pAA signal peaks were too close to baseline to provide accurate integrations. However, for the lower grafting ratios of 0.5 and 0.25 the predicted values at 11 latent variables (19-20%) were closer to the actual % conjugation (23-24%). Though at 27 latent variables the predicted results (~12%) were not as accurate at 11 latent variables. It appears that increasing the number of latent variables beyond 16, while reducing RMSECV error, did not make the model more accurate for the prediction of % PEG conjugation onto pAA.

3.4 Conclusions and future recommendations

In conclusion, following the hypothesis that the FTIR spectra of pAA-*g*-PEG is a composition of pAA and PEG spectra, two models were created to attempt to predict this

composition. FTIR of pAA and PEG mixtures alongside pure pAA and PEG spectra were analyzed using either SVD or PLS. While SVD successfully correlated the spectra to known pAA mass fractions, its predictive power is very weak and had significant error. PLS on the other hand, produced an effective linear prediction model between the spectra and known pAA mass fractions at 11 latent variables that could more effectively predict the % conjugation of the lower grafting ratio (0.5, 0.25) polymers. However, for pAA(60)-2-PEG(2) and pAA(60)-1-PEG(2) with the larger grafting ratios, neither SVD nor PLS could accurately predict the % conjugation. This may be because at grafting ratios of 2 or 1, the pAA-*g*-PEG's is mostly composed of PEG and hence its spectra resembles that of PEG. Also the smallest pAA mass fraction used to create the calibration/prediction curves, other than 0, used for the FTIR was 0.1 corresponding to 33% conjugation of PEG onto pAA. Due to this, it is the recommendation of this author that even smaller pAA mass fractions should be used for calibration/prediction curves to accommodate the analysis of highly grafted pAA-*g*-PEG's.

3.5 References

1. Yang, W. J. *et al.* Biomimetic anchors for antifouling and antibacterial polymer brushes on stainless steel. *Langmuir* **27,** 7065–76 (2011).

2. Muszanska, A. K. *et al.* Antiadhesive polymer brush coating functionalized with antimicrobial and RGD peptides to reduce biofilm formation and enhance tissue integration. *Biomacromolecules* **15,** 2019–26 (2014).

3. Fan, X., Lin, L. & Messersmith, P. B. Cell fouling resistance of polymer brushes grafted from ti substrates by surface-initiated polymerization: effect of ethylene glycol side chain length. *Biomacromolecules* **7,** 2443–8 (2006).

4. Hwangbo, K.-H., Kim, Y.-J. & Cho, K. Y. Fabrication of protein-resistant blend based on PVDF-HFP and amphiphilic brush copolymer made from PMMA and PEGMA. *Appl. Surf. Sci.* **263,** 291–296 (2012).

5. Gao, G. *et al.* Antibacterial surfaces based on polymer brushes: investigation on the influence of brush properties on antimicrobial peptide immobilization and antimicrobial activity. *Biomacromolecules* **12,** 3715–27 (2011).

6. Roosjen, A., Mei, H. C. Van Der, Busscher, H. J. & Norde, W. Microbial Adhesion to Poly (ethylene oxide) Brushes : Influence of Polymer Chain Length and Temperature. 10949–10955 (2004).

7. Nejadnik, M. R. *et al.* Bacterial colonization of polymer brush-coated and pristine silicone rubber implanted in infected pockets in mice. *J. Antimicrob. Chemother.* **62,** 1323–5 (2008).

8. Nejadnik, M. R., van der Mei, H. C., Norde, W. & Busscher, H. J. Bacterial adhesion and growth on a polymer brush-coating. *Biomaterials* **29,** 4117–21 (2008).

9. Raviv, U. *et al.* Lubrication by charged polymers. *Nature* **425,** 163–5 (2003).

10. Nomura, A., Okayasu, K., Ohno, K., Fukuda, T. & Tsujii, Y. Lubrication Mechanism of Concentrated Polymer Brushes in Solvents: Effect of Solvent Quality and Thereby Swelling State. *Macromolecules* **44,** 5013–5019 (2011).

11. Bielecki, R. M., Crobu, M. & Spencer, N. D. Polymer-Brush Lubrication in Oil: Sliding Beyond the Stribeck Curve. *Tribol. Lett.* **49,** 263–272 (2012).

12. Loiseau, J. *et al.* Synthesis and characterization of poly (acrylic acid) produced by RAFT polymerization. Application as a very efficient dispersant of CaCO3, kaolin, and TiO2. *Macromolecules* **36,** 3066–3077 (2003).

13. Sheiko, S. S., Sumerlin, B. S. & Matyjaszewski, K. Cylindrical molecular brushes: Synthesis, characterization, and properties. *Prog. Polym. Sci.* **33,** 759–785 (2008).

14. Neugebauer, D., Zhang, Y. & Pakula, T. Densely-grafted and double-grafted PEO brushes via ATRP. A route to soft elastomers. *Macromolecules* **36,** 6746–6755 (2003).

15. Rinaldi, D. & Hamaide, T. copolymerization of methacrylic acid and poly (ethylene glycol) methyl ether methacrylate in the presence of a hydrophobic chain transfer agent in organic solution. *J. Polym. Sci. Part A Polym. Chem.* **47,** 3045–3055 (2009).

16. Müller, M., Lee, S., Spikes, H. & Spencer, N. The influence of molecular architecture on the macroscopic lubrication properties of the brush-like co-polyelectrolyte poly (L-lysine)-g-poly (ethylene glycol)(PLL-g-PEG) adsorbed on oxide surfaces. *Tribol. Lett.* **15,** 395–405 (2003).

17. Perrino, C., Lee, S., Choi, S. W., Maruyama, A. & Spencer, N. D. A Biomimetic Alternative to Poly (ethylene glycol) as an Antifouling Coating: Resistance to Nonspecific Protein Adsorption of Poly (L -lysine)-graft-dextran. *Langmuir* **24,** 8850–8856 (2008).

18. Ederle, Y., Isel, F., Grutke, S. & Lutz, P. J. Anionic polymerization and copolymerization of macromonomers: kinetics, structure control. *Macromol. Symp.* **132,** 197–206 (1998).

19. Tsarevsky, N. V & Matyjaszewski, K. “Green” atom transfer radical polymerization: from process design to preparation of well-defined environmentally friendly polymeric materials. *Chem. Rev.* **107,** 2270–99 (2007).

20. Behavior, A. *et al.* Bioinspired Bottle-Brush Polymer Exhibits Low Friction and Amontons-like Behavior. *J. Am. Chem. Soc.* **136,** 6199–6202 (2014).

21. Schmolke, H., Hartwig, S. & Klages, C.-P. Poly(acrylic acid)-graft-poly(ethylene glycol) preparation and adsorption on polyelectrolyte multilayers (PEMs) for custom-made antiadhesive surfaces. *Phys. Status Solidi* **208,** 1290–1300 (2011).

22. Practical, I. A., Data, M., Berrar, A. D. P. & Dubitzky, W. in *A Pract. Approach to Microarray Data Anal.* 91–109 (2003).

23. Hug, S. J., Lewis, J. W., Einterz, C. M., Thorgeirsson, T. E. & Kliger, D. S. Nanosecond photolysis of rhodopsin: evidence for a new blue-shifted intermediate. *Biochemistry* **29,** 1475–85 (1990).

24. Furnas, G. W., Landauer, T. K., Dumais, S. T., Lochbaum, K. E. & Streeter, L. A. Information Retrieval using a Singular Value Decomposition Model of Latent Semantic Structure. in *Proceeding SIGIR '88 Proc. 11th Annu. Int. ACM SIGIR Conf. Res. Dev. Inf. Retr.* 465–480 (1988).

25. Turney, P. D. Mining the Web for Synonyms : PMI-IR Versus LSA on TOEFL. in *Proc. Twelth Eur. Conf. Mach. Learn.* 451–502 (2001).

26. Martens, H. & Martens, M. *Multivariate Analysis of Quality: An Introduction*. (2001).

27. Wold, H. in *Quant. Sociol. Int. Perspect. Math. Stat. Model Build.* 307–357 (Academic Press, 1975).

28. Pelet, J. M. & Putnam, D. Poly(acrylic acid) Undergoes Partial Esterification During RAFT Synthesis in Methanol and Interchain Disulfide Bridging Upon NaOH Treatment. *Macromol. Chem. Phys.* **213,** 2536–2540 (2012).

3.6 Appendix

3.6.1 Initial FTIR analysis data utilizing SVD (n=1 for each sample)

A series of pAA-*g*-PEG's were initially analyzed using SVD to determine % conjugation of PEG side chain groups onto pAA. The methodology involved only n=1 samples for each calibration pAA mass ratios and unknown pAA-*g*-PEG's, thus reducing the robustness of the both the calibration curves and the results; hence was not included in the main chapter text. Spin coating was not applied and these results were obtained using SVD. The data is presented in **Table 3**, and a multivariate linear regression model was applied to analyze the effect of the independent variables of pAA backbone size, PEG side chain size, grafting ratio and their cross-correlations on the resulting % conjugation of PEG onto pAA (**Table 4**). No significant conclusions can be drawn from the data, though PEG side chain size and pAA backbone appeared to have the strongest non-significant effects ($p=0.099$, $p=0.146$). Multivariate linear regression on the same variables but against hydrodynamic size instead of % conjugation also indicates that side chain size and backbone size have the largest effects. However, no definitive conclusion can be drawn from these small sample sets.

Table 3.2 Table of initial % conjugation of pAA-*g*-PEG using SVD

Polymer[a]	% conjugation by SVD[b]	Calculated MW (kg/mol)[c]
pAA(60)-2-PEG(2)	78	1,348,527
pAA(60)-1-PEG(2)	25	472,989
pAA(60)-0.5-PEG(2)	14	291,274
pAA(60)-2-PEG(5)	31	1,346,461
pAA(60)-0.5-PEG(5)	5	267,494
pAA(60)-2-PEG(10)	18	1,556,354
pAA(105)-2-PEG(5)	15	1,217,092
pAA(105)-1-PEG(5)	41	3,141,250
pAA(105)-2-PEG(10)	4.4	742,268
pAA(145)-2-PEG(2)	36	1,593,114
pAA(146)-1-PEG(10)	17	829,359

[a] Nomenclature is pAA(α)-*g*-PEG(β) where α and β is M_n of pAA and PEG respectively; *gr* is grafting ratio of [PEG]:[AA] during conjugation.

[b] Calculated from FTIR (see section 3.2.2)

[c] Calculated using % conjugation and Mn of pAA.

Table 3.3 Table of % Conjugation Multivariate Linear Regression Modeling Coefficients

Variables investigated	**Coefficient estimate**	**p-value (significance)[a]**
side chain size	$-5.66 \times 10^{-3} \pm 2.39 \times 10^{-3}$	0.0988
(backbone size)*(grafting ratio)	$-8.40 \times 10^{-4} \pm 4.29 \times 10^{-4}$	0.1456
(backbone size)*(side chain side)*(grafting ratio)	$7.23 \times 10^{-08} \pm 1.04 \times 10^{-7}$	0.5377
(backbone size)*(side chain side)	$-2.94 \times 10^{-8} \pm 5.62 \times 10^{-8}$	0.6372
backbone size	$1.07 \times 10^{-4} \pm 2.46 \times 10^{-4}$	0.6925
grafting ratio	2.50 ± 11.3	0.8396
(side chain side)*(grafting ratio)	$-8.40 \times 10^{-4} \pm 4.37 \times 10^{-3}$	0.8598

[a] Arranged by descending degree of p-value

3.6.2 MATLAB Single Value Decomposition (SVD) code

```
close all

    clear all
    clc

    %number of calibration samples?
    nstan=54;

    %number of concentration sets?
    nset=6;

    %number of unknown samples?
    %nukn=12;
    nukn=10;




    %%%%%%%%%%%%%%%%%%%%%%%%%%%%%%%%%%%%%%%%%%%%%%%%%%%%%%%%%%%%%%%%%%%%%%%%%
    %%%%%%%%%%%%%%%%%%%%%%%%%%%%%%%%%%%%%%%%%%%%%%%%%%%%%%%%%%%%%%%%%%%%%%%%%
    % Load data

    %%%%%%%%%%%%%%%%%%%%
    % Load the calibration data:

    % Input sections of the file names corresponsing to concentration,
    % replicate letter, date, and pAA fraction
    conc={'0to1','1to0','01to09','05to05','025to075','075to025'};
    samp={'1','2','3','4','5','6','7','8','9'};
    pAAfracLIST={0, 1, 0.1, 0.5, 0.25, 0.75};
    nsamp=length(samp);

    field1='conc';
    for i=1:nset
        for j=1:nsamp;
            value1(j+(i-1)*nsamp)=conc(i);
        end
    end

    field2='sample';
    value2=repmat(samp,1,nset);

    field3='pAAfrac';
    for i=1:nset
        for j=1:nsamp;
            value3(j+(i-1)*nsamp)=pAAfracLIST(i);
        end
    end
```

```
%This structure contains info on all spectra
info=struct(field1,value1,field2,value2,field3,value3);

exdata=load('C:\Users\Tanmingchee\Documents\FTIR@bakerLabs\pAAPEGonCaF2_MeO
H_spinCoating750rpm_042214_All\pAAPEGratio0to1_10mgml_1.CSV');
% Manually load first two files into data cell
data{2}=load('C:\Users\Tanmingchee\Documents\FTIR@bakerLabs\pAAPEGonCaF2_Me
OH_spinCoating750rpm_042214_All\pAAPEGratio0to1_10mgml_1.CSV');
data{1}=load('C:\Users\Tanmingchee\Documents\FTIR@bakerLabs\pAAPEGonCaF2_Me
OH_spinCoating750rpm_042214_All\pAAPEGratio1to0_10mgml_1.CSV');

% Add spectra files to data matrix, while skipping over files which don't
exist
% Since not all concentration sets have the same number of spectra, some
% elements of struture 'info' do not correspond to spectra


j=0;
%data=zeros(size(exdata,1),2,nstan);
pAAfrac=zeros(nstan,1);
pAAfrac(1)=1; pAAfrac(2)=0;
% Add the rest of spectra into data cell
for k=3:nstan;
 if
isequal(exist(['C:\Users\Tanmingchee\Documents\FTIR@bakerLabs\pAAPEGonCaF2_
MeOH_spinCoating750rpm_042214_All\pAAPEGratio'...
         info(k+j).conc '_10mgml_' info(k+j).sample '.CSV'],'file'),2);

data{k}=load(['C:\Users\Tanmingchee\Documents\FTIR@bakerLabs\pAAPEGonCaF2_M
eOH_spinCoating750rpm_042214_All\pAAPEGratio' ...
               info(k+j).conc '_10mgml_' info(k+j).sample '.CSV']);
            pAAfrac(k)=info(k+j).pAAfrac;
 else
     while
~exist(['C:\Users\Tanmingchee\Documents\FTIR@bakerLabs\pAAPEGonCaF2_MeOH_sp
inCoating750rpm_042214_All\pAAPEGratio'...
             info(k+j).conc '_10mgml_' info(k+j).sample '.CSV'],'file');
            j=j+1;


     end

data{k}=load(['C:\Users\Tanmingchee\Documents\FTIR@bakerLabs\pAAPEGonCaF2_M
eOH_spinCoating750rpm_042214_All\pAAPEGratio' ...
         info(k+j).conc '_10mgml_' info(k+j).sample '.CSV']);
      pAAfrac(k)=info(k+j).pAAfrac;

 end
end

% Larger range 831-3600
% minval=500; maxval=3367;

%smaller range 1000-2000 - also the ones used in PLS
```

```
minval=675; maxval=1707;


% Create x-axis values for plots
x=cell2mat(data(2));
x=x(minval:maxval,1);

i=1;
while i<=nstan;
    dummyVar=cell2mat(data(i));
    y(1:(maxval-minval+1), i)=dummyVar(minval:maxval,2);
    i=i+1;
    clear dummyVar
end

   % Pure pAA and pure PEG respectively
y1=y(:,1);
y2=y(:,2);


% Add unknown samples to spectra
 sampU={'1','2','3'};

    field2U='sample';
    value2U=sampU;

    infoU=struct(field2U,value2U);

    for k=1:nukn;
        if k<=3;

dataU{k}=load(['C:\Users\Tanmingchee\Documents\FTIR@bakerLabs\pAA_g_PEGonCa
F2_MeOH_spinCoating750rpm_050614\'...
            '60-2-2_fr061313_1_10mgml_on050614_' infoU(k).sample '.CSV']);
%
dataU(:,:,k)=load(['C:\Users\Tanmingchee\Documents\FTIR@bakerLabs\pAA_g_PEG
onCaF2_MeOH_spinCoating750rpm_052714\'...
%             '60-2-2_10mgml_fr052714_1_' infoU(k).sample '.CSV']);
        % I added this below for additional samples - by Mingchee Tan
        elseif (k>3) && (k<7);

dataU{k}=load(['C:\Users\Tanmingchee\Documents\FTIR@bakerLabs\pAA_g_PEGonCa
F2_MeOH_spinCoating750rpm_120314\'...
            '60-2-025_fr090413_10mgml_on120314_'         infoU((k-3)).sample
'.CSV']);
        elseif (k>6) && (k<9);

dataU{k}=load(['C:\Users\Tanmingchee\Documents\FTIR@bakerLabs\pAA_g_PEGonCa
F2_MeOH_spinCoating750rpm_120314\'...
            '60-2-05_fr081913_10mgml_on120314_'          infoU((k-6)).sample
'.CSV']);
        else
```

```
dataU{k}=load(['C:\Users\Tanmingchee\Documents\FTIR@bakerLabs\pAA_g_PEGonCa
F2_MeOH_spinCoating750rpm_120614\'...
            '60-2-05_fr081913_10mgml_on120614_'          infoU((k-8)).sample
'.CSV']);
        end
    end



i=nstan+1;
while i<=(nstan+nukn);
    dummyVar=cell2mat(dataU(i-nstan));
    y(1:(maxval-minval+1), i)=dummyVar(minval:maxval,2);
    i=i+1;
    clear dummyVar
end


[U,S,V]=svd(y);

%Reduce the matrices to remove noise. Reduce to n bases:
n=size(y,2);
Up=U(:,1:n);
Sp=S(1:n,1:n);
Vp=V(:,1:n);

%Re-constitute A using reduced matrices
Ap=Up*Sp*Vp';


% set initial values for Pi matrix
a1=10;
a2=.11; b2=+0.63;
a3=0.8; b3=+0.15;
a4=+.11; b4=-0.3;
a5=-0.02; b5=-0.02;
a6=+0.10; b6=+0.01;
a7=+0.01; b7=0.01;
a8=+0.01; b8=0.01;
a9=0.01; b9=0.01;
a10=0.2; b10=0.1;
a11=0.1; b11=0.1;
a12=0.1; b12=0.01;
a13=0.1; b13=0.01;
a14=0.1; b14=0.01;
a15=0.1; b15=0.01;
a16=0.1; b16=0.01;
a17=0.1; b17=0.01;
a18=0;

Pi=eye(size(y,2));
 Pi(1,1)=a1;
```

```
 Pi(2,1)=a2; Pi(1,2)=a2;
 Pi(3,1)=a3; Pi(1,3)=a3;
 Pi(4,1)=a4; Pi(1,4)=a4;
 Pi(5,1)=a5; Pi(1,5)=a5;
 Pi(6,1)=a6; Pi(1,6)=a6;
 Pi(7,1)=a7; Pi(1,7)=a7;
 Pi(8,1)=a8; Pi(1,8)=a8;
 Pi(9,1)=a9; Pi(1,9)=a9;
 Pi(10,1)=a10; Pi(1,10)=a10;
 Pi(11,1)=a11; Pi(1,11)=a11;
 Pi(12,1)=a12; Pi(1,12)=a12;
 Pi(13,1)=a13; Pi(1,13)=a13;
 Pi(14,1)=a14; Pi(1,14)=a14;
 Pi(15,1)=a15; Pi(1,15)=a15;
 Pi(16,1)=a16; Pi(1,16)=a16;
 Pi(17,1)=a17; Pi(1,17)=a17;
 Pi(18,1)=a18; Pi(1,18)=a18;
 Pi(2,2)=b2;
 Pi(2,3)=b3; Pi(3,2)=b3;
 Pi(2,4)=b4; Pi(4,2)=b4;
 Pi(2,5)=b5; Pi(5,2)=b5;
 Pi(2,6)=b6; Pi(6,2)=b6;
 Pi(2,7)=b7; Pi(7,2)=b7;
 Pi(2,8)=b8; Pi(8,2)=b8;
 Pi(2,9)=b9; Pi(9,2)=b9;
 Pi(2,10)=b10; Pi(10,2)=b10;
 Pi(2,11)=b11; Pi(11,2)=b11;
 Pi(2,12)=b12; Pi(12,2)=b12;
 Pi(2,13)=b13; Pi(13,2)=b13;
 Pi(2,14)=b14; Pi(14,2)=b14;
 Pi(2,15)=b15; Pi(15,2)=b15;
 Pi(2,16)=b16; Pi(16,2)=b16;
 Pi(2,17)=b17; Pi(17,2)=b17;
%  Pi(2,18)=b7; Pi(18,2)=b7;

% Recursion to determine coefficients via brute force method
for time=1:50;
h=1;
 while h<=(nstan+nukn);
    clear i % column index
    clear j % row index
    i(1)=(-1); % set intial recursion at -1
    j=1; % keeps track of the recursive values to be tested
        while i(j)<=(+1);
            Pi(1,h)=i(j); Pi(h,1)=i(j);
            Xg=Up*Pi;
            y1scal=(max(Xg(:,1))/max(y1))*y1;
            sumSquares(j)=sum((Xg(:,1)-y1scal).^2);
            j=j+1;
            i(j)=i(j-1)+.01; % sets next recursive value for matrix
            clear Xg
            clear y1scal
        end
    [C, mini]=min(sumSquares);
```

```
    Pi(1,h)=i(mini);  Pi(h,1)=i(mini);  % set matrix value to coefficient
value that returns smallest least squares residual
    clear sumSquares
    clear i
    if (h<nstan) && (h>1); % determine values of Pi matrix that affects the
PEG spectra
        i(1)=(-1); % set intial recursion at -1
        j=1; % keeps track of the recursive values to be tested
        while i(j)<=(+1);
            Pi(2,h)=i(j); Pi(h,2)=i(j);
            Xg=Up*Pi;
            y2scal=(max(Xg(:,2))/max(y2))*y2;
            sumSquares(j)=sum((Xg(:,2)-y2scal).^2);
            j=j+1;
            i(j)=i(j-1)+.01; % sets next recursive value for matrix
            clear Xg
            clear y2scal
        end
    [D, mini1]=min(sumSquares);
    Pi(2,h)=i(mini1); Pi(h,2)=i(mini1);
    clear sumSquares
    end
    clear C
    clear mini
    h=h+1;
 end
end

% Pi(1,1)=a1;


% Transformed basis vectors and coefficient matrix:
Xg=Up*Pi;
VpPi=Vp*Pi;


% Plots of transformed basis sets:
% For pAA component
% load pure pAA for y1
y1scal=(max(Xg(:,1))/max(y1))*y1;
figure;
axes('FontSize',14)
plot(x,y1scal,x,Xg(:,1))
legend('transformed & scaled','transformed')
xlabel('frequency (cm-1)','FontSize',16);
ylabel('absorbance','FontSize',16);
title('pAA component fit','FontSize',20);

% For PEG component
% load pure PEG for y2
y2scal=(max(Xg(:,2))/max(y2))*y2;
figure;
axes('FontSize',14)
plot(x,y2scal,x,Xg(:,2))
```

```
legend('transformed & scaled','transformed')
xlabel('frequency (cm-1)','FontSize',16);
ylabel('absorbance','FontSize',16);
title('PEG component fit','FontSize',20);

%Enter mass of pAA in each sample here
%pAAmass=[0;0;0;0;0;0;0;0;0;0;1;1;1;1;1;1;1;1;0.1;0.1;0.1;0.1;0.1;0.1;0.1;0
.1;0.1;0.25;0.25;0.25;0.25;0.25;0.25;0.25;0.25;0.25;0.5;0.5;0.5;0.5;0.5;0.5
;0.5;0.5;0.5;0.75;0.75;0.75;0.75;0.75;0.75;0.75;0.75;0.75];

%Enter mass of PEG in each sample here
%PEGmass=[1;1;1;1;1;1;1;1;1;1;0;0;0;0;0;0;0;0;0.9;0.9;0.9;0.9;0.9;0.9;0.9;0
.9;0.9;0.75;0.75;0.75;0.75;0.75;0.75;0.75;0.75;0.75;0.5;0.5;0.5;0.5;0.5;0.5
;0.5;0.5;0.5;0.25;0.25;0.25;0.25;0.25;0.25;0.25;0.25;0.25];

%The fraction of pAA per sample, by mass
%pAAfrac=pAAmass./(pAAmass+PEGmass)

%The pAA coefficient fraction for each sample
pAAcoeff=VpPi(:,1);
PEGcoeff=VpPi(:,2);
pAAcoeffrac=pAAcoeff./(pAAcoeff+PEGcoeff)

% Plot of pAA coefficient ratios along with quadratic fit.
xx=[-0.2:0.01:1.2];
%q=polyfit(pAAfrac,pAAcoeffrac(1:(nstan)),2);
q=polyfit(pAAfrac,pAAcoeffrac(1:(nstan)),2);
qfit=q(1).*xx.^2+q(2).*xx+q(3);
resFit=q(1).*pAAfrac.^2+q(2).*pAAfrac+q(3);
yresid = pAAcoeffrac(1:(nstan))-resFit;
SSresid = sum(yresid.^2);
SStotal = (length(pAAcoeffrac(1:(nstan))-1)) * var(pAAcoeffrac(1:(nstan)));
rsq=1-SSresid/SStotal
figure;
axes('FontSize',14);
plot(pAAfrac,pAAcoeffrac(1:(nstan)),'ob',xx,qfit,'-r')
xlabel('pAA fraction (by mass)','FontSize',16);
ylabel('pAA coefficient fraction','FontSize',16);
title('calibration curve','FontSize',20);
solve('pAAcoeffrac(8)=quadfity')
q

% pAA error percent
sum(sqrt((y1scal-Xg(:,1)).^2));
sum(sqrt((y1scal-Xg(:,2)).^2));


% % Solve for the pAA fraction
soln1a=(-q(2)+sqrt(q(2)^2-4*q(1)*(q(3)-pAAcoeffrac(55)*2)))/(2*q(1))
soln2a=(-q(2)+sqrt(q(2)^2-4*q(1)*(q(3)-pAAcoeffrac(56)*2)))/(2*q(1))
soln3a=(-q(2)+sqrt(q(2)^2-4*q(1)*(q(3)-pAAcoeffrac(57)*2)))/(2*q(1))
soln4a=(-q(2)+sqrt(q(2)^2-4*q(1)*(q(3)-pAAcoeffrac(58)*2)))/(2*q(1))
soln5a=(-q(2)+sqrt(q(2)^2-4*q(1)*(q(3)-pAAcoeffrac(59)*2)))/(2*q(1))
soln6a=(-q(2)+sqrt(q(2)^2-4*q(1)*(q(3)-pAAcoeffrac(60)*2)))/(2*q(1))
```

```
soln7a=(-q(2)+sqrt(q(2)^2-4*q(1)*(q(3)-pAAcoeffrac(61)*2)))/(2*q(1))
soln8a=(-q(2)+sqrt(q(2)^2-4*q(1)*(q(3)-pAAcoeffrac(62)*2)))/(2*q(1))
soln9a=(-q(2)+sqrt(q(2)^2-4*q(1)*(q(3)-pAAcoeffrac(63)*2)))/(2*q(1))
soln10a=(-q(2)+sqrt(q(2)^2-4*q(1)*(q(3)-pAAcoeffrac(64)*2)))/(2*q(1))
```

3.6.3 MATLAB Partial Least Squares (PLS) code (See hard drive for library files)

```
close all
%%%%%%%%%%%%%%%%%%%%%%%%%%%%%%%%%%%%%%%%%%%%%%%%%%%%%%%%%%%%%%%%%%%%%%%%%%%%%%%%
%%%%%%%%%%%%%%%%%%%%%%%%%%%%%%%%%%%%%%%%%%%%%%%%%%%%%%%%%%%%%%%%%%%%%%%%%%%%%%%%
%Tasks to complete? 0=no, 1=yes
%Reload data and clear all
task_load=0;
%Set/change frequency range
task_freq=1;
%Plot baseline shift corrected absorbance spectra of calibration
task_absplot=1;
%Outlier detection (Monte Carlo)
task_outlier=1;
%Remove outliers
task_remove=0;
%Partition between training and test data. Test model (Kennard-Stone)
task_ks=1;
%Moving window PLS
task_MW=0;
%Monte Carlo uninformative variable detection
task_MCUVE=0;
%Plot calibration spectra
task_calplot=1;
%Plot unknowns
task_unkplot=1;
%Cross validation of whole data set
task_CV=1;
%PLS model for whole set + solution for uknowns
task_PLS=1;

if task_load==1;
    clear all
    clc

    %number of calibration samples?
    ncal=54;

    %number of concentration sets?
    nset=6;

    %number of unknown samples?
    %nukn=12;
    nukn=10;

    %Number of latent variables?
    nLV=26;



%%%%%%%%%%%%%%%%%%%%%%%%%%%%%%%%%%%%%%%%%%%%%%%%%%%%%%%%%%%%%%%%%%%%%%%%%%%%%%%%

%%%%%%%%%%%%%%%%%%%%%%%%%%%%%%%%%%%%%%%%%%%%%%%%%%%%%%%%%%%%%%%%%%%%%%%%%%%%%%%%
    % Load data
```

```
    %%%%%%%%%%%%%%%%%%%%
    % Load the calibration data:

    % Input sections of the file names corresponsing to concentration,
    % replicate letter, date, and pAA fraction
    conc={'0to1','1to0','01to09','05to05','025to075','075to025'};
    samp={'1','2','3','4','5','6','7','8','9'};
    pAAfracLIST={0, 1, 0.1, 0.5, 0.25, 0.75};
    nsamp=length(samp);

    field1='conc';
    for i=1:nset
        for j=1:nsamp;
            value1(j+(i-1)*nsamp)=conc(i);
        end
    end

    field2='sample';
    value2=repmat(samp,1,nset);

    field3='pAAfrac';
    for i=1:nset
        for j=1:nsamp;
            value3(j+(i-1)*nsamp)=pAAfracLIST(i);
        end
    end


%This structure contains info on all spectra
info=struct(field1,value1,field2,value2,field3,value3);

exdata=load('C:\Users\Tanmingchee\Documents\FTIR@bakerLabs\pAAPEGonCaF2_MeO
H_spinCoating750rpm_042214_All\pAAPEGratio0to1_10mgml_1.CSV');

% Add spectra files to data matrix, while skipping over files which don't
exist
% Since not all concentration sets have the same number of spectra, some
% elements of struture 'info' do not correspond to spectra


j=0;
data=zeros(size(exdata,1),2,ncal);
pAAfrac=zeros(ncal,1);
for k=1:ncal;
 if
isequal(exist(['C:\Users\Tanmingchee\Documents\FTIR@bakerLabs\pAAPEGonCaF2_
MeOH_spinCoating750rpm_042214_All\pAAPEGratio'...
         info(k+j).conc '_10mgml_' info(k+j).sample '.CSV'],'file'),2);

data(:,:,k)=load(['C:\Users\Tanmingchee\Documents\FTIR@bakerLabs\pAAPEGonCa
F2_MeOH_spinCoating750rpm_042214_All\pAAPEGratio' ...
                info(k+j).conc '_10mgml_' info(k+j).sample '.CSV']);
```

```
            pAAfrac(k)=info(k+j).pAAfrac;
 else
     while
~exist(['C:\Users\Tanmingchee\Documents\FTIR@bakerLabs\pAAPEGonCaF2_MeOH_sp
inCoating750rpm_042214_All\pAAPEGratio'...
             info(k+j).conc '_10mgml_' info(k+j).sample '.CSV'],'file');
            j=j+1;


     end

data(:,:,k)=load(['C:\Users\Tanmingchee\Documents\FTIR@bakerLabs\pAAPEGonCa
F2_MeOH_spinCoating750rpm_042214_All\pAAPEGratio' ...
         info(k+j).conc '_10mgml_' info(k+j).sample '.CSV']);
      pAAfrac(k)=info(k+j).pAAfrac;

 end
end

    %%%%%%%%%%%%%%%%%%%%
    %Load the unknown data:

    % Again, input file name elements. These are for unknown (unknown
conc).
%     code={'0to1','1to0','01to09','05to05','025to075','075to025'};
%     sampU={'9'};
%
%     field1U='code';
%     value1U=code;
%     field2U='sample';
%     value2U=sampU;
%
%     infoU=struct(field1U,value1U,field2U,value2U);
%
%     for k=1:nukn;
%
dataU(:,:,k)=load(['C:\Users\Tanmingchee\Documents\FTIR@bakerLabs\pAAPEGonC
aF2_MeOH_spinCoating750rpm_042214_All\pAAPEGratio'...
%             infoU(k).code '_10mgml_' infoU(k).sample '.CSV']);
%     end
%
%
%     data=cat(3,data,dataU);

    sampU={'1','2','3'};

    field2U='sample';
    value2U=sampU;

    infoU=struct(field2U,value2U);

    for k=1:nukn;
        if k<=3;
```

```
dataU(:,:,k)=load(['C:\Users\Tanmingchee\Documents\FTIR@bakerLabs\pAA_g_PEG
onCaF2_MeOH_spinCoating750rpm_050614\'...
            '60-2-2_fr061313_1_10mgml_on050614_' infoU(k).sample '.CSV']);
%
dataU(:,:,k)=load(['C:\Users\Tanmingchee\Documents\FTIR@bakerLabs\pAA_g_PEG
onCaF2_MeOH_spinCoating750rpm_052714\'...
%             '60-2-2_10mgml_fr052714_1_' infoU(k).sample '.CSV']);
        % I added this below for additional samples - by Mingchee Tan
        elseif (k>3) && (k<7);

dataU(:,:,k)=load(['C:\Users\Tanmingchee\Documents\FTIR@bakerLabs\pAA_g_PEG
onCaF2_MeOH_spinCoating750rpm_120314\'...
            '60-2-025_fr090413_10mgml_on120314_'         infoU((k-3)).sample
'.CSV']);
        elseif (k>6) && (k<9);

dataU(:,:,k)=load(['C:\Users\Tanmingchee\Documents\FTIR@bakerLabs\pAA_g_PEG
onCaF2_MeOH_spinCoating750rpm_120314\'...
            '60-2-05_fr081913_10mgml_on120314_'          infoU((k-6)).sample
'.CSV']);
        else

dataU(:,:,k)=load(['C:\Users\Tanmingchee\Documents\FTIR@bakerLabs\pAA_g_PEG
onCaF2_MeOH_spinCoating750rpm_120614\'...
            '60-2-05_fr081913_10mgml_on120614_'          infoU((k-8)).sample
'.CSV']);
        end
    end


    data=cat(3,data,dataU);


%Smooth using moving average filter:
    for i=1:size(data,3)
        Xfilt_trans(i,:)=movavgFilt(transpose(data(:,2,i)),25,'Center');
    end
    Xfilt=transpose(Xfilt_trans);

%Smooth using golay filter:
    %Xall=sgolayfilt(data(:,2,:),3,13); %all absorbance values
    %Xall=sgolayfilt(data(:,2,:),3,7); %all absorbance values

    %Differentiate absorbance data (takes derivative)
    Xall=diff(Xfilt);
    Xallfreq=data(:,1,:); %all frequency values


end

if task_freq==1;
    %Create X matrix (absorbance data for calibration+unknown
```

```
    %Set wavenumber limits for fitting
    %Use units of wavenumbers
    wavenumber=data(:,1,1);
    minval=searchclosest(wavenumber, 1000);
    mincut=searchclosest(wavenumber, 1200);
    maxcut=searchclosest(wavenumber, 1500);
    maxval=searchclosest(wavenumber, 2000);
%
%     minval=searchclosest(wavenumber,830);
%     mincut=searchclosest(wavenumber,1500);
%     maxcut=searchclosest(wavenumber,1500);
%     maxval=searchclosest(wavenumber,3999)

    %Absorbance for calibration spectra
    %substract baseline by substracting min of "deadzone"
    ABSall=data(minval:maxval,2,1:ncal); %all calibration abs values
    FREQall=data(minval:maxval,1,1:ncal); %all calibration freq values
%     deadzoneMIN=searchclosest(FREQall(:,1),2060); %limits of "deadzone"
%     deadzoneMAX=searchclosest(FREQall(:,1),2250);
    %deadzoneMIN=searchclosest(FREQall(:,1),1950); %limits of "deadzone"
    %deadzoneMAX=searchclosest(FREQall(:,1),1950);
    for i=1:size(ABSall,3) %number of calibration spectra
        for j=1:size(ABSall,1); %number of frequencies
            ABScorr(j,1,i)=ABSall(j,1,i);                                  %-
min(ABSall(deadzoneMIN:deadzoneMAX,1,i));
        end
    end



    %Sum of absorbance values
    ABSsum=sum(ABScorr,1);
    ABSsum=transpose(squeeze(ABSsum)); %resize to match dim of y (pAA frac)

    %The y-values (known pAA frac) for the ncal spectra
    y=pAAfrac';



    %Apply wavenumber limits

    X=Xall([minval:mincut,maxcut:maxval],1:ncal);      %All      calibration
standards
    Xukn=Xall([minval:mincut,maxcut:maxval],(ncal+1):(ncal+nukn));      %all
unknowns

XfreqCAL=reshape(Xallfreq([minval:mincut,maxcut:maxval],1,1:ncal),length(X)
,ncal);
    %frequency values in chosen range

    %Save calibration spectra in .csv:
    % 1. wavenumber
    % 2. absorbance (all calibration spectra)
```

```
    cal_data=[XfreqCAL(:,1) X];
    dlmwrite('cal_spectra_diff.csv', cal_data);

end

if task_absplot==1;
    figure (1);
    plot(squeeze(FREQall),squeeze(ABScorr));
    xlabel('frequency (cm-1)','FontSize',16);
    ylabel('absorbance','FontSize',16);
    title('Baseline shift corrected calibration spectra','FontSize',20);
end

if task_outlier==1;
    %Outlier detection
    N=1000; %number of simulations
    ratio=50/65; %ratio of calibration samples to total samples (cal+test)
    MCS=mcs(X',y',nLV,'center',N,ratio);
    figure(4);
    plotmcs(MCS);
    title('Mean    of    prediction    error,    by    calibration    column
#','FontSize',20);

    figure(5); %Plot of mean error vs. pAA fraction
    plot(y,MCS.MEAN,'bo')
    xlabel('pAA fraction','FontSize',16);
    ylabel('mean error','FontSize',16);
    title('Mean    error    per    calibration    spectrum    vs.    pAA
fraction','FontSize',20);

    figure(6); %Plot of mean error vs absorbance sum (general intensity)
    plot(ABSsum,MCS.MEAN,'ro')
    xlabel('absorbance sum (spectral intensity)','FontSize',16);
    ylabel('mean error','FontSize',16);
    title('Mean error per calibration spectrum vs. abs sum','FontSize',20);
end


if task_remove==1;
  %Give index numbers of outlies to remove
  list=[4,6,9];
  %Delete these spectra from X
  X(:,list)=[];
  %Delete corresponding pAA frac from y
  y(:,list)=[];
  nremove=length(list);
else
    nremove=0;
end

%Rank calibration spectra by Kennard-stone algorithm
nCAL=12; %Number of calibration standards in calibration (not test) group
XTran=X'; %transpose of X
yTran=y'; %transpose of y
```

```
Rank=ks(XTran); %sort calibration standards into model and test groups
if task_ks==1;
    %Separate calibration and unknown values

    %Break up calibration spectra into calibration and test. We will
validate
    %the model make from calibration standards with test standards.

    A=XTran(Rank(1:nCAL),:); %Pick how many calibration standards for model
    Xcal=A'; %Xcal contains model spectra
    B=XTran(Rank(nCAL+1:(ncal-nremove)),:); %The rest of the spectra go to
test
    Xtest=B';
    C=yTran(Rank(1:nCAL),:); %partition off y (pAA frac) for calibration
    ycal=C';
    D=yTran(Rank(nCAL+1:(ncal-nremove)),:); %y for test
    ytest=D';

    CVcal=plscv(Xcal',ycal',nCAL-1,nCAL);
    figure(2);
    plot(CVcal.RMSECV,'bo-','linewidth',2)
    xlabel('number of latent variables','FontSize',16);
    ylabel('RMSECV','FontSize',16);
    set(gcf,'color','w');
    title('RMSECV for calibration set','FontSize',20);

    %Build model from calibration set.
    PLScal=pls(Xcal',ycal',nLV,'center');
    PLScal

    %Make predictions on test set using model from calibration set
    [ypred,RMSEP]=plsval(PLScal,Xtest',ytest');
    display('error from rest of calibration')
    RMSEP
    figure(3);
    plot(ytest,ypred,'.',ytest',ytest,'r');
    % showing values of sample prediction from calibration set
    xlabel('experimental','FontSize',16);
    ylabel('predicted','FontSize',16);
    title('Prediction power of model','FontSize',20);
end


if task_MW==1;
    %Moving window PLS. Use full set of calibration spectra (no partition)
    %This looks at the frequency dependence of the error for each latent
    %variable
    A=nLV; %choose number of LV's
    width=25; %frequency window size. Must be odd.
    [WP,RMSEF]=mwpls(X',y',A,width);
    figure(7)
    WPfreq=XfreqCAL(WP,1); %Convert window center index# to frequency
    plot(WPfreq,RMSEF(:,1:3)); %plot traces for first five LV's
    xlabel('frequency');
```

```
    ylabel('RMSEF');
    title('Error per frequency window for each latent variable');
    figure(8) %Plot the average over all latent variables
    avgRMSEF=mean(RMSEF,2);
    sumRMSEF=sum(RMSEF,2);
    plot(WPfreq,sumRMSEF);
    xlabel('frequency');
    ylabel('average RMSEF');
    title('Sum of error per frequency window for all latent variables');
end

if task_MCUVE==1;
    %Monte-Carlo Uninformative Variable Elimination (MC-UVE)
    A=nLV; %number of LV to use in PLS
    method='center'; %data pretreatment
    N=1000; %number of simulations
    ratio=50/65; %ratio of calibration samples to total samples (cal+test)
    UVE=mcuvepls(Xcal',ycal',A,method,N,ratio);
    figure(9)
    plot(XfreqCAL,abs(UVE.RI),'linewidth',2);
    xlabel('frequency');
    ylabel('reliability index');
    title('Reliability indes versus frequency')
end

if task_calplot==1;
    %Plot data
    %Plot the calibration spectra
    figure(10);


    %Coding the line color to the pAA fraction
    colormap(cool);
    map=colormap(cool);
    for i=1:length(y);
        if y(i)/max(y)==0
        intensity(i)=1;
        else
        intensity(i)=round(y(i)/max(y)*length(map));
        end
    end
    colorLINE=map(intensity,:);
    for i=1:length(y);
    ColorVal(i)={colorLINE(i,:)};
    end

    p=plot(XfreqCAL,X,'LineWidth',1.2);
    set(gcf,'color','w');
    set(p,{'color'},ColorVal');
    caxis([0,1]);
    colorbar('location','EastOutside');
    xlabel('frequency','FontSize',16);
    ylabel('absorbance','FontSize',16);
    title('Calibration spectra','FontSize',20);
```

```
end

if task_unkplot==1;
    %Plot the unknown spectra
    %Figure 3

XfreqUKN=reshape(Xallfreq([minval:mincut,maxcut:maxval],1,ncal+1:ncal+nukn)
,length(X),nukn);
    figure(11);
    plot(XfreqUKN,Xukn,'LineWidth',1.2);
    set(gcf,'color','w');
    xlabel('frequency','FontSize',16);
    ylabel('absorbance','FontSize',16);
    title('unknown spectra','FontSize',20);
end


%%%%%%%%%%%%%%%%%%%%%%%%%%%%%%%%%%%%%%%%%%%%%%%%%%%
%Decide the number of latent variables
%Figure 4

F=XTran(Rank(1:end),:); %Sort spectra by KS algorithm ranking calc above
X=F'; %X is re-ordered
G=yTran(Rank(1:end),:); %sort y (pAA frac) by KS ranking
y=G';

if task_CV==1;
    CV=plscv(X',y',ncal-1,ncal);   %by default, 'center' is used for data
pretreatment inside plscv.m.
    figure(12);
    plot(CV.RMSECV,'bo-','linewidth',2);
    xlabel('number of latent variables','FontSize',16);
    ylabel('RMSECV','FontSize',16);
    set(gcf,'color','w');
    title('RMSECV','FontSize',20);
end

if task_PLS==1;
    %%%%%%%%%%%%%%%%%%%%%%%%%%%%%%%%%%%%%%%%%%%%%%%%%%%
    %Build PLS model
    %Figure 5
    PLS=pls(X',y',nLV,'center'); % mean centering, alters first derivative
numbers such that equal number of positive and negative
    figure(13);
    plot(y,PLS.y_fit,'bo',y,y,'r-','LineWidth',1.2)
    xlabel('measured pAA frac','FontSize',16);
    ylabel('PLS y fit','FontSize',16);
    set(gcf,'color','w');
    title('Meas pAA frac vs PLS prediction','FontSize',20);

    %%%%%%%%%%%%%%%%%%%%%%%%%%%%%%%%%%%%%%%%%%%%%%%%%%%
    %Prediction
    plsval(PLS,Xukn',nLV)
    % Fit of calibration standards with model
```

```
    PLS.R2
end
```

CHAPTER 4

IN VITRO AND IN VIVO EVUALATION OF pAA-*g*-PEG AS BOUNDARY LUBRICANT FOR TREATMENT OF OSTEOARTHRITIS

4.1 Introduction

Osteoarthritis (OA) is a leading cause of disability in adults caused by acute, chronic or progressive damage to the tissues surrounding joints such as the knees, hips or ankles[1]. in the United States, there were 27 million adults with OA in 2003[2] and this population is expected to grow to 67 million people by 2030[3]. In 2005, the annual health care burden of OA exceeded $185 billion[4] and the costs will continue to increase due to an aging population and increasing obesity rates.

Current pharmacologic treatments of OA include non-steroidal anti-inflammatories[5], intra-articular corticosteroid injections[6], and chondroitin sulfate or glucosamine supplements[7]; however, they have little or no effect on disease progression. A more recent approach to the treatment of OA involves the use of injectable lubricants to minimize friction and tissue damage. A common approach involves the intra-articular injection of the natural synovial glycosaminoglycan, hyaluronic acid (HA)[8], also known as HA viscosupplementation. HA increases synovial fluid viscosity, effectively altering lubrication mode toward mixed or hydrodynamic lubrication[10]. However, the mode of lubrication with the highest friction coefficients and incidence of wear is boundary lubrication, where opposing normal forces are high. Further, the efficacy of HA injections are a topic of continued debate, with studies showing only transient effects on pain relief[9] that are minimally better than placebo[10] and inconsistent evidence of benefit in radiographic assessment of disease progression[11].

More recently, there has been great interest in understanding the role of the natural synovial fluid glycoprotein, lubricin, in joint lubrication. Lubricin acts directly as a boundary lubricant[12] by binding to the cartilage surface[13] and appears to interact with HA to enhance cartilage lubrication in multiple lubrication modes[14–16]. However, in damaged or aging cartilage, chondrocyte production of lubricin is compromised and boundary mode lubrication is reduced[15]. Intra-articular injection of supplemental lubricin, as well as the truncated recombinant lubricin construct LUB:1, slows progression of OA in rat models of disease[16,17]. However, to date, the large-scale recombinant manufacture of both lubricin and LUB:1 remains challenging owing to multiple amino acid repeats in the protein core, as well as the high degree of glycosylation[13,18].

The potent boundary mode lubricating ability of lubricin stems from two key molecular features: its C-terminus and its central mucin domain. The C-terminus facilitates lubricin binding to fibronectin and collagen on the cartilage surface[13,19]. The mucin domain is a high-density oligosaccharide brush segment that attracts and retains water in a hydrogen-bonded network[19,20]. Collectively, these two molecular structures work in tandem to trap water proximally to the cartilage surface. The network of lubricin molecules across the articular surface of cartilage promotes the formation of a thin aqueous film to facilitate lubrication under boundary mode conditions[21].

Since lubricin's lubricating ability depends on its brush-like structure consisting of the aforementioned long mucin domain with hydrophilic side chains, our hypothesis is that lubricin is comparable to brush polymers in structure and function[19,20]. Herein, we report (1) the synthesis of brush polymers with analogous structures to lubricin, (2) in vitro binding and lubrication of polymers on cartilage explants and (3) efficacy of intra-articular polymer

treatments in a rat OA model. The polymers binding time constant was found to significantly lower than synovial clearance time by 15 times, allowing efficient binding. Both in vitro and in vivo results demonstrated significant reduction in friction compared to unlubricated controls as well as significantly reducing cartilage degradation. The chondroprotective qualities of this polymer can be compared to recombinant lubricin such as LUB:1 designed by the pharmaceutical company Wyeth[17] and even full-length lubricin as investigated by the Gregory Jay of Brown University[22]. In addition, the synthetic scheme allows a simple, well-controlled method to produce lubricin-mimetic polymers at high volumes, bypassing the difficulties of lubricin biosynthesis.

4.2 Materials and Methods

4.2.1 Materials.

Acrylic acid (AA, 99.5%) stabilized with 200 ppm 4-methoxyphenol, methanol (99.8%) and sodium borate buffer were obtained from VWR (Radnor, PA, USA). 4,4'-azobis-(4-cyanopentanoic acid) (A-CPA), Dulbecco's 10X Phosphate buffered saline (PBS), sodium chloride (NaCl, >99.5%), 4-cyano-4-(phenylcarbonothioylthio)pentanoic acid (CPA-DB) (>97% HPLC) and fluorescein-5-thiosemicarbazide (~80%) was obtained from Sigma-Aldrich (St. Louis, MO, USA). Methoxy-poly(ethylene glycol)-amine powder (PEG-NH_2) was obtained from Jenkem Technologies (Beijing, PRC) and 4-(4,6-dimethoxy-1,3,5-triazin-2-yl)-4-methylmorpholinium chloride (DMTMM) was from TCI America (Portland, OR, USA). Knee joints of 1-3 day old calves were purchased from a local slaughterhouse. All chemicals were used as received unless otherwise specified.

4.2.2 Synthesis and characterization of poly(acrylic acid) backbone (pAA).

Polyacrylic acid was synthesized by RAFT polymerization using acrylic acid (AA), A-CPA as initiator (I) and CPA-DB as chain transfer agent (CTA) under anhydrous, airtight and dark conditions in methanol. AA concentration was maintained at ~3.8 mM, while [AA]:[I]:[CTA] was 762:0.25:1. The general reaction scheme is as follows: AA was added to a flame dried 5 ml brown ampule to which CPA-DB dissolved in 2.9 ml of nitrogen-purged methanol was added, followed by A-CPA dissolved in 0.7 ml of nitrogen-purged methanol. Nitrogen gas was bubbled through the reaction mixture to prevent oxygen influx. The ampule was flamed sealed and placed in a 60^{o}C oil bath for 48 hours. Ampule was then broken and cooled in ice bath. The solution was diluted with water, dialyzed against deionized water for 3 days, and then lyophilized to obtain a white, waxy powder. Characterization: ^{1}H NMR (INOVA 400 MHz, D_2O, ppm): δ1.5-2.0 (pAA-CH_2-), δ 2.25-2.75 (pAA-CH-). Molecular weight determined by Waters gel permeation chromatography (GPC) system (Waters 1515 Isocratic HPLC Pump, Waters 2414 Refractive Index Detector) using poly(methacrylic acid) standards and phosphate buffered saline (pH 7.4) as the mobile phase at 30^{o}C.

4.2.3 Synthesis of pAA-*g*-PEG polymer brushes.

The pAA-*graft*-PEG (pAA-*g*-PEG) copolymer was synthesized by polymer analogous conjugation of monoamine-functionalized PEG to the pAA backbone using DMTMM as the coupling agent. pAA is dissolved in 0.1 M borate buffer (pH 8.5) at 3.3 mg/ml, while [AA]:[DMTMM]:[PEG] is 1:2:2. The general reaction is as follows: pAA and PEG-amine were dissolved in 3 ml borate buffer in a 10 ml flask with magnetic stir bar. DMTMM dissolved in in 0.6 ml borate buffer was added drop-wise into flask with the final pH adjusted

to 6-7 using 1 N HCl. The end polymer was called pAA(60)-2-PEG(2) (60,000 g/mol pAA; grafting ratio 2; 2,000 g/mol PEG). Each conjugation reaction was conducted for 24 hours at room temperature, dialyzed against deionized water for 3 days and lyophilized to obtain a white powder. Molecular weight was characterized by a multi-angle laser light scattering size exclusion chromatography (MALLS/SEC) performed at Biophysics Resource of Keck Facility at Yale University.

4.2.4 Bovine cartilage preparation & in vitro evaluation of pAA(60)-2-PEG(2).

For both kinetics and dose response experiments, cartilage plugs were taken from the patellofemoral groove of 1-3 day old bovine calves. Native lubricin was removed from the plugs using a 1.5 M NaCl solution. pAA(60)-2-PEG(2) were tagged with fluorescein-5-thiosemicarbazide via DMTMM chemistry in ~0.1M borate buffer (pH 8.5) following a similar protocol to PEG conjugation onto pAA but without pH adjustment. The tagged polymer was dissolved in saline and cartilage plugs were incubated in these solutions. Following the incubation, the plugs were rinsed twice with saline to remove any unbound lubricants from the articular surface and then imaged with a Zeiss 710 confocal microscope.

In parallel, cartilage plugs denuded and incubated in solutions of pAA(60)-2-PEG(2)were loaded into our custom tribometer[13] to determine their frictional behavior. A 40% compressive normal strain was induced on each cartilage plug, and 60 minutes was allowed for the hydrostatic pressure within the porous tissue to equilibrate. The tribometer then linearly oscillated each plug in a saline solution at a speed of 0.3 mm/s.

To assess binding kinetics, cartilage plugs were incubated in a 3mg/ml pAA(60)-2-PEG(2)solution for incubation times of 0, 15, 30, 60, 90, and 120 min. For dose response

experiments, plugs were incubated for 120 min in lubricin-mimetic solutions of 0.03, 0.1, 0.3, 1, and 3 mg/ml. Binding kinetics were assessed by measuring fluorescence intensity as a function of time and fitting this data to a first order binding model of the form $Z = A - Be^{(-t/\tau)}$. Where *Z* is fluorescence (AU), *A* is final fluorescence, (*A*-*B*) is initial fluorescence, *t* is time, and τ is binding time constant.

4.2.5 Rat model of OA & in vivo evaluation of pAA-*g*-PEG.

The pAA(60)-2-PEG(2)'s were sterilized in 95% ethanol for ~0.5 hours and then dried, lyophilized and re-suspended in saline at 3 mg/ml. The anterior cruciate ligament (ACL) of each hind leg was transected in 11 Sprague-Dawley rats. Starting one week post-surgery, 50 µl of pAA-*g*-PEG solutions were injected intra-articularly into one knee, with the contralateral receiving a saline vehicle. The injections were repeated once per week for 3 weeks, and rats were sacrificed 3 weeks after the final injection. All animal studies were conducted in compliance with the Institutional Animal Care and Use Committee. Legs from six rats were examined histologically, while the other five were mechanically evaluated through tribometry and profilometry. Histologic samples were decalcified, embedded, sectioned, and stained with safranin-O. For mechanical evaluation, 3 mm cartilage samples were taken from the tibial plateau, one each from the medial and lateral compartments. Samples were loaded into a custom tribometer to determine their frictional behavior[13]. A compressive normal stress of 250-300 kPa was induced on each tibial plug and 60 minutes was allowed for the hydrostatic pressure within the tissues to equilibrate. The tribometer then linearly oscillated each explant in a saline solution at speeds of 0.1, 0.3, 1, 3, and 10 mm/s.

To observe roughening of cartilage, each tibial was then imaged on an ADE Phase Shift MicroXAM optical interferometric profiler and height measurements were taken over three different 849 μm x 631 μm scans. Histograms of the measured heights at each pixel of the scanned image were made. The deviations of these histograms are the surface roughness measure S_q.

4.3 Results and Discussion

4.3.1 Polymer Synthesis & Characterization.

To mimic the molecular composition and function of native lubricin, brush-like copolymers were designed and synthesized to impart both cartilage binding and hydrogen bonding domains. Specifically, polyethylene glycol (PEG) chains were grafted to a poly(acrylic acid) (pAA) core to mimic the central mucin domain of lubricin and the thiol terminus to allow binding to cartilage (**Fig 4.1a**). A library of 27 polymers in total were produced investigating the parameters of pAA sizes, PEG sizes and grafting ratios of PEG:AA (See chapter 1). In collaboration with the Bonassar Lab, several polymer were tested on their tribological equipment. However, one set of paramaters demonstrated the greatest efficacy in boundary lubrication and hence become the sole topic of this chapter.

The synthesis of the lubricin mimetic was carried out using a robust, two-step synthesis. The pAA backbone was polymerized via RAFT polymerization of acrylic acid (AA) to produce a polymer M_n of 60,000 with a polydispersity of ~1.3 (**Fig 4.1b**). The pAA was conjugated with methoxy-PEG-amine (M_n 2,000) using DMTMM as the condensing agent (**Fig 1c**) with a final a M_n of $1.4*10^6$ with 80% degree of PEG substitution to the pAA backbone. The resulting polymer is called pAA(60)-2-PEG(2) following the assigned

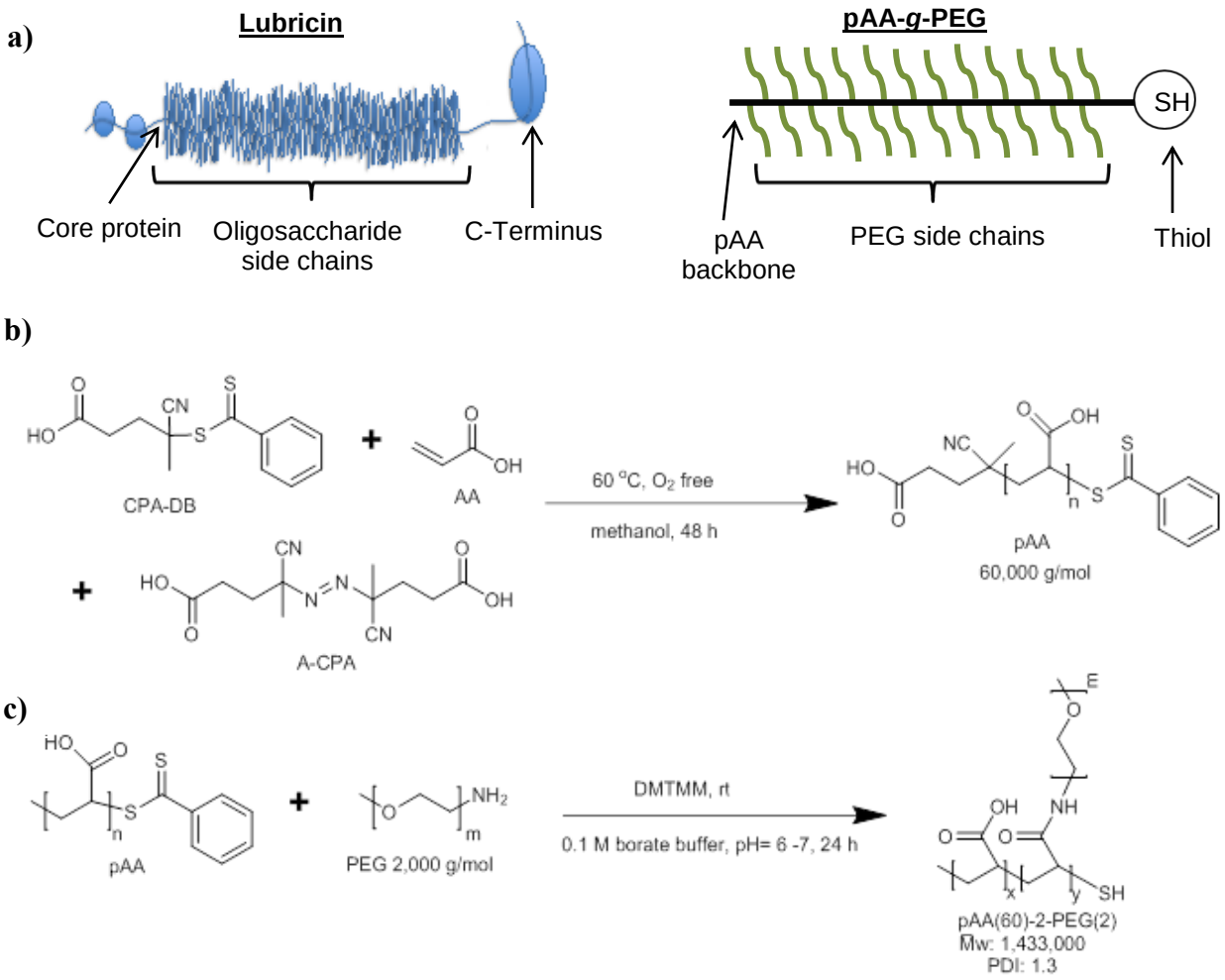

Figure 4.1: a) The design of pAA-*g*-PEG mimics the general structure of lubricin following the hypothesis that the lubrication properties is due to brush-like shape. In particular, the polymer pAA backbone, hydrophilic PEG side chains and thiol functional group mimics lubricin's core protein backbone, oligosaccharide chains and C-terminus respectively. **b)** RAFT polymerization of acrylic acid to produce poly(acrylic acid) (pAA). Molecular weight was determined done using aqueous SEC with poly(methacrylic acid) standards. **c)** Condensation chemistry with pAA and PEG using DMTMM to yield a statistical graft copolymer called poly(acrylic acid)-*graft*-PEG or pAA(60)-2-PEG(2). Aqueous MALLS/SEC was used to determine absolute molecular weight of pAA-*g*-PEG.

nomenclature for the polymer brushes of pAA(*a*)-*gr*-PEG(*b*), where *a* and *b* are molecular weights of pAA and PEG respectively, and *gr* is the grafting ratio defined by the moles of PEG grafted to the pAA backbone divided by the moles of AA monomers in the pAA backbone. Both of the polymer materials applied are biocompatible and are used extensively in the biomedical field. The success of this research has to potential to overcome the barriers associated with lubricin production and provide a powerful, simple therapeutic for the treatment of OA.

4.3.2 Evaluation of in vitro treatments.

To quantify the binding kinetics of pAA(60)-2-PEG(2) to cartilage, denuded bovine cartilage plugs were immersed in a solution of the polymer over various incubation times (**Fig 4.2a,c**). The pAA(60)-2-PEG(2) bound to the cartilage surfaces with a first order binding time constant of 16±1 min, reaching a maximum saturation after about 60(±2) min of incubation. Similarly, cartilage friction coefficients, measured under boundary mode conditions, decreased as incubation time increased with a first order time constant of 20±1 min, reaching a minimum friction coefficient after about 60(±2) min of exposure. These are encouraging results, considering that the synovial clearance times for synovial fluid (about 5 hrs)[23] is an order of magnitude larger than the reported binding constants. So, injected pAA(60)-2-PEG(2) would bind to cartilage surfaces long before being expelled from the joint. Furthermore, overall friction coefficients decreased from μ=0.28±0.01 for denuded cartilage (cartilage surfaces without lubricin or pAA(60)-2-PEG(2)) to μ=0.14±0.02 for cartilage surfaces saturated with pAA(60)-2-PEG(2) demonstrating its efficacy as a boundary lubricant.

As a comparison, the coefficient of friction for similar systems saturated with lubricin is about $\mu=0.10\pm0.01$[12] (**Fig 4.2b**).

Dose response experiments were conducted using a constant incubation time while varying the lubricin-mimetic concentrations in which the cartilage plugs were incubated. The pAA(60)-2-PEG(2) both bound to and lubricated cartilage surfaces similarly to a first order binding model with a K_D and an EC_{50} = 1.3 mg/ml (r^2=0.98, RMSE=0.005) (**Fig 4.2d**) The EC_{50} of lubricin is 11μg/ml[12]. Currently, saturation has not yet been observed for dosage suggesting a possible enhancement of lubrication at higher concentrations beyond those tested thus far.

We synthesized brush-like polymers with analogous structures to lubricin that rapidly bound to and effectively lubricated articular cartilage surfaces. Relatively low binding constants underscore the therapeutic potential of the pAA-*g*-PEG in that they may be able to bind to the cartilage surface well before being expelled from the joint. Additionally from these binding studies, lubrication was correlated with the amount of polymer bound to the surface (r=0.98), suggesting a dose-dependent effect for lubricant binding and function. Furthermore, the significant drop in friction for the pAA-*g*-PEG treated cartilage was comparable to that of lubricin and greater than that of the truncated lubricin mutant LUB:1 (**Fig 4.2c)**, both of which have demonstrated chondroprotection in rat OA models[17,22]. Collectively, these results imply that pAA-*g*-PEG will effectively bind to and lubricate cartilage surfaces in vivo with potential chondroprotective results.

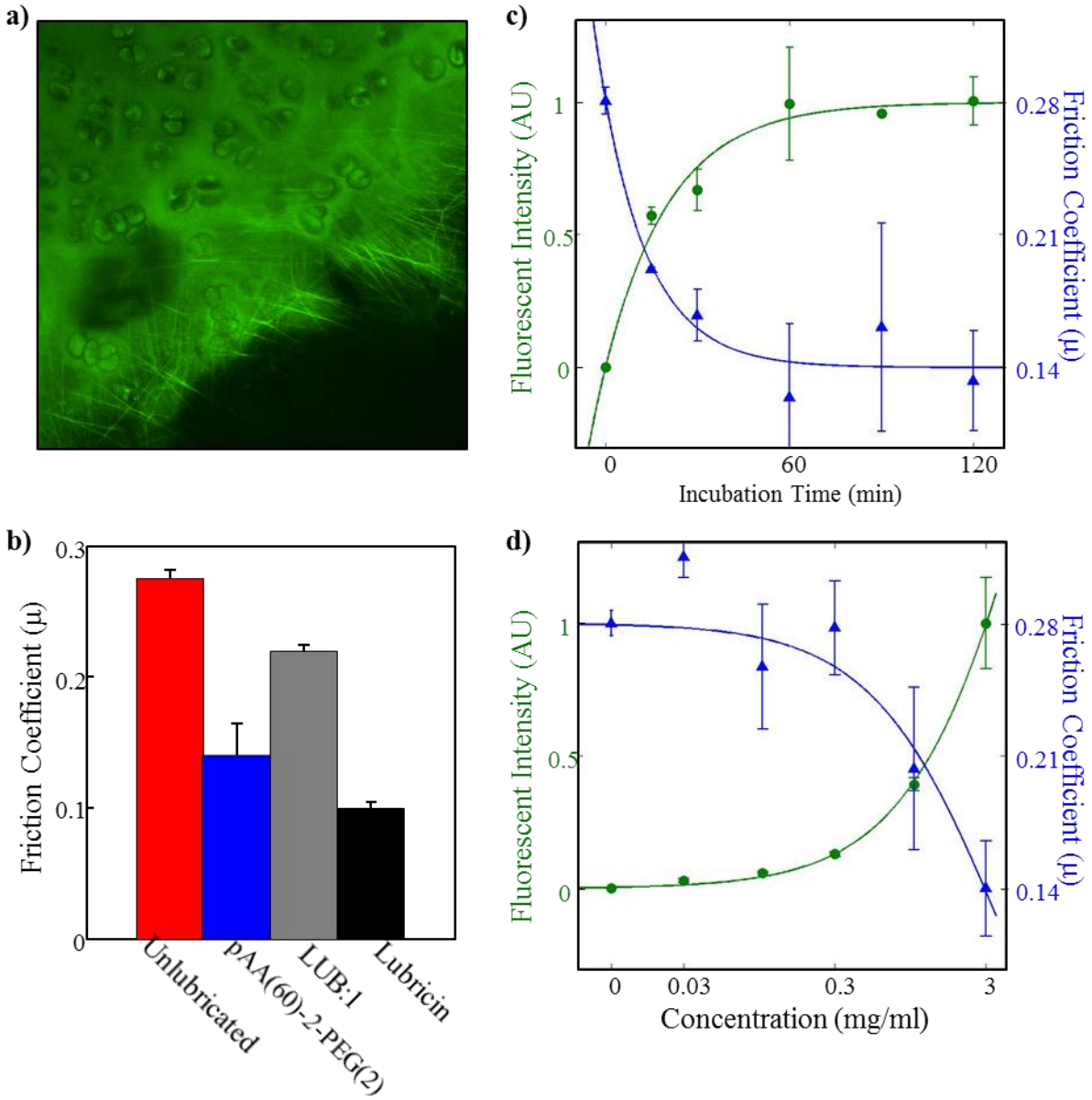

Figure 4.2: a) The image above shows fluorescently-tagged pAA(60)-*2*-PEG(2) (green) bound to cartilage surfaces. **b)** The pAA(60)-*2*-PEG(2) effectively lubricated cartilage surfaces ($p<0.05$). More effective than LUB:1 but not lubricin. **c)** The biomimetic lubricants quickly bound to cartilage surfaces following first-order behavior (τ=16 min). **d)** dose-dependent behavior for both binding and lubrication. At 3 mg/ml, saturation points have yet to be reached.

4.3.3 Mechanical and histological evaluation of in vivo treatment.

The chondroprotective ability of the pAA(60)-2-PEG(2) was assessed using the widely-used anterior cruciate ligament transection (ACLT) model for OA in the rat knee[16,17,22,24,25]. The ACL of each hind leg of eleven Sprague-Dawley rats was transected. One limb of each rat was intraarticularly treated with a saline vehicle, while the contralateral received injections of a pAA(60)-2-PEG(2) solution. Plugs from the tibial plateaus of 6 of the rats were mechanically evaluated through friction testing and optical profilometry. Friction coefficients of the tibial plugs from the pAA(60)-2-PEG(2) treated group were similar to those from healthy rats that had not undergone the ACLT procedure, and significantly lower than those from the saline-treated group (**Fig 4.3a**). The cartilage surfaces of the saline control group were significantly rougher than that of the lubricin-mimetic-treated group as well as the healthy group (**Fig 4.3b,c,d**). Thus, the pAA(60)-2-PEG(2) was able to preserve the lubricating ability and the morphology of the cartilage surface.

Histological grading was done for both the tibial and femoral surfaces of each joint of five rats using the OARSI scoring system[26] (**Fig 4.4**). No differences were seen in the scores of the tibial surfaces. However, in the femoral surfaces safranin-O staining of the histologic specimens revealed the presence of articular cartilage lesions, associated subchondral bone remodeling, evidence of significant proteoglycan loss, and focal regions of hypertrophy and cloning in the meniscus in the saline controls. In contrast, knees receiving injections of the pAA(60)-2-PEG(2) minimal changes in the articular surface, bone, or meniscus morphology and maintained healthy columnar cell arrangement throughout the cartilage. The OARSI score of each pAA(60)-2-PEG(2) treated distal femur was lower than that of the contralateral. The mean score of the femoral surfaces of the saline control group was a 4.0, corresponding to the

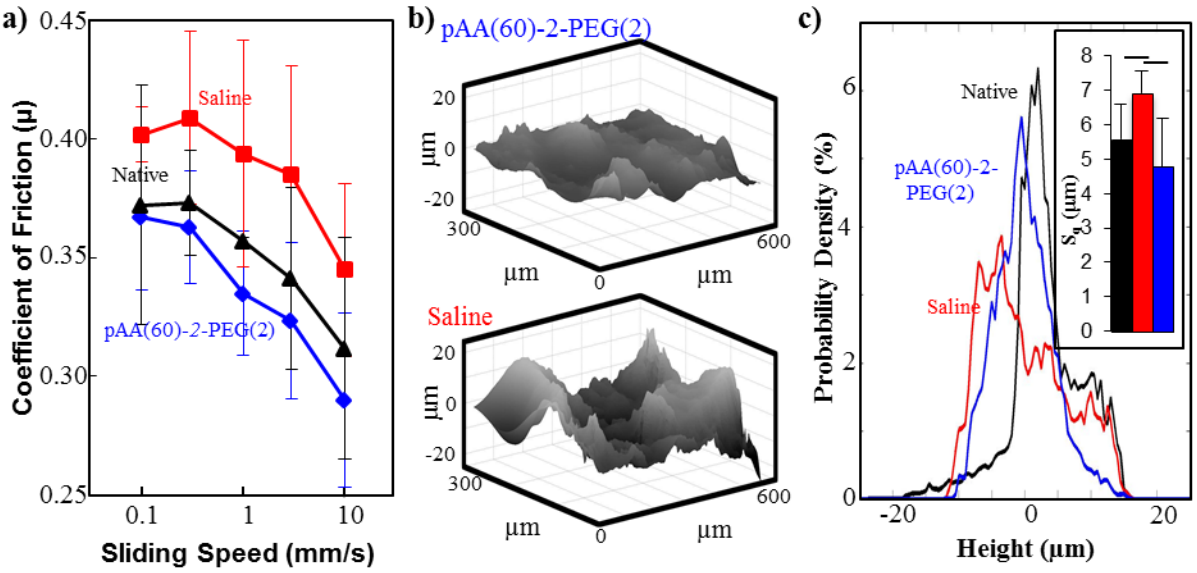

Figure 4.3. a) Intraarticular treatments with lubricin-mimetics preserved the low-friction bearing surface of the joint, evidenced by significantly lower friction coefficients for the polymer-treated group compared to saline-treated controls, $p<0.001$. The frictional behavior of the polymer-treated joints were similar to that seen in uninjured native joints. **b-c)** Intraarticular treatments with lubricin-mimetics also demonstrated chondroprotection by maintaining the smooth articular surface. Topographic images of the articular surfaces sample taken via optical profilometry showed narrower height distributions for polymer-treated cartilage compared to the saline-treated controls. The roughness of polymer-treated cartilage was similar to uninjured native surfaces.

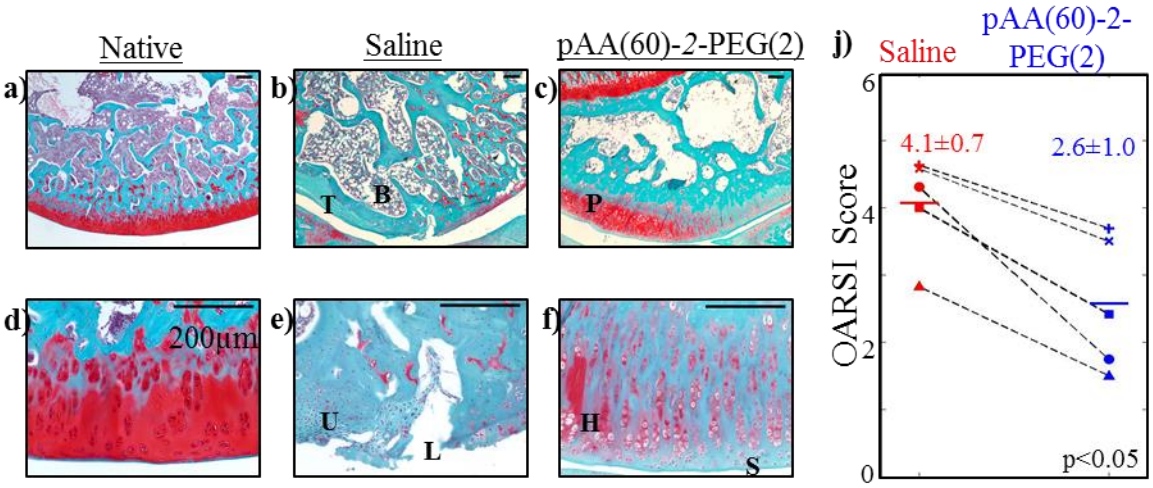

Figure 4.4. a-f) Chondroprotection by intraarticular treatments with lubricin-mimetics was evident in safranin-O stained histology. The polymer-treated joints showed better retention of proteoglycans (P) while maintaining a relatively intact and undisturbed articular surface (S). The saline-treated controls had large cartilage lesions (L), cartilage thinning (T) and morphologic subchondral bone changes (B), characteristic of advanced OA. Cells in the polymer-treated joints had healthy morphology and columnar arragement (H) similar to that in uninjured native joints. Cells in the saline-treated controls were unhealthy and near apoptotic (U). **j)** Chondroprotection by the pAA(60)-2-PEG(2) treatments were quantified through OARSI scoring of each distal femur surface. Joints from the same rat are shown connected by dashed lines. Treatment group with pAA(60)-2-PEG(2) had lower OARSI scoring compared to saline control (2.6 vs 4.1, $p<0.05$).

complete removal of the superficial zone of the cartilage as well as partial erosion of the middle zone. In contrast, the mean score for the femoral surfaces of the pAA(60)-2-PEG(2) treated group was 2.5, corresponding to some disruption of the articular surface. This amounts to a 37.5% mean reduction in OARSI score compared to control; in comparison Teeple et al. by supplementing ACLT rats with either lubricin or lubricin+HA reduced mean OARSI scores by 15% and 32% respectively[24] suggesting that supplementation of pAA(60)-2-PEG(2) is comparable to lubricin +HA in chondroprotection in rat ACLT models.

pAA(60)-2-PEG(2) prevented the progression of cartilage degeneration when introduced into ACL transected rat knees. Intraarticular injection of pAA(60)-2-PEG(2) prevented changes in cartilage, bone, and meniscus, functionally manifest in lower tissue roughness and friction coefficient. Notably the biggest cartilage changes were on the femoral condyles, yet roughening and changes in friction coefficient occurred on tibial cartilage.

Local administration of the pAA(60)-2-PEG(2) appeared to be therapeutically effective in preventing cartilage degeneration. The decrease in coefficients of friction for the pAA(60)-2-PEG(2) treated group compared to the saline-treated group was $\Delta\mu=0.05$. Similar frictional changes have been seen between healthy and ACL-deficient joints as well as lubricin-deficient and wildtype rats ($\Delta\mu=0.03$[24] and 0.04[27], respectively). The introduced synthetic lubricants maintained levels of lubrication that have been previously observed in healthy, lubricin-rich joints. The lower friction coefficients in pAA(60)-2-PEG(2) treated joints are consistent with the idea that cartilage degeneration is being mitigated, and the articular surface minimally disturbed. Such changes suggest that the injected lubricants not only bound to the cartilage but prevented surface roughening and perhaps prevented loss of endogenous lubricants.

The cartilage surfaces of the polymer treated group were smoother that those of the PBS treated group, having less variation in measured height across the surface. The relative smoothness is an indicator of preservation of cartilage health and also provides a lower friction bearing surface which will slow any degeneration through wear. Furthermore, histologic analysis of rat knees treated with the pAA(60)-2-PEG(2) compare favorably to histologic results from similar studies using the truncated lubricin mutant LUB:1[17] and full length lubricin[16,22,24,28] at preventing the formations of cartilage lesions and hypertrophy. No gross damage to the articular cartilage or subchondral bone was observed in the histologic specimens for the polymer-treated group, which suggests that the pAA(60)-2-PEG(2) could be used as a potential therapy to treat degenerative diseases such as OA.

4.4 Conclusion

A polymer was synthesized mimicking the structure and function of lubricin as a boundary lubricant for the potential treatment of osteoarthritis. Composed of pAA grafted with PEG called it is called pAA-*g*-PEG or pAA(60)-2-PEG(2) (60,000 g/mol pAA; grafting ratio 2; 2,000 g/mol PEG). In vitro boundary lubrication tests demonstrated significant reduction in coefficient of friction compared to control, greater even that of LUB:1 and a binding time constant that is ~15 times less than that of synovial clearance time. In vivo studies of pAA(60)-2-PEG(2) in rat models of OA also demonstrated significant reduction in friction compared to untreated resembling the friction of healthy cartilage and in OARSI histology grading. Overall, the polymer pAA(60)-2-PEG(2) demonstrates excellent boundary lubrication and chondroprotection of cartilage in rat models of OA.

4.4 References

1. Guccione, A. The effects of specific medical conditions on the functional limitations of elders in the Framingham Study. *Am. J. Public Health* **84,** 351–358 (1994).

2. Lawrence, R. C. *et al.* Estimates of the prevalence of arthritis and other rheumatic conditions in the United States. Part II. *Arthritis Rheum.* **58,** 26–35 (2008).

3. Hootman, J. M. & Helmick, C. G. Projections of US prevalence of arthritis and associated activity limitations. *Arthritis Rheum.* **54,** 226–9 (2006).

4. Kotlarz, H., Gunnarsson, C. L., Fang, H. & Rizzo, J. a. Insurer and out-of-pocket costs of osteoarthritis in the US: evidence from national survey data. *Arthritis Rheum.* **60,** 3546–53 (2009).

5. Scott, D. L. *et al.* The long-term effects of non-steroidal anti-inflammatory drugs in osteoarthritis of the knee: a randomized placebo-controlled trial. *Rheumatology (Oxford).* **39,** 1095–101 (2000).

6. Arroll, B. & Goodyear-Smith, F. Corticosteroid injections for osteoarthritis of the knee: meta-analysis. *BMJ* **328,** 869 (2004).

7. Sinusas, K. Osteoarthritis: diagnosis and treatment. *Am. Fam. Physician* **85,** 49–56 (2012).

8. Mabuchi, K., Tsukamoto, Y., Obara, T. & Yamaguchi, T. The effect of additive hyaluronic acid on animal joints with experimentally reduced lubricating ability. *J. Biomed. Mater. Res.* **28,** 865–70 (1994).

9. Bannuru, R. R., Natov, N. S., Dasi, U. R., Schmid, C. H. & McAlindon, T. E. Therapeutic trajectory following intra-articular hyaluronic acid injection in knee osteoarthritis--meta-analysis. *Osteoarthritis Cartilage* **19,** 611–9 (2011).

10. Chang, K.-V., Hsiao, M.-Y., Chen, W.-S., Wang, T.-G. & Chien, K.-L. Effectiveness of intra-articular hyaluronic acid for ankle osteoarthritis treatment: a systematic review and meta-analysis. *Arch. Phys. Med. Rehabil.* **94,** 951–60 (2013).

11. Jubb, R., Piva, S., Beinat, L., Dacre, J. & Gishen, P. A one-year, randomised, placebo (saline) controlled clinical trial of 500-730 kDa sodium hyaluronate (Hyalgan) on the radiological change in osteoarthritis of the knee. *Int. J. Clin. Pract.* **57,** 467–474 (2003).

12. Gleghorn, J. P., Jones, A. R. C., Flannery, C. R. & Bonassar, L. J. Boundary mode lubrication of articular cartilage by recombinant human lubricin. *J. Orthop. Res.* **27,** 771–7 (2009).

13. Jones, A. & Gleghorn, J. Binding and localization of recombinant lubricin to articular cartilage surfaces. *J. Orthop. Res.* **12,** 10–12 (2007).

14. Das, S. *et al.* Synergistic interactions between grafted hyaluronic acid and lubricin provide enhanced wear protection and lubrication. *Biomacromolecules* **14,** 1669–77 (2013).

15. Elsaid, K. a *et al.* The impact of forced joint exercise on lubricin biosynthesis from articular cartilage following ACL transection and intra-articular lubricin's effect in exercised joints following ACL transection. *Osteoarthritis Cartilage* **20,** 940–8 (2012).

16. Jay, G. D. *et al.* Prevention of cartilage degeneration and restoration of chondroprotection by lubricin tribosupplementation in the rat following anterior cruciate ligament transection. *Arthritis Rheum.* **62,** 2382–91 (2010).

17. Flannery, C. R. *et al.* Prevention of cartilage degeneration in a rat model of osteoarthritis by intraarticular treatment with recombinant lubricin. *Arthritis Rheum.* **60,** 840–7 (2009).

18. Jay, G. D. Lubricin and surfacing of articular joints. *Curr. Opin. Orthop.* **15,** 355–359 (2004).

19. Coles, J. M., Chang, D. P. & Zauscher, S. Molecular mechanisms of aqueous boundary lubrication by mucinous glycoproteins. *Curr. Opin. Colloid Interface Sci.* **15,** 406–416 (2010).

20. Zappone, B., Ruths, M., Greene, G. W., Jay, G. D. & Israelachvili, J. N. Adsorption, lubrication, and wear of lubricin on model surfaces: polymer brush-like behavior of a glycoprotein. *Biophys. J.* **92,** 1693–708 (2007).

21. Chang, L. Effects of thermally induced inhomogeneous shear and surface thermal boundary conditions on the shear stress in sliding elastohydrodynamic contacts. 227–240 (2009). doi:10.1002/ls

22. Jay, G. D. *et al.* Prevention of cartilage degeneration and gait asymmetry by lubricin tribosupplementation in the rat following anterior cruciate ligament transection. *Arthritis Rheum.* **64,** 1162–71 (2012).

23. Dulin, J. & Drost, W. Influence of exercise on the distribution of technetium Tc 99m medronate following intra-articular injection in horses. *Am. J. Vet. Res.* **73,** 418–25 (2012).

24. Teeple, E. *et al.* Effects of supplemental intra-articular lubricin and hyaluronic acid on the progression of posttraumatic arthritis in the anterior cruciate ligament-deficient rat knee. *Am. J. Sports Med.* **39,** 164–72 (2011).

25. Lee, D. W., Banquy, X. & Israelachvili, J. N. Stick-slip friction and wear of articular joints. *Proc. Natl. Acad. Sci. U. S. A.* **110,** E567–74 (2013).

26. Pritzker, K. P. H. *et al.* Osteoarthritis cartilage histopathology: grading and staging. *Osteoarthritis Cartilage* **14,** 13–29 (2006).

27. Waller, K. a *et al.* Role of lubricin and boundary lubrication in the prevention of chondrocyte apoptosis. *Proc. Natl. Acad. Sci. U. S. A.* **110,** 5852–7 (2013).

28. Teeple, E. *et al.* Coefficients of friction, lubricin, and cartilage damage in the anterior cruciate ligament-deficient guinea pig knee. *J. Orthop. Res.* **26,** 231–7 (2008).

CHAPTER 5

CONCLUSIONS AND RECOMMENDATIONS

Synthetic biomimicry of natural molecules is an ever expanding field in biomedical engineering and the life sciences. Fields such as tissue engineering are becoming more relevant, as it becomes clear that some of the best engineered structures are not man-made but exist in the natural world. An example is the load-bearing knee joint which can sustain an incredible amount of loading, both statically and dynamically, and yet maintain its structural integrity for decades. However, even the best engineered structures can break down over time requiring replacement or proper maintenance. Here synthetic biomimicry can be especially useful for treating medical disorders such as osteoarthritis (OA) involving degradation of the joints. Naturally, the body creates biolubricants to protect and maintain the integrity of joint cartilage. One of these biolubricants called lubricin is extremely important for boundary mode lubrication of the cartilage where the greatest frictional forces and wear occurs. Unfortunately, the production of lubricin is impaired in people with OA, and is cannot be easily synthesized in the laboratory. In this work, we synthesized a library of polymer brushes to mimic the structure of lubricin for use as a boundary lubricant. Our goal was to characterize these polymers and determine their effectiveness in treating OA.

Employing a combinatorial approach to polymer synthesis, 27 different polymer brushes were created composed of poly(acrylic acid) (pAA) with poly(ethylene glycol) (PEG) side chains to mimic the structure of lubricin, which itself has a long backbone and dense, hydrophilic oligosaccharide side chains. Human lubricin has a length of ~173 nm with a molecular weight of ~200,000 g/mol. We utilized RAFT polymerization to create the (pAA)

backbone's of molecular weights ($\bar{M}_n$) 60,000; 105,000; and 145,000 g/mol (0.5X, 1X, 1.5X size of lubricin). This allowed for well-controlled polymerizations with relatively narrower polydispersity indices (PDI). Following synthesis of the pAA backbones methoxy-PEG-amine side chains of molecular weights 2,000; 5,000 and 10,000 g/mol were conjugated onto the pAA using condensation chemistry with 4-(4,6-dimethoxy-1,3,5-triazine-2-yl)-4-methylmorpholinium chloride (DMTMM) as the condensing/activating agent to form amide bonds. The role of PEG is to add hydrophilicity and rigidity to the pAA backbone and mimic the oligosaccharide side chains of lubricin. AA:DMTMM:PEG grafting ratios were employed during the reaction of 1:0.5:0.5, 1:1:1 and 1:2:2 to study the effect of side chain densities. The resulting polymer brushes are called poly(acrylic acid)-*graft*-poly(ethylene glycol)'s (pAA-*g*-PEG) and are of varying size and grafting parameters ranging from pAA(60)-0.5-PEG(2) (60,000 g/mol pAA, grafting ratio 1:0.5:0.5, 2,000 g/mol PEG) to pAA(145)-2-PEG(10) (145,000 g/mol pAA, grafting ratio 1:2:2, 10,000 g/mol PEG). This two-step synthesis provided a quick and simple way to produce polymer brushes; the relatively mild conditions required for the synthesis allow scalability and low cost.

In addition, forced degradation experiments were performed to study the stability of the pAA-*g*-PEG's and to determine what potential environmental stressors can degrade the polymer over time. This is important not only to determine ideal storage conditions but to determine if any toxic byproducts are formed and is accomplished through accelerated chemical degradation of the materials. For a material to become a clinically available drug product or drug substance, stability studies are crucial for FDA approval. Here the forced degradation study of pAA(60)-2-PEG(2), pAA and PEG under oxidation (3% hydrogen peroxide phosphate buffered saline (PBS), pH=7.4) and hydrolytic conditions (0.1 N HCl or

0.1 N NaOH). These environments were chosen assuming that pAA(60)-2-PEG(2) would be drug substance stored in an aqueous media. It was found that pAA(60)-2-PEG(2) appeared to only degrade under the oxidative conditions studied. In particular, the PEG component of the polymer was very susceptible to oxidation potentially forming aldehydes, esters, hydroperoxides or carboxylates but resistant to acid or base hydrolysis.

Beyond the synthesis and stability testing of pAA-*g*-PEG, we sought to determine the percent conjugation of PEG onto the pAA backbones as well. Unfortunately, this proved far more difficult than originally conceived. Many of the polymer brushes were too large to be injected into gel permeation chromatography (GPC) columns, where they are not well equipped for analyzing non-linear polymers. Proton nuclear magnetic resonance (NMR) had difficulties quantifying the polymers with higher grafting ratios such that the spectra resembled pure PEG spectra. This is a result of the polymer brushes being composed mostly of PEG by mass. To overcome this difficulty, a novel method was developed and investigated using Fourier transform infrared spectroscopy (FTIR) to determine percent conjugation. The assumption that the FTIR spectra pAA-*g*-PEG's are a combination of pAA and PEG spectra. To exploit this method a series of pure pAA and PEG physical mixtures along with their pure forms were spin coated on CaF_2 crystals and their FTIR spectra captured. The spectra were then mathematically decomposed along the frequency range of 1000-2000 cm^{-1} using either single value decomposition (SVD) or partial least squares (PLS) in Matlab. The results were plotted as a graph comparing the mathematical decomposition of the spectra against the known mass fraction of pAA in the spectra. The spectra of the pAA-*g*-PEG can then be compared to this curve to determine the mass fraction of pAA to determine percent conjugation. Of the two mathematical decompositions employed, PLS was the most robust

and demonstrated greater precision and accuracy of determining percent conjugation of lower grafting ratios (0.5, 0.25). However, neither of the methods could predict the percent conjugation of the highest grafting ratio of 2. In fact, the results seem to suggest that the polymer pAA(60)-2-PEG(2) is pure PEG. While this methodology utilizing FTIR seems to hold promise, more work must be done to confirm the potential of this in determining the percent conjugation of high density graft copolymers. It is the recommendation of this author that more mass fractions of pAA (pAA/(pAA+PEG)) should be added to the calibration spectra in future studies, especially in the range of 0-10% mass fractions. This is to compensate for the disparity of pAA to PEG in highly grafted pAA-*g*-PEG, which could be less than 5% pAA by mass.

Finally, the pAA-*g*-PEG's were evaluated in collaboration with the Bonassar Laboratory to determine the efficacy of polymer binding and lubrication on cartilage in in vitro and in vivo experiments. Among the polymers pAA(60)-2-PEG(2) demonstrated the greatest efficacy in terms of boundary friction reduction and efficient binding onto cartilage. In vitro testing of pAA(60)-2-PEG(2) dissolved in PBS on bovine cartilage stripped of natural lubricin showed a significant reduction of friction compared to unlubricated ($p<0.05$) and produced lower friction values than even LUB:1, a recombinant form of lubricin shown to have chondroprotective affects in rat models of OA. The binding time constant of pAA(60)-2-PEG(2) was determined to be ~20 minutes, significantly lower than the known synovial clearance time (~5 hours) suggesting quick binding in the synovial cavity. In vivo studies were conducted with Sprague-Dawley rat models of OA, where OA was induced by tearing the anterior-cruciate ligaments (ACL) of the hind-legs and supplemented with either polymer or PBS as control daily for three weeks. After six weeks total post-transection, the rats were

sacrificed and their knee sections were tribologically analyzed and histologically graded based on the Osteoarthritis Research Society International (OARSI) grading scheme in a blinded and randomized manner. The results showed significant reduction in coefficient of friction on the tibeal plateau when supplemented with pAA(60)-*g*-PEG(2) compared to control ($p<0.01$) and similar to native, undamaged cartilage. The OARSI grading of the distal femur surface showed significant reduction ($p<0.05$) compared to PBS control demonstrating chondroprotection of the cartilage surface. These results show that pAA(60)-2-PEG(2) significantly reduces friction in the boundary mode on cartilage, provides chondroprotection in rat models of OA compared to PBS control treatments and is comparable to LUB:1 in inhibiting OA disease progression.

For future studies, pAA(60)-2-PEG(2) can be further evaluated in larger animal studies such as dogs with hip dysplasia or race horses with injury-induced OA. This would determine if the chrondroprotective effect observed in the small animal (rat) trials would translate to larger and more load-bearing joints. In these models, the polymer brush would be tested on animals with existing OA, instead of the early treatment model of the rats. In the rat model of OA, pAA(60)-2-PEG(2) was utilized as an early treatment of OA in the hopes of preventing disease progression. Potentially in these larger animals that already suffer from OA, the polymer treatment can be evaluated for more moderate to severe conditions in treating pain, degradation and mobility. In addition, the next step might be to enhance the binding efficacy of the pAA-*g*-PEG's by attaching peptides with affinities to cartilage and other synovial fluid components; native lubricin is known to have several binding domains that interact with other fluid components as well as cartilage tissue.

In summary, a library of polymer brushes were synthesized to mimic the structure and function of lubricin. pAA-*g*-PEG was found to be resistant to hydrolysis but prone to oxidation in forced degradation studies especially the PEG component. A novel method utilizing FTIR and PLS was developed in an attempt to quantify the percent conjugation of PEG in pAA-*g*-PEG, but was found to be ineffective at the highest grafting ratio and may need further development. In vitro and in vivo evaluation of pAA-*g*-PEG's as boundary lubricants found that pAA(60)-2-PEG(2) was the most effective in reducing boundary mode friction, had the fastest binding time constant (~20 minutes) and provided significant chronoprotection of cartilage in rat models of OA.

APPENDIX

HYDRODYNAMIC SIZE ANALYSIS OF pAA-*g*-PEG's

Hydrodynamic size of lubricin measured through light scattering is approximiately 173 nm[35] while it's contour length is ~200 nm[44]. This means that hydrodynamic size is an excellent approximation of lubricin's contour length; this may be due to lubricin's extended structure in the presence of water[30] forcing it to adopt a stiff conformation in solution. As a consequence, hydrodynamic size characterization was employed on the pAA-*g*-PEG's to determine the effect of the varying the backbone size, side chain size and grafting density on hydrodynamic size and relation to contour length of the polymer backbones. The pAA-*g*-PEG's were dissolved in 1X PBS to better mimic physiological conditions at 3 mg/ml and characterized using dynamic light scattering (DLS) in a Zetasizer Nano to determine the size of the polymers. Solubility issues were experienced with some of the larger pAA-*g*-PEG's preventing any characterization of structural properties in solution. The collected hydrodynamic size characterization data is presented below in **Table A-1**.

The data was analyzed using multivariate linear regression to determine the individual effects of pAA backbone size, PEG side chain size and PEG:AA grafting ratio as well as their cross-correlations on hydrodynamic size. The results is presented in **Table A-2** in descending order of p-value. The only variable that had a significant effect on hydrodynamic size of the pAA-*g*-PEG's was the PEG side chain sizes ($p<0.05$). The pAA backbone size while not significant ($p=0.06$) provided the second greatest influence to hydrodynamic size, while the cross-correlation variables and grafting ratio did not appear to significantly contribute.

Table A.1: Table of hydrodynamic diameters of pAA-*g*-PEG's

Nomenclature	pAA backbone (g/mol)	MW of PEG side chains (g/mol)	PEG:AA grafting ratio	hydrodynamic diameter (nm)
pAA(145)-2-PEG(10)	145000	10000	2	
pAA(145)-1-PEG(10)	145000	10000	1	110.5
pAA(145)-0.5-PEG(10)	145000	10000	0.5	
pAA(145)-2-PEG(5)	145000	5000	2	
pAA(145)-1-PEG(5)	145000	5000	1	
pAA(145)-0.5-PEG(5)	145000	5000	0.5	89
pAA(145)-2-PEG(2)	145000	2000	2	84
pAA(145)-1-PEG(2)	145000	2000	1	
pAA(145)-0.5-PEG(2)	145000	2000	0.5	64
pAA(105)-2-PEG(10)	105000	10000	2	
pAA(105)-1-PEG(10)	105000	10000	1	
pAA(105)-0.5-PEG(10)	105000	10000	0.5	
pAA(105)-2-PEG(5)	105000	5000	2	105
pAA(105)-1-PEG(5)	105000	5000	1	103
pAA(105)-0.5-PEG(5)	105000	5000	0.5	84
pAA(105)-2-PEG(2)	105000	2000	2	81
pAA(105)-1-PEG(2)	105000	2000	1	83
pAA(105)-0.5-PEG(2)	105000	2000	0.5	88
pAA(60)-2-PEG(10)	60000	10000	2	91
pAA(60)-1-PEG(10)	60000	10000	1	
pAA(60)-0.5-PEG(10)	60000	10000	0.5	91
pAA(60)-2-PEG(5)	60000	5000	2	69
pAA(60)-1-PEG(5)	60000	5000	1	82
pAA(60)-0.5-PEG(5)	60000	5000	0.5	64
pAA(60)-2-PEG(2)	60000	2000	2	46
pAA(60)-1-PEG(2)	60000	2000	1	
pAA(60)-0.5-PEG(2)	60000	2000	0.5	63

Table A.2: Table of hydrodynamic multivariate linear regression modeling coefficients

Variables investigated	**Coefficient estimate**	**p-value (significance)[a]**
side chain size	$3.65 \times 10^{-3} \pm 1.20 \times 10^{-3}$	0.0164[b]
backbone size	$2.47 \times 10^{-4} \pm 1.15 \times 10^{-4}$	0.0634
(backbone size)*(grafting ratio)	$1.97 \times 10^{-4} \pm 2.80 \times 10^{-4}$	0.502
(side chain size)*(grafting ratio)	$1.18 \times 10^{-3} \pm 4.10 \times 10^{-3}$	0.7816
(backbone size)*(side chain size)	$6.85 \times 10^{-09} \pm 3.12 \times 10^{-8}$	0.8315
(backbone size)*(side chain size)*(grafting ratio)	$-1.21 \times 10^{-08} \pm 1.17 \times 10^{-7}$	0.92
grafting ratio	0.453 ± 9.95	0.9648

[a] Arranged by descending degree of significance

[b] $p<0.05$